공학박사 학위논문

Enhancing the performance of Vanadium based catalysts for selective catalytic reduction of nitrogen oxides with ammonia

암모니아를 사용한 질소산화물 선택적 촉매 환원을 위한 바나듐 기반 촉매계 성능 향상 연구

2023년 8월

서울대학교 대학원

화학생물공학부

전 세 원

Enhancing the performance of Vanadium based catalysts for selective catalytic reduction of nitrogen oxides with ammonia

지도 교수 김 도 희

이 논문을 공학박사 학위논문으로 제출함
2023년 7월

서울대학교 대학원
화학생물공학부
전 세 원

전세원의 공학박사 학위논문을 인준함
2023년 7월

위 원 장 이 원 보 (인)

부위원장 김 도 희 (인)

위 원 강 종 헌 (인)

위 원 김 지 만 (인)

위 원 박 영 권 (인)

Abstract

Air pollution has been a global environmental issue for decades and efforts to mitigate the global threat are a huge challenge to many environmental researchers. As the industries have been developing fast, desires for clean environment and better life have also increased for past years. The major air pollutions that have caught much attention are nitrogen gases (NO_x), sulfurous gases(SO_x), carbon dioxides(CO_2), and other greenhouse gases(GHG). For recent years, the harmfulness of these emissions has been highlighted as cause of climate change. Hence, the global goals for clean environment have implemented to reduce the environmental impacts for public health.

Among these air pollutants, NOx emission from stationary sources like coal power plants that uses fossil fuels as energy sources is a huge challenge because it can produce the secondary product when it emits to air. It also plays a critical role in increasing ozone and smog. Various technologies have been developed to suppress NOx emissions including selective catalytic reduction with NH_3, lean burn engines and so on. Although selective catalytic reduction with NH_3 as a reducing agent (NH_3-SCR) has been applied to industries as an efficient technology, especially to after treatment process, to reduce NO_x emission. The injected ammonia(NH_3) into exhaust gas stream, passing through a catalyst bed where the NOx is converted to nitrogen (N_2) and water (H_2O), which are

harmless compounds in air. The NH_3-SCR technology are advantageous over other technologies because of its lower operating costs with high efficiency. However, new technology on NH_3-SCR system must be introduced to fulfill the NOx emission regulations placed by governments and SOx are usually present in after treatment process of power plants. During the NH_3-SCR process, the present of SOx must be considered as well because it can affect the lifetime of catalyst and efficiency.

Various types of metal oxide-based catalysts and zeolite-based catalysts have been utilized in NH_3-SCR systems depending on their properties and operating factors like temperature and composition of exhaust gas. Among various DeNOx catalysts, vanadium oxide-based catalysts are most used in after treatment process of stationary sources for its high thermal stability and affordable prices. Although the vanadium oxide-based catalysts (V_2O_5/TiO_2 or V_2O_5/WO_3-TiO_2) are world widely used for its advantages, there are practical issues to meet the recent obligations. First, the high NOx conversion of the conventional vanadium oxide-based catalysts can only achieve only at high temperature above 300 ^oC while the recent operating temperature in actual industries are mostly below 300 ^oC. In addition, since SO_2 and water exist during the after-treatment process. When SO_2 are oxidized to SO_3 and react with NH_3 and H_2O, ammonium bisulfate (ABS) is produced and it causes sulfur poisoning on catalysts, leading to reduce efficiency and lifetime of catalysts. Hence, innovative NH_3-SCR technology that acquires high sulfur resistance with less energy

consumptions and higher NOx removal efficiency at low temperature simultaneously are required as for environment-friendly industrial applications. Therefore, this research provides innovative insights to improve sulfur resistance of vanadium oxide-based catalysts via simple synthesis method that can be advantageous applying to practical industrial fields.

In details, this study discussed that a series of V_2O_5/WO_3-TiO_2 and alumina calcined at different temperatures are prepared by physical mixing to enhance sulfur resistance and regenerability at low temperatures. Among the mechanically alumina mixed catalysts (V_2O_5/WO_3-TiO_2 + Al), the V_2O_5/WO_3-TiO_2 mixed with alumina calcined at 900 ^oC achieved the highest sulfur resistance due to increase of strongly adsorbed acid sites. This research also demonstrated that ABS formed on vanadia sites migrated to the mixed alumina sites and vanadia active sites were protected from sulfur poisoning, resulted in superior sulfur resistance at low temperature. The physical mixed V_2O_5/WO_3-TiO_2 catalyst with alumina can enhance sulfur resistance of V_2O_5/WO_3-TiO_2 catalyst and accomplish regenerability at low temperature.

This study also discussed the physically mixed vanadia catalyst with surface modified zeolite that can resolve physical and chemical deactivation simultaneously. When V_2O_5/WO_3-TiO_2 catalysts and Al-rich zeolite Y (Si:Al_2=5.1) were mechanically mixed are designed for sulfur-resistant deNOx catalysts, degradation of activity was observed with

improved sulfur resistance. The main cause of degradation was the chemical interaction between VOx and mobile AlOx species, most likely extra-framework Al species, on zeolite surface during the mechanical mixing, which were confirmed by various characterizations including H_2-temperature-programmed reduction (H_2-TPR) and line energy dispersive X-ray spectroscopy (line-EDS). To resolve the problem, octadecyltrichlorosilnae (OTS) was coated on zeolite surface first and mechanically mixed with V_2O_5/WO_3-TiO_2 catalysts. In summary, the developed catalyst V_2O_5/WO_3-TiO_2 + OTSY catalyst obtained high NOx conversion and enhanced sulfur resistance by suppressing the physical and chemical poisoning simultaneously.

The present study also investigated ball milling effect over hybrid catalyst composed of V_2O_5/WO_3-TiO_2 + zeolite Y catalysts. It included how the ball milling process affected on catalytic properties and activity depending on synthesis method.

Keyword : Selective catalytic reduction with NH_3 (NH_3-SCR), Vanadium oxide-based catalyst, Physical mixing, Sulfur resistance, Zeolite, Alumina.
Student Number : 2017-25668

Table of Contents

List of Tables

List of Figures

Chapter 1. Introduction

1.1. Study Background

As various industrials have grown quickly and taken places in many parts of lives of human being, massive concerns regarding the impacts on environment has been increasing for decades. One of the major concerns is to slow down the global warming and to protect the environment for descendants. As environmental issues have been considered as global issue, the regarding regulations have become stringent to resolve the issues with priority [1, 2].

Especially, power plants using fossil fuels as energy sources have been facing large energy consumption of electrical and thermal energy and emissions of air pollutants, such as fine particulate matters (PM_{10}, $PM_{2.5}$), nitrogen gases(NO_x), sulfur oxides(SO_x), and greenhouse gases (GHG) as illustrated in Fig. 1-1 [3-5]. Nitrogen gases(NO_x) emissions have caught a huge attention because not only itself can be a serious air pollutant, but when it emits to the air, it can also form the second air pollutants including smog, ultrafine particulate matters, acid rain, and so on. With the reasons, human beings have tremendous concern on its emission from industrial areas and plants.

Especially, recent research has shown that South Korea is the most heavily polluted country by ultrafine dust particles in the world. According to an analysis conducted by the international environmental organization

Greenpeace[6], South Korea ranked first among OECD member countries for air pollution, based on annual average ultrafine dust particles concentration. The concentration of ultrafine dust particles has increased to 24.8 μg/m^3 in comparison to 24 μg/m^3 in 2018, and the proportion of the hourly average concentration of ultrafine dust particles that fall under the "Bad" category has increased from 6% in 2018 to 6.5% in 2019. This increase in air pollution has led to increased health risks [6, 7].

Therefore, global obligations on NO_x emissions following Euro 6 have been strengthened to mitigate the issue for past years as the paradigm of energy shifts to clean energy and environment as shown in Fig 1-2 [1, 7]. The biggest challenge for the industry in recent years is to satisfy the global demands for the improved environment. The goals for setting environment-friendly plants in near future are obvious and reducing energy consumption for net zero emissions are clear. Although massive research has been studied to improve the previous ways or to develop new breakthroughs to accomplish these goals, many industries have been still struggling to find innovative methods. Hence, developing air purification technologies is necessary by practicing research on exhaust gas.

Fig 1-1. Major Air pollutants and schematic of fine particulate matters.

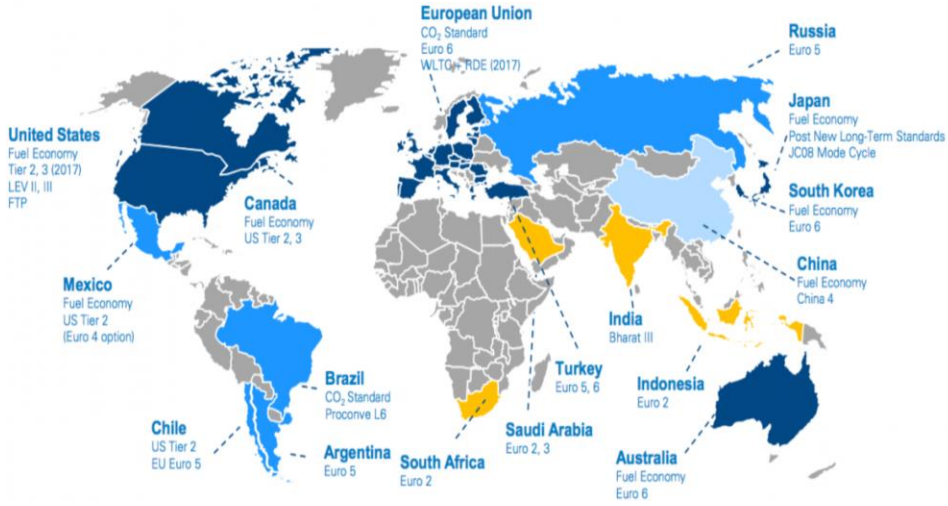

Fig 1-2. NO_x Emission standards of mobile sources on worldwide.

1.2. Selective catalytic reduction of NO_x with NH_3

One of the widely applied techniques for removal of NO_x emission is selective catalytic reduction with NH_3 as a reducing agent (NH_3-SCR). NH_3-SCR system has been applied for transportations and stationary sources. During NH_3-SCR reaction, the reducing agent NH_3 can reduce nitrogenous gases to nitrogen and water, which is unharmful to emit in air.

Generally, metal oxide-based catalysts and zeolite-based catalysts are often utilized in majority of industrial NH_3-SCR systems. Most metal oxide-based catalysts can be used as both active sites of catalysts and support regarding its properties. They are sometimes advantageous over the zeolite-based catalysts for affordable prices and ease to supply. Various metal oxide-based catalysts, such as MnOx, CeOx, and Pd/ceria, are known to have high NOx removal ability [8].

In addition, zeolite-based catalysts or metal supported on zeolite catalysts, such as Cu/zeolite, Fe/zeolite catalysts, can be utilized in many industries. Zeolite itself can be also used as ion exchange, acid catalysts, support, and some reactions can even occur within the pores of zeolite [9]. Various properties of zeolites including pore size, thermal conductivity, and so on can influence the catalytic process and targeting reactions. In that way, both metal oxide-based and zeolite based deNOx catalysts are applied depending on their catalytic properties, operating conditions and so on.

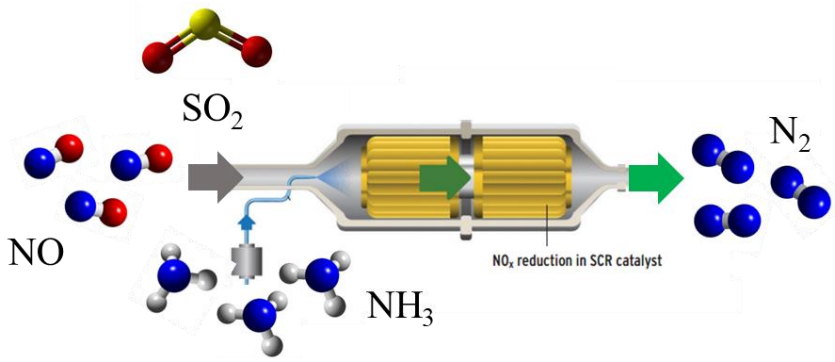

$$2\,NO + 2\,NH_3 + \tfrac{1}{2}O_2 \longrightarrow 2\,N_2 + 3\,H_2O$$
$$NO_2 + 2\,NH_3 + \tfrac{1}{2}O_2 \longrightarrow \tfrac{3}{2}N_2 + 3\,H_2O$$
$$NO + NO_2 + 2\,NH_3 \longrightarrow 2\,N_2 + 3\,H_2O$$

Fig 1-3. The scheme of selective catalytic reduction with NH_3.

1.3. Purpose of Research

Globally, air pollutants including NOx emission have brought negative effects on human lives and health. One of the major challenges in industries using fossil fuels as energy sources NOx emission. NOx not only play a main air pollutant, but it also can produce the secondary air pollutants, acid rain, fine particulate matters, and smog. As many environmental researchers have put their efforts to resolve the emission, NH_3-SCR system is utilized as one of the efficient technologies to reduce NOx emission in various applications like aftertreatment process in off road sources. However, the policies over the amount of emitting NOx emission have become stricter every year, allowing only small amount of NOx emission as possible. So innovative way to develop NH_3-SCR system are necessary.

Vanadium oxide-based catalysts have been utilized as a NH_3-SCR catalyst due to its high stability to sulfur at high temperature, especially to after treatment in stationary sources like coal-power plants. However, it is difficult to satisfy the strengthened obligations with the conventional vanadium oxide-based catalysts. The temperature of exhaust gases in stationary sources are often below 300 ℃. At such low temperature range, the conventional vanadium oxide-based catalysts achieve high NOx removal ability mostly at higher temperatures and sulfur poisoning on the catalyst is accelerated, which leads to additional heat energy consumption and shortening lifetime of catalyst. Also, during the heating process, the risk of producing greenhouse gases is increasing, which is contradicting result to

realizing environment-friendly industries.

Therefore, vanadium oxide-based catalysts were synthesized via simple physical mixing with alumina to enhance sulfur resistance of the conventional vanadium oxide-based catalysts at low temperatures. The lifetime and possibility of multiple use of the developed catalysts were examined vis regnerability and reusability tests. In addition, mechanically mixed vanadium oxide-based catalysts with surface modified zeolite were designed to suppress physical and chemical poisoning simultaneously in presence of sulfur at low temperature.

Hence, in this study, the purpose of this research is to suggest new insights on developing efficient vanadium oxide-based NH_3-SCR catalysts via simple synthesis way that can maintain superior sulfur resistance at low temperatures. Additionally, the purpose of this research is to suggest breakthroughs that can be possibility used to soothe global NO_x emissions in industrial fields and realize the environment-friendly catalytic system for public health.

Chapter 2. Enhanced SO_2 resistance of V_2O_5/WO_3-TiO_2 catalyst physically mixed with alumina for the selective catalytic reduction of NO_x with NH_3

2.1. Introduction

As NO_x emission regulations have been strengthened to mitigate environmental issues, the demand for effective NO_x removal technology that can satisfy the current regulations has increased remarkably. Selective catalytic reduction with NH_3 (NH_3-SCR) is known as the most effective NO_x removal technology applied to many industrial areas [10-14]. The overall reaction mechanism and corresponding catalysts have been studied for many years [15-18].

Among many SCR catalysts, supported vanadium oxide catalysts have been widely applied in industrial applications [19-22]. However, conventional vanadia-based catalysts require modifications, such as the addition of promoters or the increase in the loading of V_2O_5, for high NOx removal ability [23-33]. Such modifications could promote the aggregation of the promoter or acceleration of SO_2 oxidation. This makes it difficult for the catalyst to maintain a high activity under SO_2 containing flue gas while achieving high stability at low temperatures, because SO_2 oxidation also accelerates the formation of ammonium bisulfate (ABS) on active sites, thus physically blocking the active sites and eventually decreasing the catalytic activity at low temperatures [34-38].

In our previous study [39], vanadium oxide supported on tungsten titania catalyst (V_2O_5/WO_3-TiO_2) was mixed with zeolite Y in a certain mass ratio, which yielded a significantly enhanced SO_2 resistance compared to the conventional V_2O_5/WO_3-TiO_2 catalyst. Since our previous study demonstrated that a greater number of alumina sites in zeolite is closely related to stronger sulfur resistance, it is expected that physical mixing with alumina would also enhance the sulfur resistance of vanadia catalysts [39]. In this study, we found that V_2O_5/WO_3-TiO_2 catalysts achieved high sulfur resistance upon the physical mixing with alumina. We also obtained different degrees of sulfur resistance when the physically mixed alumina was calcined at different temperatures (600 ℃, 900 ℃, and 1000 ℃). In addition, the alumina mixed catalyst exhibited remarkable regenerability, while maintaining its catalytic activity at low temperatures, and acquired a noticeable reusability even after repetitive SO_2 aging tests. Hence, this study aims to improve the SO_2 resistance of V_2O_5/WO_3-TiO_2 catalysts by physical mixing with alumina and elucidate the role of alumina in enhancing sulfur resistance.

2.2. Experimental

2.2.1. Catalyst preparation

A series of supported vanadium oxide catalysts was prepared using the wet impregnation method [40, 41]. Ammonium metavanadate (Sigma-Aldrich) was used as a vanadium oxide precursor and was dissolved in oxalic acid and stirred overnight. A calculated amount of commercial WO_3-TiO_2 (DT-52) was added to the solution as a support and the solution was stirred for 2 h. The stirred solution was dehydrated in a rotary evaporator in a water bath at 80 ℃ and dried overnight in an oven at 105 ℃. The vanadium oxide content was fixed at 5 wt.% and the dried samples were calcined in a muffle furnace at 500 ℃ for 4 h under static air. Then, the 5 wt.% V_2O_5/WO_3-TiO_2 catalyst was mixed with silica in a mortar for a few minutes with a 2:1 mass ratio of 5 wt.% V_2O_5/WO_3-TiO_2 to silica. The sample was simply denoted as 5VWTi. The mixed silica presumably had negligible effects on the catalytic activity and SO_2 resistance of the vanadia catalyst.

In this study, boehmite (Sasol) was used as an alumina precursor and calcined at 600 ℃, 900 ℃, and 1000 ℃ before it was physically mixed with the 5VWTi catalyst [42]. The 5VWTi and calcined alumina were mechanically mixed in a mass ratio of 2:1 (5VWTi to alumina) in a mortar for a few minutes. The catalysts are denoted as 5VWTi + (x)cal Al, where x represents the calcination temperature of alumina.

2.2.2. Reaction condition

SCR catalytic activity profiles were acquired under 500 ppm NO, 600 ppm NH_3, 10% O_2, 5% CO_2, 10% H_2O (balanced with N_2) with Gas hourly space velocity (GHSV) = 100,000 h^{-1}. To compare samples under the same space velocity, the same amount of V_2O_5/WO_3-TiO_2 was mixed with silica with the mass ratio of 5 wt.% V_2O_5/WO_3-TiO_2 to silica at 2:1. A SO_2 aging test was conducted with 500 ppm NO, 600 ppm NH_3, 10% O_2, 5% CO_2, 10% H_2O, and 30 ppm or 100 ppm SO_2 with N_2 balance. The gas hourly space velocity (GHSV) was fixed at 100,000 h^{-1} and the reaction temperature was 220 ℃. A regeneration test was conducted under a flow of 10% O_2, 5% CO_2, and 10% H_2O with N_2 balance at 350 ℃ for 2 h and with a gas hourly space velocity (GHSV) fixed at 100,000 h^{-1}. NO_x measurements were collected on a NO_x analyzer (42i high level, Thermo Scientific).

To compare deactivation rates of catalysts during SO_2 aging fairly, we conducted the deactivation rate of catalysts based on the normalized activity where the initial NOx conversion is denoted as 1. NOx conversion of catalyst would decrease during SO_2 aging test, and its decreasing slope of the normalized activity was calculated as a deactivation rate by using a linear fitting in Origin software.

2.2.3. Characterizations

To determine the sulfur species distribution after the SO_2 aging test, temperature-programmed desorption-mass spectroscopy (TPD-MS) results were obtained using a mass spectrometer (Hiden Analytical, model QGA). The TPD-MS characterization was performed at a heating rate of 10 ℃/min up to 900 ℃ under a N_2 flow of 100 mL/min and then maintained at 900 ℃ for 30 min. Powder X-ray diffraction (XRD) was performed using an X-ray diffractometer (Bruker, D8 Advance model) with a Cu Kα detector to determine the structural changes of the crystallites in the catalyst. An aberration corrected transmission electron microscope (Cs-TEM) of the JEM-ARM200F model was used to observe the crystal structure of the catalysts, and line energy dispersive X-ray spectroscopy (line-EDS) was performed on the catalyst to investigate the chemical composition of the catalysts after SO_2 aging.

Elemental analysis after SO_2 aging was performed using a Thermo Fisher Scientific Elemental Analyzer (Flash 2000 model) to determine the residual S content of the sample. NH_3-temperature programmed desorption (NH_3-TPD) peaks were collected using a BELCAT 50 from BEL JAPAN INC. The catalyst was pretreated at 400 ℃ for 1 h with an O_2/He mixture as the carrier gas. The adsorption was performed under NH_3/He mixture flow gas at 50 ℃ for 1 h. Desorption was performed up to 900 ℃ at a rate of 10 ℃/min under He gas flow. The N_2 adsorption and desorption isotherms were obtained at 77 K. The textural properties were acquired using a

Belsorp-mini (BEL Japan), which was calculated using the Brunauer–Emmett–Teller (BET) method. Solid-state nuclear magnetic resonance (NMR) spectra were collected on a Bruker Avance III HD (Bruker, Germany) under ambient conditions (25 ℃). ^{27}Al NMR spectra were measured at 130 MHz and a spinning rate of 10 kHz using a 2.5 mm MAS probe, with a pulse length of 2 μs, and a delay time of 0.1 s.

2.3. Results and discussions

2.3.1. SO_2 aging tests over the physically mixed vanadia catalysts with alumina

The catalytic activities of the physically mixed 5VWTi + 900cal Al catalyst and the conventional 5VWTi catalyst were compared in the absence of SO_2. As shown in Fig. 2-1, no significant difference in SCR activity was observed between the two catalysts over the entire temperature range, indicating that alumina does not affect the intrinsic SCR activity of the physically mixed sample. The catalytic activities of 5VWTi + 900cal Al and 5VWTi catalysts were compared at 220 ℃ in the presence of 30 ppm SO_2. As demonstrated in Fig. 2-2, the NO_x conversion of the 5VWTi catalyst decreased from 55% to 38% after 22 h of reaction, while that of 5VWTi + 900cal Al only decreased from 53% to 48%. This result strongly indicates that the tolerance to sulfur improved more significantly for 5VWTi + 900cal Al than the commercial 5VWTi alone in the presence of SO_2. In other words, physical mixing with 5VWTi and alumina did not affect the catalytic activity in the absence of SO_2 over the entire temperature range, although deactivation by SO_2 was significantly suppressed by the addition of alumina.

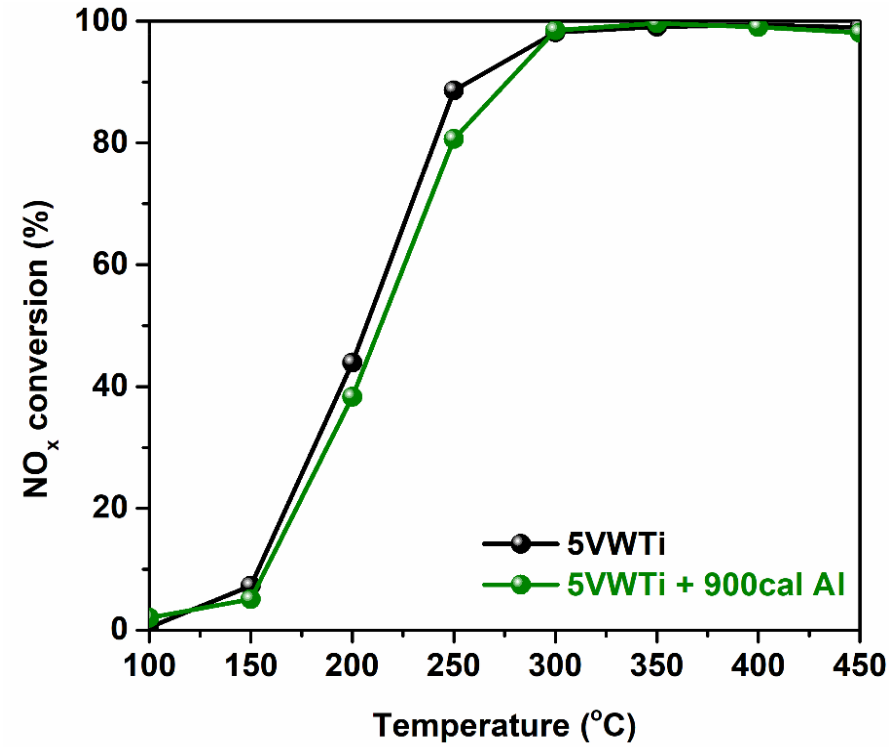

Fig. 2- 1. SCR catalytic activity profiles of the 5VWTi and 5VWTi + 900cal Al catalysts.

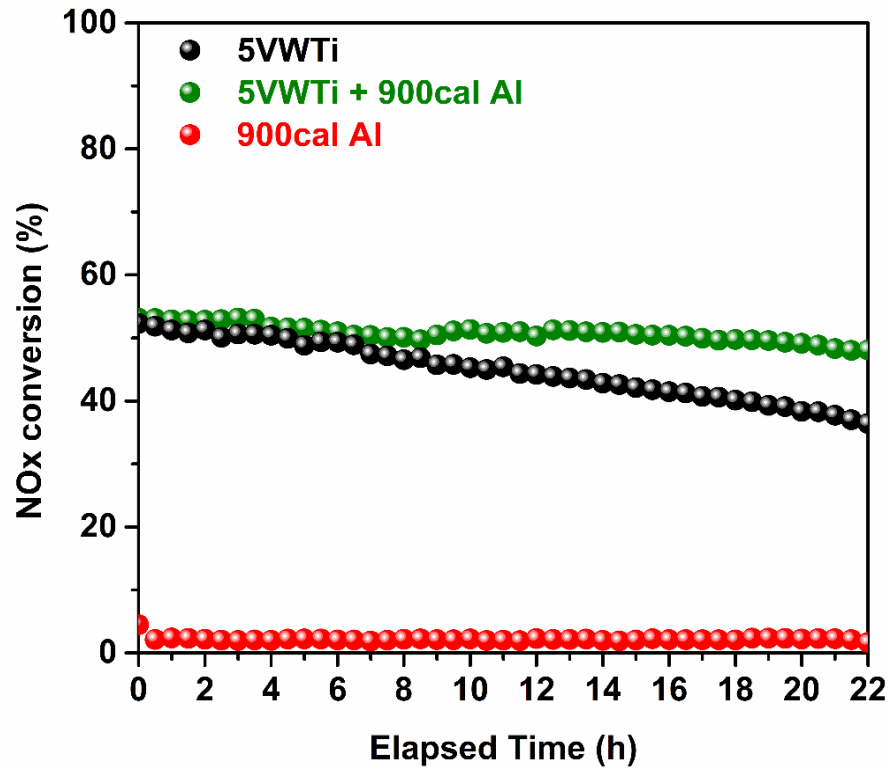

Fig. 2- 2. NO_x conversion profile of 5VWTi, 900cal Al and 5VWTi + 900cal Al catalysts during SO_2 aging at 220 ℃ for 22 h.

Furthermore, we found that calcination of alumina at different temperatures resulted in different sulfur resistances, as shown in Fig. 2-3. Interestingly, when the calcination temperature of alumina changed, the degree of suppression of deactivation by SO_2 was different, as shown in Fig. 2-3 and Fig. 2-4. As mentioned previously, 5VWTi + 900cal Al demonstrated a higher sulfur resistance, whereas the 5VWTi + 600cal Al and 5VWTi + 1000cal Al catalysts obtained much lower sulfur resistances. Among the several alumina mixture catalysts, the vanadia catalyst physically mixed with alumina calcined at 900 ℃ yielded the lowest deactivation rate. However, note that every alumina mixture catalyst achieved higher sulfur stability than the 5VWTi catalyst, regardless of the calcination temperature of the mixed alumina. From the SO_2 aging of the mixed catalysts, it was found that the physically mixed alumina calcined at different temperatures resulted in different sulfur resistances.

In addition, during the fast SO_2 aging test conducted under 100 ppm of a SO_2-containing flow for 22 h, physical mixing with Al contributed to the suppression of deactivation by SO_2, as shown in Fig. 2-5(a). Compared to the 5VWTi catalyst, the 5VWTi + 900cal Al catalyst achieved an improved SO_2 resistance with a much smaller deactivation rate, even after the 100 ppm SO_2 aging test, as displayed in Fig. 2-5(b). The results are also noticeable that the physically mixed alumina catalyst maintained a stable SCR performance, even at higher sulfur concentrations.

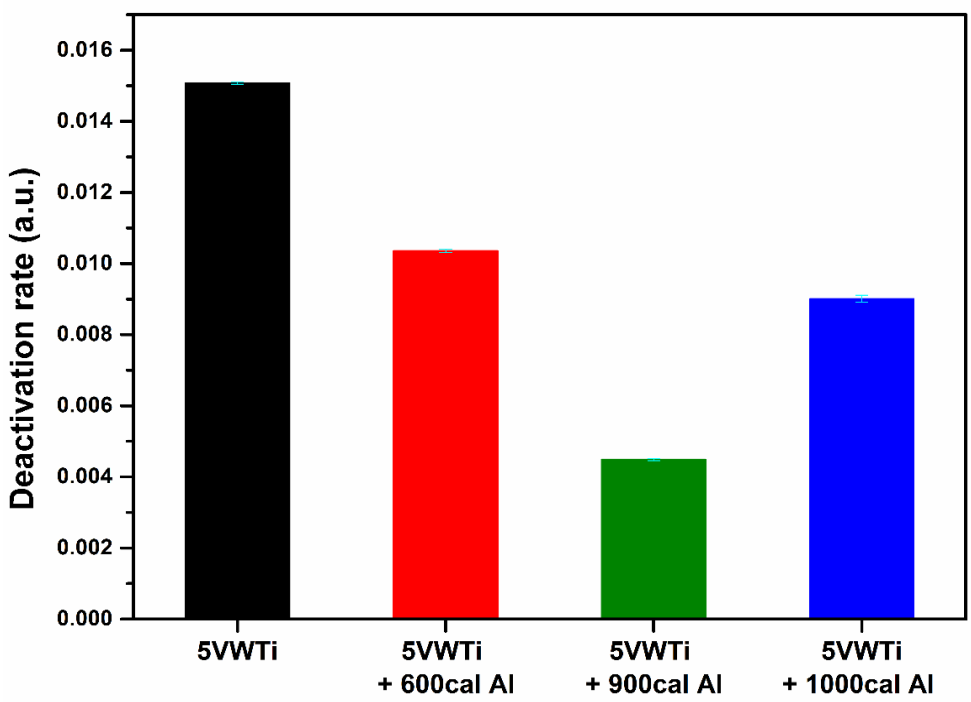

Fig. 2- 3. Deactivation rates of the physically mixed vanadia catalysts with calcined alumina at different temperatures (600 ℃, 900 ℃, and 1000 ℃) after SO_2 aging at 220 ℃.

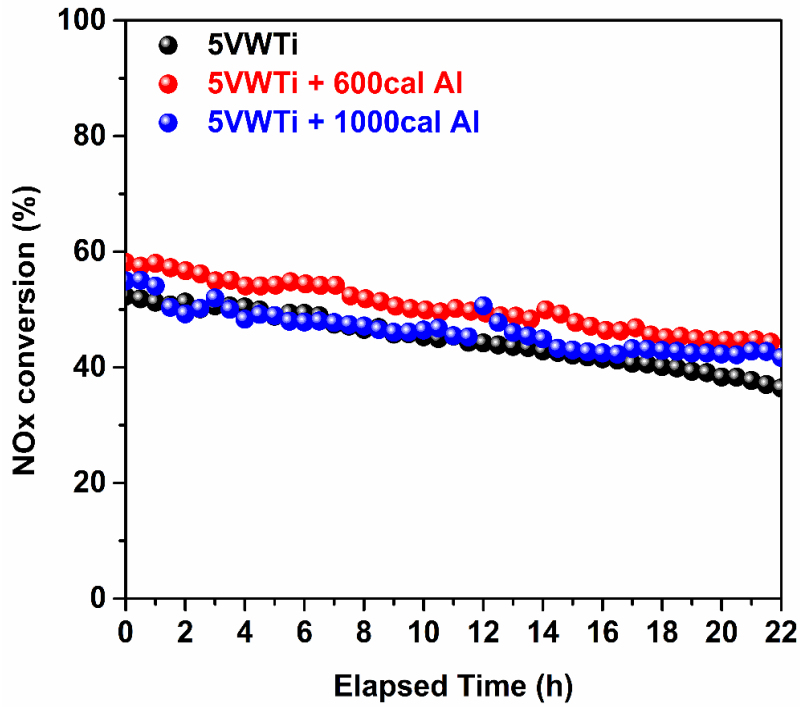

Fig. 2- 4. NOx conversion profiles of the physically mixed vanadia catalysts with calcined alumina at different temperatures (600 ℃ and 1000 ℃) at 220 ℃ for 22 h.

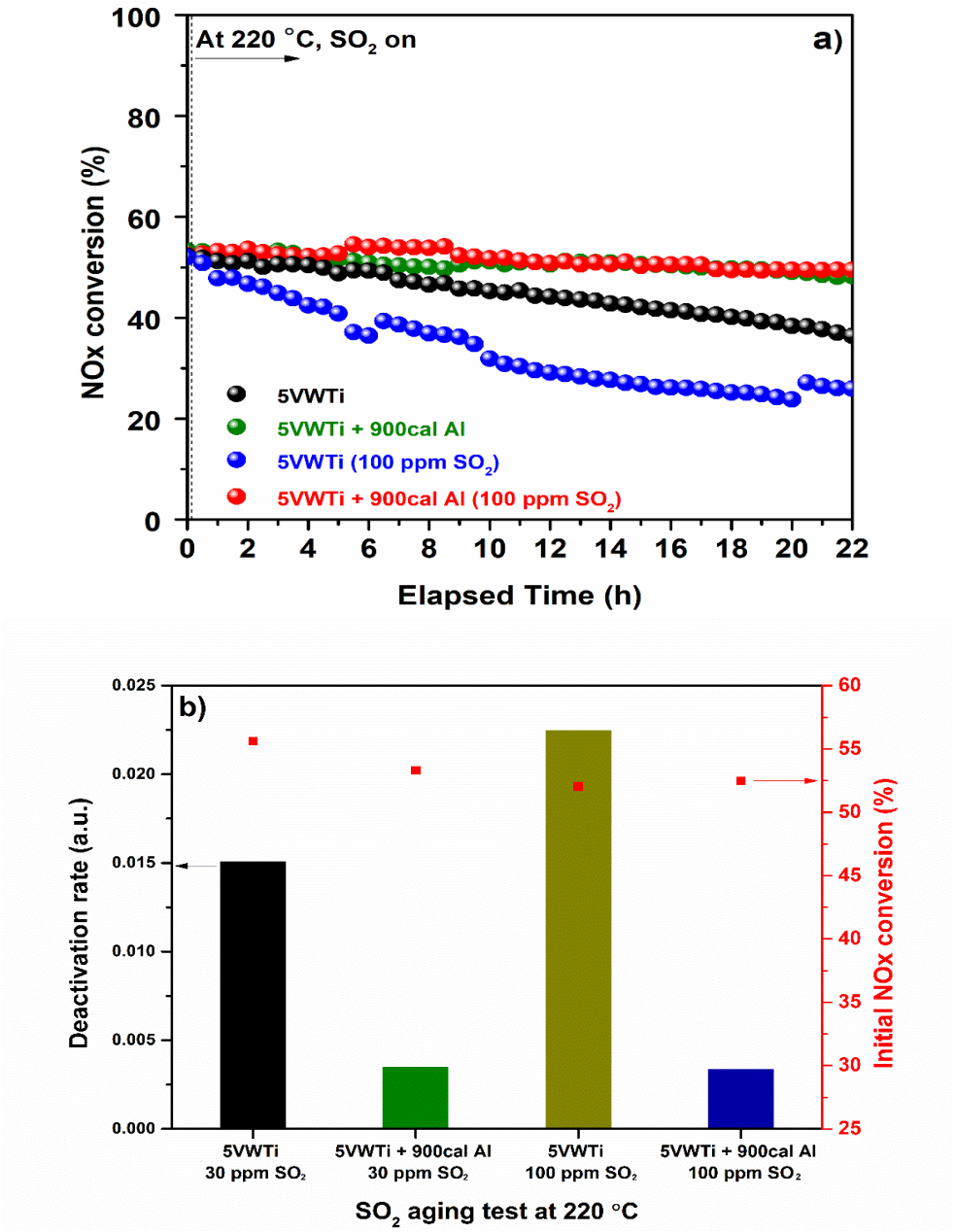

Fig. 2- 5. (a) NO_x conversion profiles of the 5VWTi and 5VWTi + Al catalysts during SO_2 aging at 220 °C and (b) deactivation rates of the samples after SO_2 aging.

2.3.2. Sulfur distribution in the physically mixed vanadia catalysts with alumina

To elucidate the role of alumina in preventing the deactivation of the catalyst from SO_2 poisoning, Cs-TEM and line-EDS analyses of the 5VWTi and 5VWTi + calcined Al samples after SO_2 aging with 30 ppm SO_2 were conducted. As shown in Fig. 2-6(a) and Fig. 2-6(b), when the EDS line scanning was performed over the SO_2 aged 5VWTi catalyst, the S intensity peak overlapped the intensity peaks of V and Ti. This could be interpreted as sulfur accumulating on the vanadia sites during exposure to SO_2. Fig. 2-7 showed the Cs-TEM and EDS analyses of SO_2 aged 5VWTi + 600cal Al, SO_2 aged 5VWTi + 900cal Al, and SO_2 aged 5VWTi + 1000cal Al catalysts, respectively, to verify the distribution of sulfur species in the samples. In the case of the 5VWTi + 600cal Al catalyst in Fig. 2-7(a) and Fig. 2-7(b), the EDS line scan of S overlapped with Ti and Al evenly, indicating that some sulfur existed on the alumina sites, although some S remained on the vanadia sites.

However, for the 5VWTi + 900cal Al sample, the intensity peak of S mostly overlapped that of Al rather than that of Ti, as shown in Fig. 2-7(c) and Fig. 2-7(d). Furthermore, in the case of the 5VWTi + 1000cal Al catalyst in Fig. 2-7(e) and Fig. 2-7(f), the EDS line scan of S overlapped with that of Ti rather than Al, which demonstrated that S remained on the vanadia sites rather than on the alumina sites. These results implied that when calcined alumina, especially at 900 °C, was physically mixed with

5VWTi, sulfur was mainly present on the alumina sites, not on the vanadia sites, whereas sulfur was accumulated on the vanadia sites in the conventional 5VWTi catalyst. Based on the characterization results, it could be concluded that sulfur piled up on the alumina sites, which suppressed the deactivation of the vanadia catalyst in the physically mixed sample.

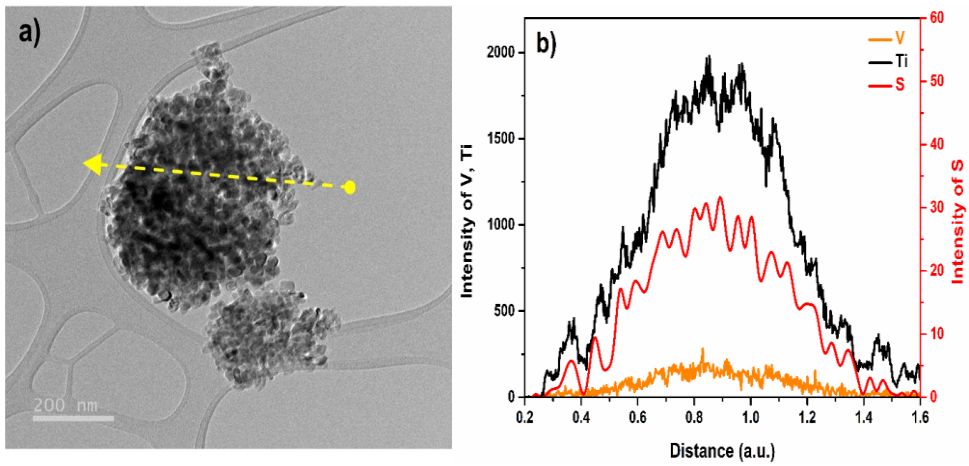

Fig. 2- 6. (a) Corrected transmission electron microscope (Cs-TEM) image and (b) line energy dispersive X-ray spectroscopy (line-EDS) scans of 5VWTi catalyst after sulfur aging under 30 ppm of a SO_2-containing flow at 220 ℃ for 22 h.

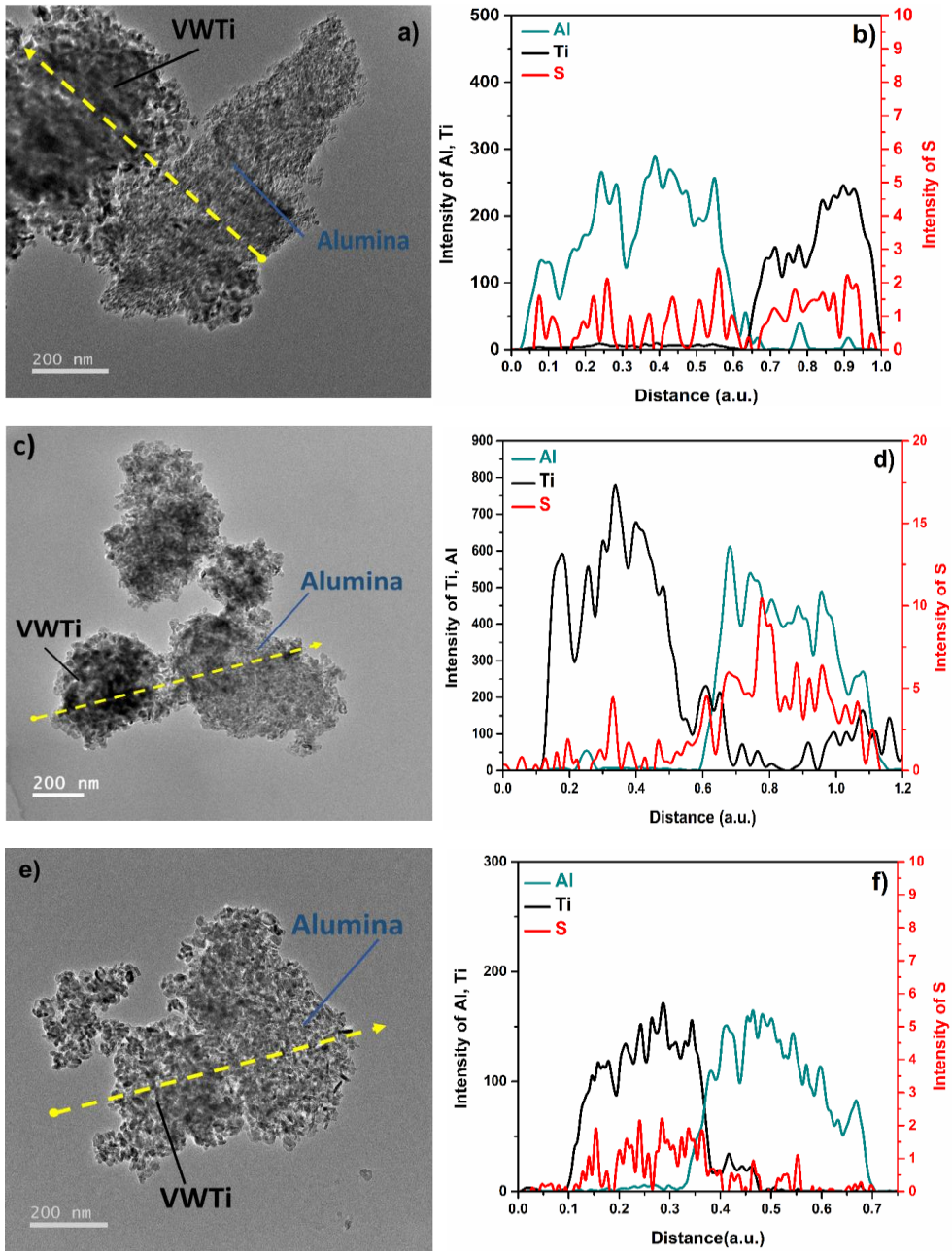

Fig. 2- 7. (a, c, and e) Cs-TEM images and (b, d, and f) line-EDS scans of 5VWTi + 600cal Al, 5VWTi + 900cal Al, and 5VWTi + 1000cal Al catalysts, respectively, after sulfur aging under 30 ppm of a SO_2-containing flow at 220 ℃ for 22 h.

To assess the characteristics of the adsorbed species over the catalysts, temperature-programmed desorption-mass spectroscopy (TPD-MS) was performed up to 900 ℃ after reaction at 220 ℃ for 22 h in the presence of SO_2. As shown in Fig. 2-8, for the SO_2 aged 5VWTi, the sample exhibited two SO_2 desorption peaks at 419 ℃ and 689 ℃. The peak at a lower temperature of 419 ℃ arose from the decomposition of ammonium bisulfate(ABS) formed on the vanadia sites [43]. This was also confirmed in the TPD-MS of the pre-impregnated 2 wt.% ABS/5VWTi catalyst, as shown in Fig. 2-9(a). When 2 wt.% ABS in the liquid phase was impregnated on 5VWTi, the SO_2 desorption peak at low temperature of approximately 400 ℃ was referred to the decomposition of ammonium bisulfate. Based on the results, the peak at a lower temperature of approximately 400 ℃ can be clearly assigned to the decomposition of ammonium bisulfate on the catalyst.

The peak at the higher temperature peak of 689 ℃ originated from the decomposition of sulfate on the titania sites initially presented in the 5VWTi catalyst, as the peak appeared at 726 ℃ in the TPD-MS results of the fresh 5VWTi shown in Fig. 2-9(b). Noda et al., demonstrated that the decomposition of sulfate on a TiO_2 sample was observed at approximately 680 ℃ based on TGA analysis, which corresponded well with our TPD-MS results [44]. However, in the case of the 5VWTi + 900cal Al catalyst, only SO_2 desorption was observed at 766 ℃, which was assigned to the decomposition of aluminum sulfate, whereas the decomposition of ammonium bisulfate shown in 5VWTi was not observed in this catalyst. The

TGA results also confirmed that the decomposition of aluminum sulfate was observed at approximately 760 ℃ [45, 46]. In the 5VWTi + 600cal Al catalyst, however, the peak at a lower temperature of approximately 384 ℃ was obtained, which was ascribed to the decomposition of ammonium bisulfate on vanadia sites, in addition to the peak corresponding to the decomposition of aluminum sulfate at approximately 800 ℃. Similar result was obtained from the TPD-MS profile of the 5VWTi + 1000cal Al catalyst. The peak at a lower temperature of approximately 391 ℃ was dominantly obtained, while the small peak appeared at approximately 846 ℃, which was assigned to the decomposition of aluminum sulfate.

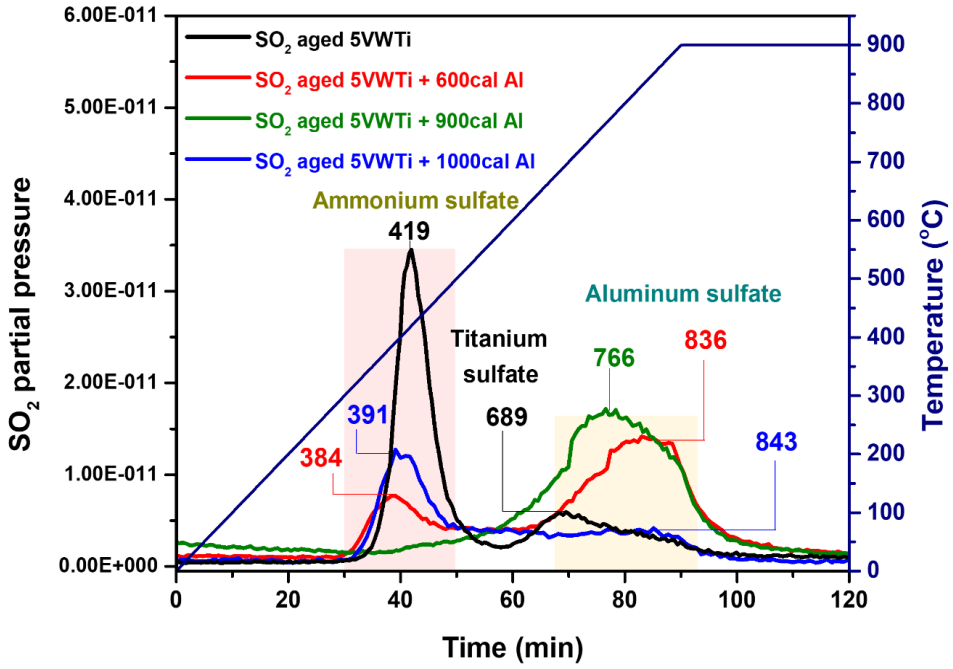

Fig. 2- 8. TPD-MS analyses of the SO_2 aged 5VWTi and the SO_2 aged alumina mixture catalysts (SO_2 aged under 30 ppm of a SO_2-containing flow at 220 ℃ for 22 h) under 100 mL/min of a N_2 flow at a heating rate of 10 ℃/min up to 900 ℃.

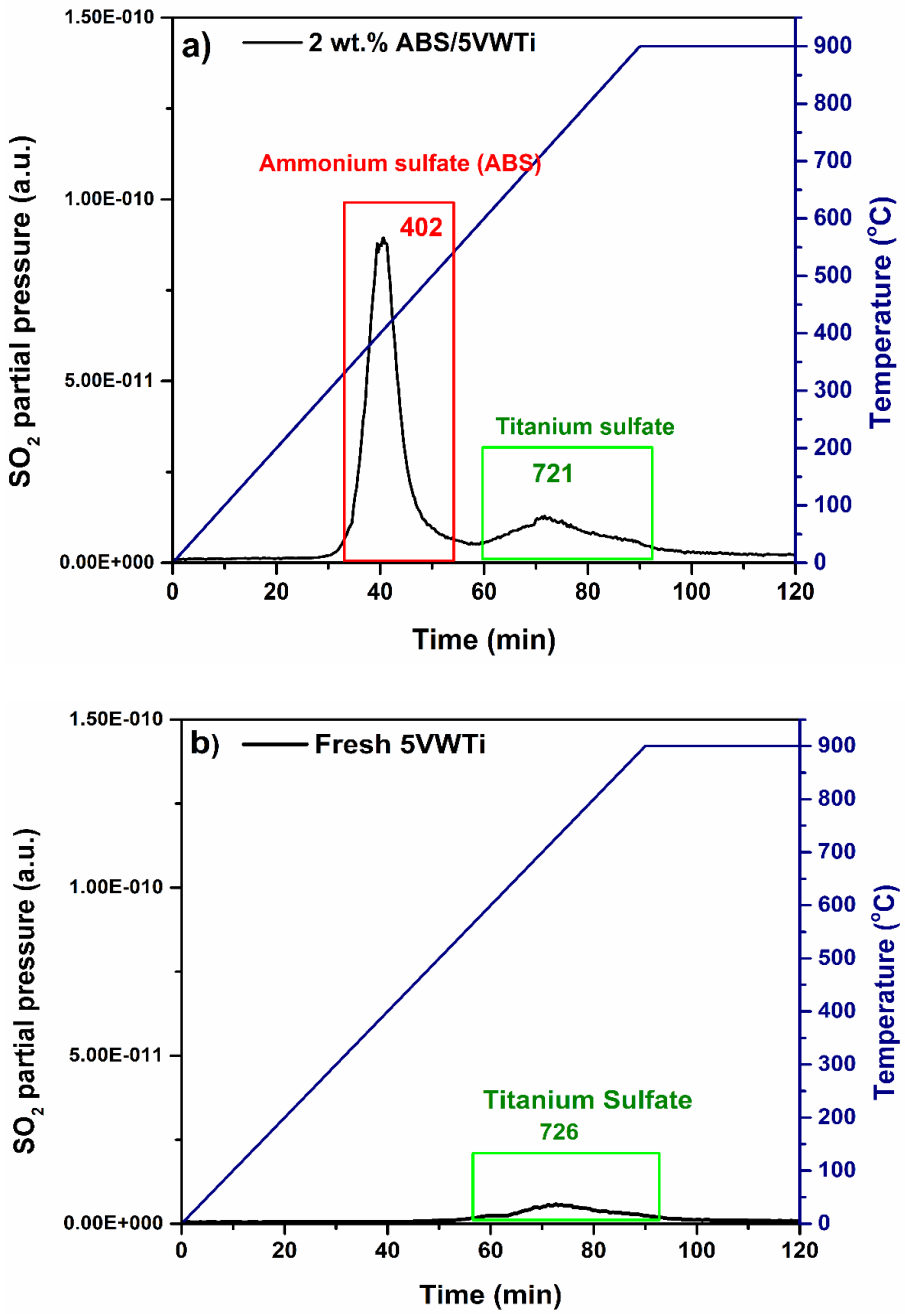

Fig. 2- 9. Temperature-programmed desorption-mass spectroscopy (TPD-MS) analyses of (a) the 2 wt.% of ABS pre-impregnated 5VWTi and (b) the fresh 5VWTi catalysts under 100 mL/min of a N_2 flow at a heating rate of 10 ℃/min up to 900 ℃.

As the peak at the low temperature was observed in the mixed samples, the intensity of the peak at high temperature was relatively reduced simultaneously. The relatively decreased intensity of the peak at high temperature confirmed that some of the sulfur remained as ABS on vanadia rather than converted to aluminum sulfate. The residual ABS on the vanadia sites in 5VWTi + 600cal Al and 5VWTi + 1000cal Al catalysts was the major factor contributing to its high deactivation rate compared to other alumina mixture catalysts. From the characterization results, we found that in the presence of physically mixed alumina calcined at 900 °C, ammonium bisulfate was not observed on the vanadia sites of the catalyst and instead, sulfur tended to exist on the alumina sites. Hence, the 5VWTi + 900cal Al catalyst exhibited higher activity without significant deactivation, thus revealing highly enhanced SO_2 resistance compared to the traditional 5VWTi.

In addition, Table 2-1 presents the residual sulfur contents of SO_2 aged catalysts obtained from elemental analysis. According to these elemental analyses, 0.5 wt.% of sulfur remained in the SO_2 aged 5VWTi while 0.4 wt.% of residual sulfur remained in the SO_2 aged 5VWTi + calcined Al samples. The similar amount of residual sulfur in every catalyst implied that the physically mixed alumina catalysts likely did not deter the formation of ABS nor decompose it. Instead, it trapped sulfate at the alumina sites. As a result, trapping sulfate on the alumina sites could protect the vanadia active sites in the alumina mixed catalyst by preventing the

formation of ABS on the vanadia sites, resulting in superior catalytic stability.

(Unit: wt.%)

Catalyst	N	C	H	S
5VWTi	0.3	0.1	0.3	0.5
5VWTi + 600cal Al	0.3	0.1	0.4	0.5
5VWTi + 900cal Al	0.3	0.1	0.3	0.4
5VWTi + 1000cal Al	0.3	0.1	0.3	0.5

Table 2- 1. Elemental analysis on 5VWTi + Al mixture catalysts after SO_2 aging under 30 ppm of a SO_2-containing flow at 220 ℃ for 22 h.

2.3.3. ABS migration through physical contact between vanadia and alumina

In the presence of alumina, especially alumina calcined at 900 °C, we found that sulfur species existed on the alumina sites rather than on the vanadia sites. Hence, we proposed two possibilities for the enhanced SO_2 resistance of the alumina mixture catalyst. The first hypothesis states that sulfur oxide was trapped in the alumina sites in the gas phase. Another hypothesis is that the adsorbed ABS on vanadia sites migrated from the vanadia sites to the alumina sites through physical contact between 5VWTi and alumina. Given the better sulfur resistance, we selected alumina calcined at 900 ℃ to investigate the physical mixing system in this study.

To validate the first hypothesis of direct SO_2 trapping on alumina sites, a loosely contacted catalyst was prepared, assuming that no close physical contact existed in the catalyst. The 5VWTi catalyst and alumina were individually sieved through 45-60 mesh, and these two were mixed in a 2:1 mass ratio in a 10 mL vial by handshaking for a few minutes. Such loosely contacted sample was denoted as 5VWTi + 900cal Al-L. To justify the adsorption of gas-phase sulfur oxide, the NO_x conversion profiles of the traditional 5VWTi, the physically mixed catalyst, and the loosely contacted alumina catalyst are compared in Fig. 2-10.

In the case of the 5VWTi sample, the NO_x conversion decreased from 55% to 38%. The NO_x conversion of the loosely contacted 5VWTi + 900cal Al-L deteriorated until it reached approximately 34%, showing a

slightly increased deactivation rate compared to the conventional 5VWTi catalyst. The results revealed that in the absence of close physical contact between vanadia and alumina, the mixture catalyst demonstrated a similar SO_2 resistance to fresh 5VWTi, implying that separate alumina did not participate in improving its sulfur stability at all. For the physically mixed 5VWTi + 900cal Al catalyst, NO_x conversion decreased by only approximately 5%, which indicated that the close contact between vanadia and alumina was essential for alumina to protect 5VWTi from sulfur poisoning and SO_2 was not directly trapped on the alumina sites in the gas phase.

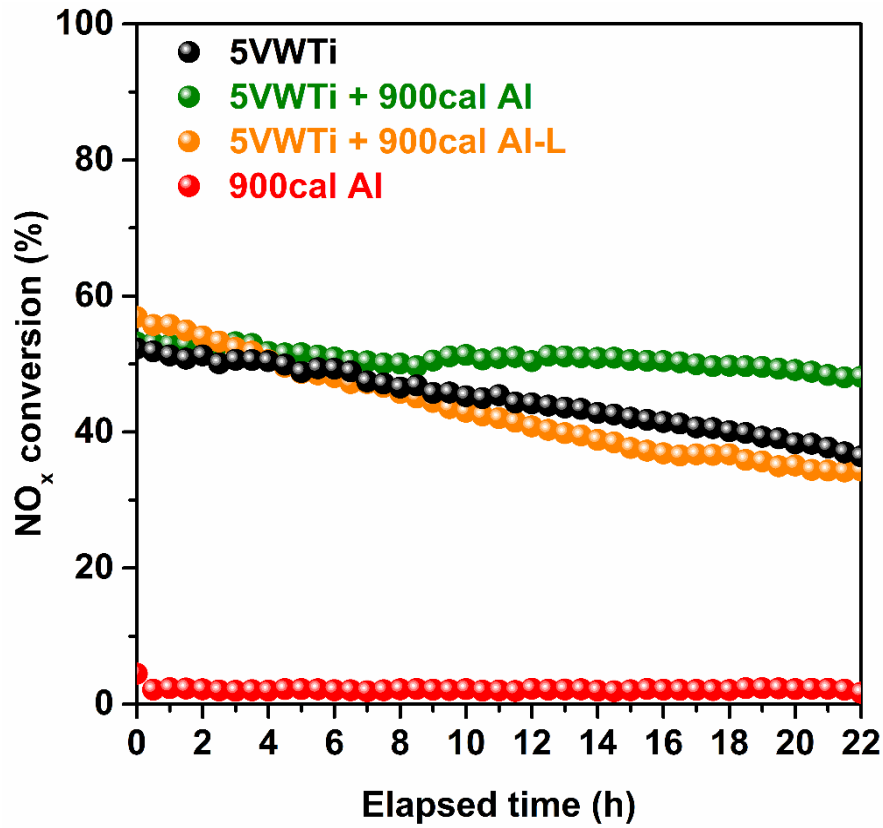

Fig. 2- 10. Comparison of the NO_x conversion of physically contacted 5VWTi + 900cal Al and loosely contacted 5VWTi + 900cal Al (5VWTi + 900cal Al-L) catalysts during SO_2 aging at 220 ℃ for 22 h.

These results were consistent with the Cs-TEM and line EDS results shown in Fig. 2-11. Fig. 2-7(c) showed that the physically mixed 5VWTi + 900cal Al was well mixed. Further, when the EDS line scans crossed the vanadia and alumina sites, the intensity peak of S overlapped that of Al rather than that of Ti as shown in Fig. 2-7(d). In the case of the loosely contacted catalyst, the separation between the alumina and vanadia sites was clearly shown in Fig. 2-11(a), indicating that no physical contact existed in the catalyst, as we designed. Unlike the physically mixed catalyst, the EDS result of S shown in Fig. 2-11(b) overlapped with that of Ti rather than Al, which demonstrated that S remained on vanadia sites more abundantly for the loosely contacted alumina mixture catalyst. These results implied that sulfur oxide was likely to be deposited on vanadia sites such as the VWTi catalyst in the absence of close contact between vanadia and alumina. Instead, it exhibited negligible sulfur absorbing ability and only plays an insignificant role in enhancing SO_2 stability in the absence of close contact with vanadia.

The reason for the poor sulfur absorbing ability of alumina was that SO_2 cannot be oxidized on alumina sites [47]. To form ABS, SO_2 must first be oxidized to SO_3 first, which subsequently reacts with NH_3, resulting in ABS formation, as described in the Introduction. Because SO_2 cannot be oxidized to SO_3 on alumina, ABS cannot be formed and trapped as ABS on alumina. However, when there was close contact with 5VWTi, SO_2 oxidation occurred on the vanadia sites and thus formed SO_3, which reacted

with NH_3 to form ABS on the vanadia sites. In other words, close contact played an essential role in forming ABS on the vanadia sites, which migrated and was then consequently trapped in the alumina sites. As shown in Fig. 2-12, the TPD result also reflected its poor sulfur absorbing ability when only Al_2O_3 was used. Only a negligible SO_2 peak was observed at a high temperature of 900 ℃, which originated from the decomposition of aluminum sulfate. The figure also demonstrated that alumina alone did not exhibit a notable SO_2 absorbing ability because the adsorption of SO_2 in the gas phase barely occurred as well.

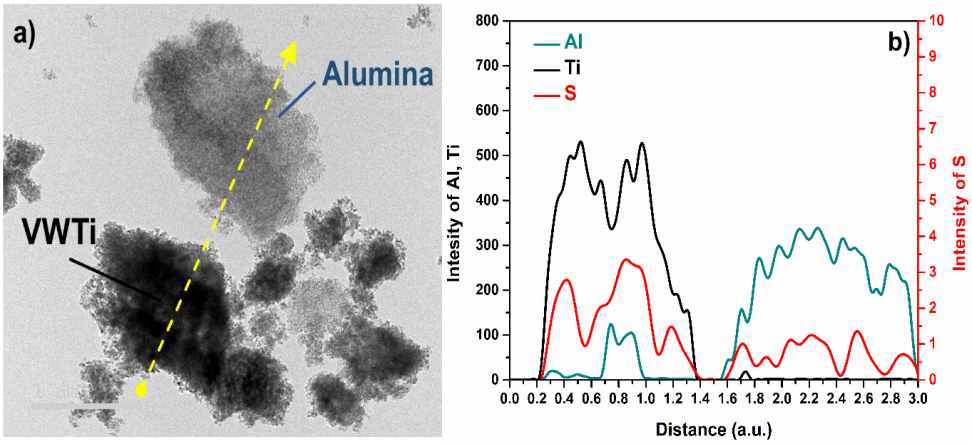

Fig. 2- 11. (a) Cs-TEM image and (b) line-EDS scans of loosely contacted 5VWTi + 900cal Al-L catalyst after sulfur aging at 220 ℃ for 22 h.

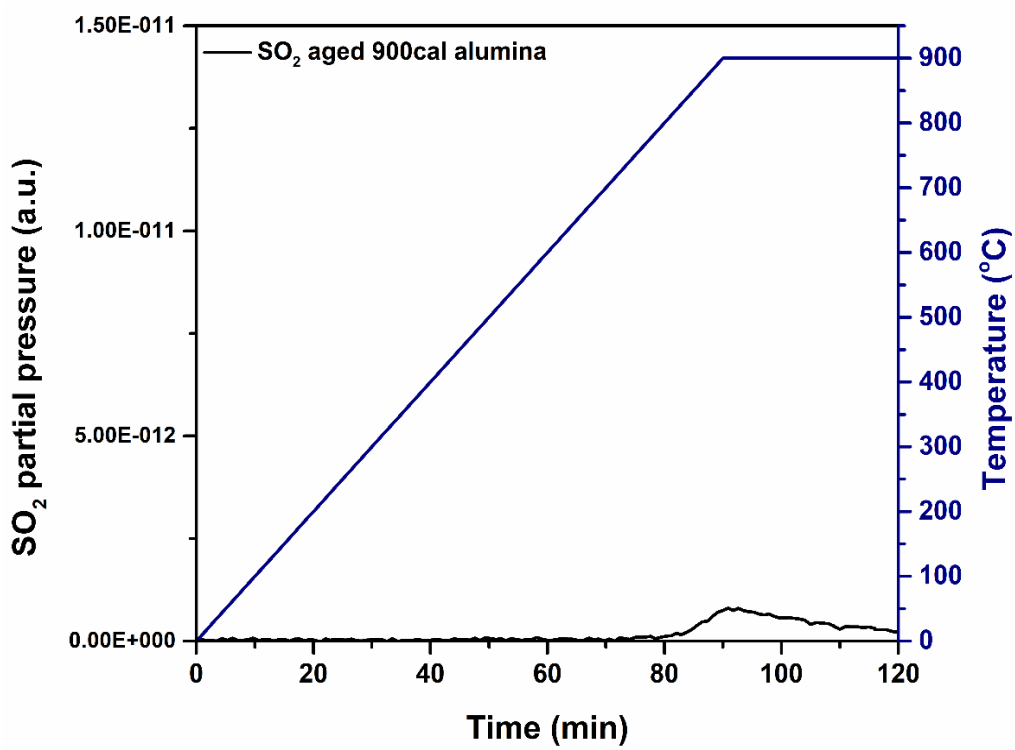

Fig. 2- 12. TPD-MS analysis of the SO_2 aged 900cal alumina (30 ppm of SO_2-containing flow at 220 ℃ for 22 h) under 100 mL/min of a N_2 flow at a heating rate of 10 ℃/min up to 900 ℃.

To test the second hypothesis about the migration of sulfur through the physical contact between vanadia and alumina, we synthesized the mixture catalysts via two different methods. Firstly, the 2 wt.% ABS was pre-impregnated onto vanadia supported on tungsten titania and this sample was denoted as 2 wt.% ABS/5VWTi. Then, 2 wt.% ABS/5VWTi was mechanically mixed with alumina in a mortar in a 2:1 mass ratio, denoted as 2 wt.% ABS/5VWTi + 900cal Al. Secondly, loosely contacted 2 wt.% ABS/5VWTi and alumina was prepared after individual sieving and mixing in a 10 mL vial via simple handshaking. The catalyst was labeled as 2 wt.% ABS/5VWTi + 900cal Al-L assuming no physical contact between vanadia and alumina. The SCR performances of the catalysts were obtained during slow temperature ramping at a heating rate of 1 ℃/min from 100 ℃ to 220 ℃, as shown in Fig. 2-13, to justify the second hypothesis on the migration of the adsorbed deactivation material, ABS, from the vanadia to the alumina sites. The mechanically mixed catalyst achieved a maximum NO_x conversion of approximately 63%, while that of the loosely contacted sample reached 46%.

Although the same amount of ABS was impregnated onto 5VWTi, the mechanically mixed 5VWTi + 900cal Al mixture catalyst exhibited higher NO_x conversion than the loosely contacted 5VWTi + 900cal Al mixture catalyst, whose SCR performance was almost the same as that of the fresh 5VWTi catalyst. Considering that the deactivation occurred in the presence of ABS on 5VWTi, it can be inferred that there was less ABS on

the 5VWTi of the physically mixed catalyst than on the loosely contacted catalyst, which implied that some of the pre-impregnated ABS migrated to the alumina sites during the slow ramping in the low-temperature range. Based on these results, we propose that the pre-impregnated ABS on 5VWTi migrated from vanadia sites to alumina sites by physical contact arising from the physical mixing in the 5VWTi + 900cal Al, resulting in a higher catalytic activity than in the 5VWTi + 900cal Al-L. It can be summarized that the physical contact between vanadia and alumina in the physically mixed 5VWTi + 900cal Al causes ABS to migrate to alumina sites, resulting in a high SO_2 resistance, as shown in Fig. 2-14.

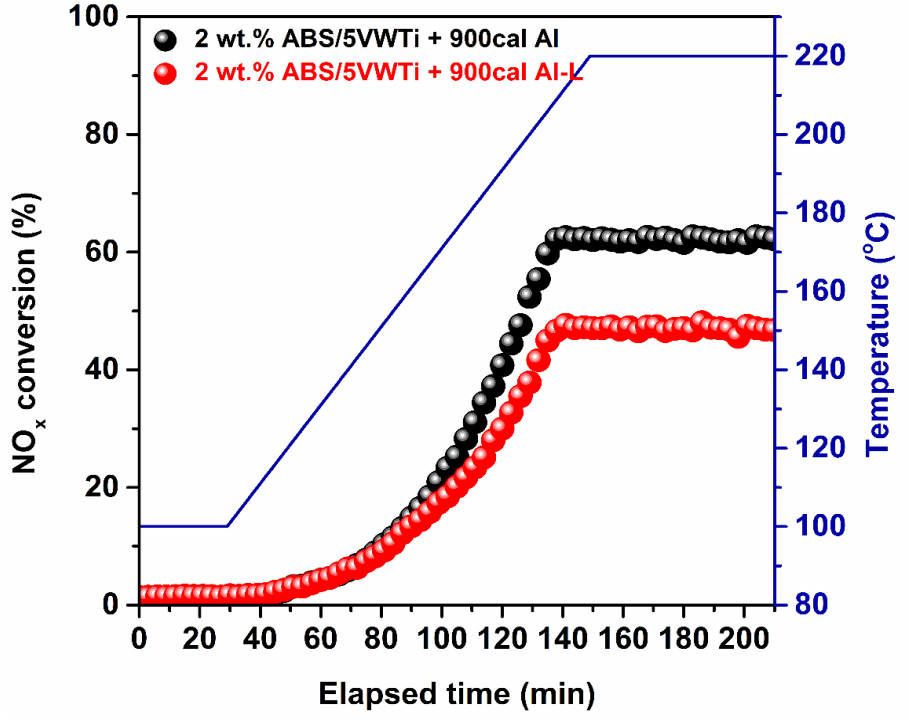

Fig. 2- 13. NO_x conversion profiles of ABS pre-impregnated 5VWTi + 900cal Al and 5VWTi + 900cal Al-L catalysts at a heating rate of 1 ℃/min from 100 ℃ to 220 ℃ .

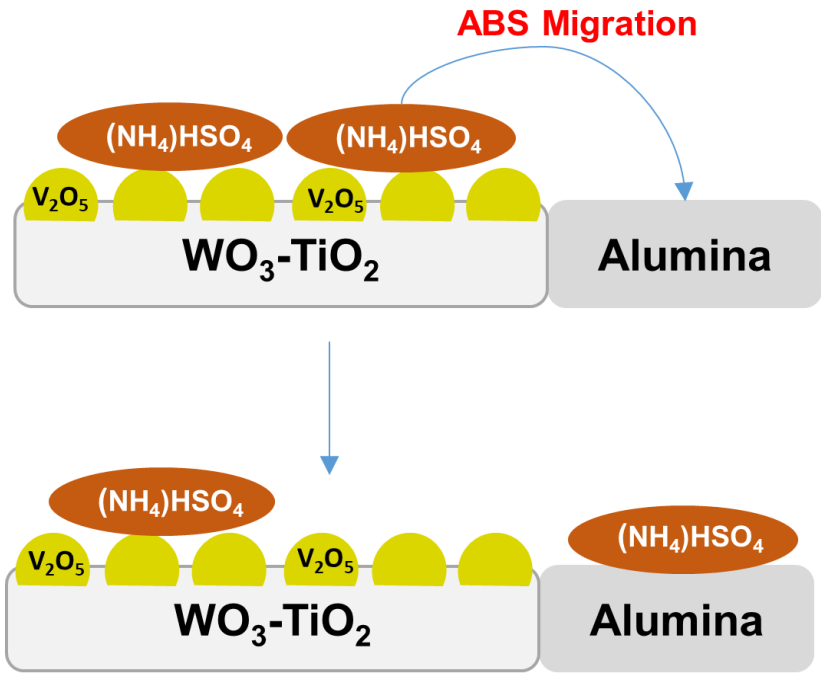

Fig. 2- 14. Schematic of ABS migration through physical contact in 5VWTi + Al catalyst.

2.3.4. Sulfur resistance depending on the calcination temperature of physically mixed alumina

In this study, we observed that, in the presence of physically mixed alumina, the deposited ABS on vanadia migrated to the alumina sites, suppressing the deactivation by SO_2 poisoning. Based on the results, it was found that ABS migration to the alumina sites proceeded in every alumina mixture catalyst through physical contact between the two materials. However, the ABS absorbing ability of each alumina mixture catalyst differed depending on the calcination temperature, which yielded different sulfur resistances.

To assess the ABS absorbing ability of each alumina mixture catalyst, herein, we prepared 5VWTi pre-impregnated with 2 wt.% of liquid-phase ABS before the mechanical mixing with alumina, which was designated as 2 wt.% ABS/5VWTi. Then, it was physically mixed with alumina, which was denoted as 2 wt.% ABS/5VWTi + (x)cal Al. The activities under the SCR reaction conditions were collected by increasing the temperature from 100 ℃ to 220 ℃, as shown in Fig. 2-15. The reaction results of the alumina mixture catalysts were in accordance with TPD-MS results. It was confirmed that the degree of ABS absorbing ability differed depending on the calcination temperature of the physically mixed alumina.

The properties of calcined alumina resulted in varied ABS absorbing abilities. Fig. 2-16(a) depicted the NH_3-TPD profiles of the calcined alumina, where two significant peaks were observed.

Corresponding to the NH_3 profiles, 900cal alumina showed a larger peak at high temperatures, which was indicative of desorbing ammonia from strong acid sites. On the other hand, desorption of weakly adsorbed ammonia at low temperatures was dominant in other alumina samples calcined at different temperatures. Such difference in acidity might correlate with the interaction with ABS. According to our previous study [39], a catalyst with a large number of stronger acid sites demonstrated a stronger interaction with migrating ABS from vanadia sites, leading to a stronger ABS absorbing ability. The increase in pore size with increasing calcination temperature might also attribute to absorbing ABS ability, as shown in Fig. 2-16(b) and Table 2-2. In the present study, the physically mixed catalyst with alumina, which had a larger pore size, deactivated less severely. As confirmed in a previous study [39], the larger pore size of alumina would accelerate the rate of ABS migration, restraining ABS to accumulate on the vanadia active sites. The suggested principle could be also applied to the present system. Although the pore size of alumina calcined at 1000 ℃ slightly increased, it could be inferred that less amount of strong acid site in alumina calcined at 1000 ℃ affected ABS absorbing ability more dominantly, inducing a larger deactivation rate. On the other hand, note that the crystallinity of calcined alumina did not play a key role in varying the ABS absorbing ability, as shown in Fig. 2-16(c).

Although slight differences in phases, such as appearance of delta and theta phases, were observed as the calcination temperature increased,

the gamma phase was dominant in the overall alumina [48, 49]. In addition, the chemical structure of the calcined alumina did not affect the ABS absorbing ability. According to the solid-state ^{27}Al NMR results, two broad asymmetric components at approximately 65 and 10 ppm were observed, which were associated with Al in tetrahedral and octahedral coordination, respectively [50]. Only an insignificant difference was observed in the Al coordination of the alumina samples calcined at different temperatures, as displayed in Figure Fig. 2-16(d). Based on these characterizations of calcined alumina, both the crystallinity and chemical structure of the calcined alumina did not contribute to the varied ABS absorbing ability as well as activity. In the present system, the affinity of the mixed alumina to ABS was determined by its acidity and pore size. In addition, the interaction of ABS formed on vanadia and alumina induced different ABS absorbing abilities of physically mixed 5VWTi and calcined alumina.

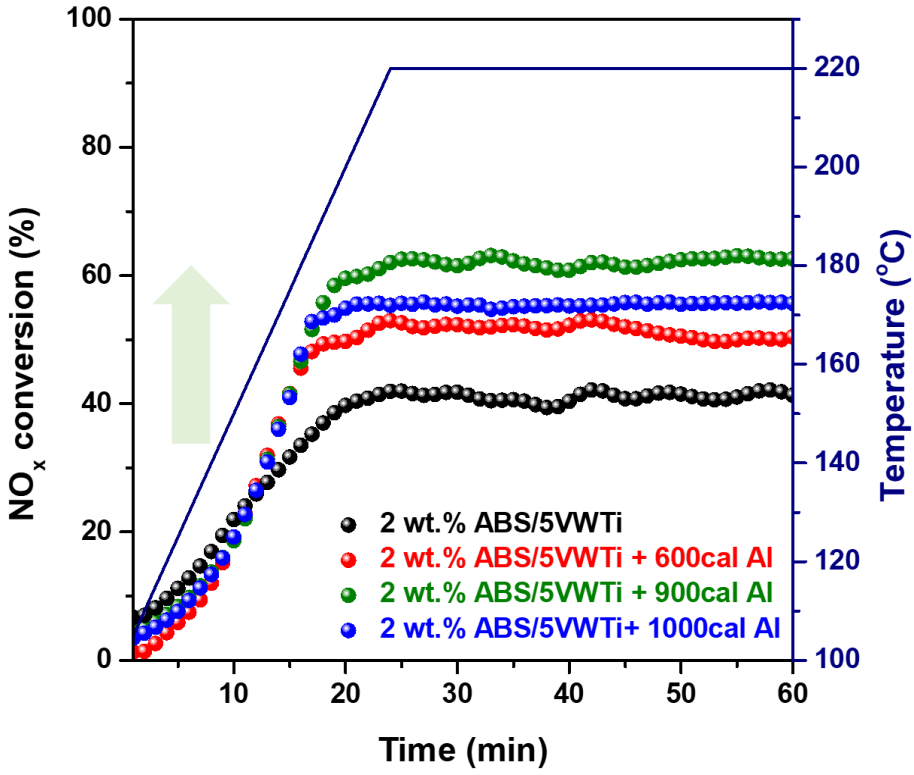

Fig. 2- 15. Catalytic activities of the 2 wt.% ABS/5VWTi and 2 wt.% ABS/5VWTi + calcined alumina catalysts from 100 ℃ to 220 ℃ at a ramping rate of 5 ℃/min.

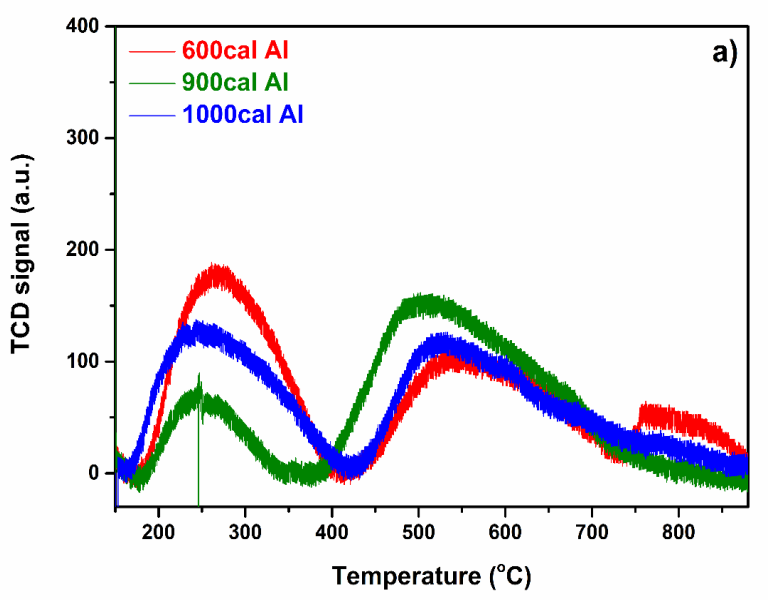
a)
600cal Al
900cal Al
1000cal Al
TCD signal (a.u.)
Temperature (°C)
400
300
200
100
0
200
300
400
500
600
700
800

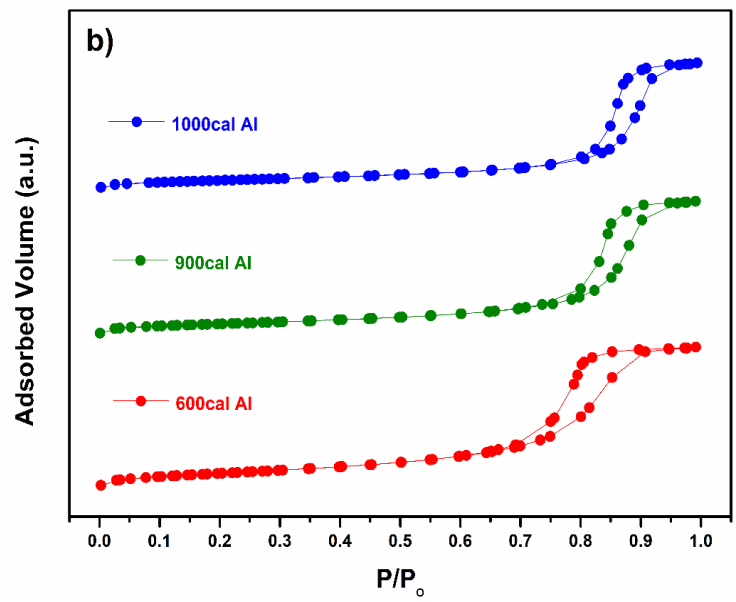
b)
1000cal Al
900cal Al
600cal Al
Adsorbed Volume (a.u.)
P/P$_o$
0.0
0.1
0.2
0.3
0.4
0.5
0.6
0.7
0.8
0.9
1.0

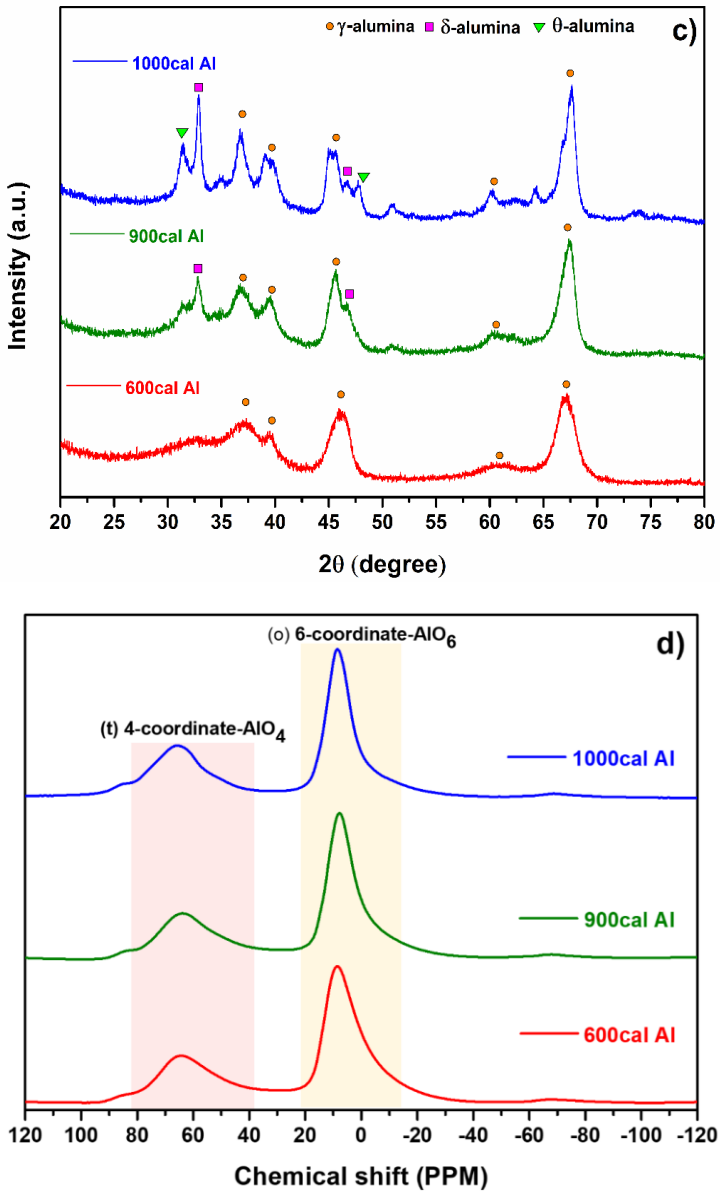

Fig. 2- 16. (a) NH_3 temperature-programmed desorption (NH_3-TPD) profiles, (b) N_2 adsorption-desorption isotherms, (c) X-ray diffraction (XRD), and (d) ^{27}Al solid-state nuclear magnetic resonance (NMR) spectra of the calcined alumina.

	600cal Al	**900cal Al**	**1000cal Al**
Surface area (m^2/g)	173	113	98
Pore volume (cm^3/g)	39.8	25.9	22.5
Pore diameter (nm)	12.0	17.0	18.0

Table 2- 2. Surface areas and pore size distributions of the alumina calcined at different temperatures, 600 ℃, 900 ℃, and 1000 ℃.

2.3.5. Regeneration test of the alumina mixture catalyst

Stability and resuability are two important factors for evaluating catalysts for industrial applications. The SO_2 aging test was performed, followed by thermal treatment at 350 ℃ for 2 h as a regeneration step to test whether the catalytic activity could be recovered after exposure to SO_2 and whether the sulfur resistance was maintained during repetitive operations. The procedure was repeated three times, as shown in Fig. 2-17(a). During the first SO_2 aging test, the NO_x conversion of the traditional 5VWTi catalyst decreased by 20%, while that of 5VWTi + 900cal Al deteriorated by only 10%. After the first regeneration process at 350 ℃ for 2 h, both 5VWTi and 5VWTi + 900cal Al catalysts recovered their initial NO_x conversions obtained before the first SO_2 aging test, which showed the complete regeneration of the catalysts resulting from thermal treatment at 350 ℃. The initial NO_x conversions after each SO_2 aging test are plotted as red dots, and the deactivation rates are shown as a black bar for 5VWTi and green bars for the alumina mixture catalyst in Fig. 2-17 (b).

After the first SO_2 aging and regeneration step, the second SO_2 aging test was performed. During the second exposure to SO_2, the NO_x conversion of 5VWTi deteriorated by approximately 20% and the NO_x conversion of 5VWTi + 900cal Al decreased from 63% to 53% with an increase in the deactivation rate. As listed in Table 2-3, approximately 1.1 wt.% of the sulfur content remained on the catalyst after the first SO_2 aging

and the first regeneration step. After the second exposure to SO_2 and the second regeneration step, the amount of residual S increased to 1.6 wt.%. We also found that the deactivation rate of the 5VWTi + 900cal Al catalyst did not increase further after the third SO_2 aging. No change in the deactivation rate indicated that the alumina mixture catalyst deactivated up to its limit.

We could assume that the residual sulfur attributed to the increased deactivation rate as sulfur aging repeated. In order to simulate the residual sulfur on alumina, 6 wt.% of ABS was pre-impregnated on 900cal alumina, which was a similar amount of residual S after the second regeneration step, as listed in Table 2-3. Then, the ABS pre-impregnated alumina was physically mixed with 5VWTi, which was denoted as 5VWTi + 6 wt.% ABS/Al, to check if ABS produced during the reaction can be migrated from vanadia to alumina already saturated with sulfur. As shown in Table 2-4, the 5VWTi + 6 wt.% ABS/Al catalyst achieved a similar deactivation rate with the measured rates during the second and third SO_2 aging tests in Fig. 2-18. The results implied that although ABS formed during the reaction and remained on alumina, the migration of ABS from vanadia sites to alumina sites still occurred to some extent, maintaining the sulfur tolerance of the physically mixed catalyst. From the experiment, we also found that the increased deactivation rate during repeated sulfur aging originated from residual sulfur on alumina. Some of the sulfur species could remain on the alumina sites and not undergo complete decomposition, even after the

thermal treatment. However, even when the alumina was saturated with sulfur, the phsycially mixed catalyst could maintain a high sulfur stability after repetitive SO_2 aging, so that it could be utilized multiple times, as shown in Fig. 2-17.

The deactivation rate of the alumina mixture catalyst increased slightly after repetitive SO_2 aging due to residual sulfur, while the zeolite mixture catalyst introduced in our previous study was fully regenerated without increasing deactivation [39]. However, the alumina mixture catalyst still obtained lower deactivation rates than that of 5VWTi (0.015) after every SO_2 aging test, and the initial conversion was fully recovered after every regeneration step, similar to what was observed for the zeolite mixture catalyst. The results showed that the ABS absorbing ability and SO_2 resistance of the 5VWTi + 900cal Al catalyst degraded more drastically than the 5VWTi + zeolite catalyst in our previous study, but the alumina mixture catalyst could be regenerated and reused to some extent even after repetitive SO_2 exposure [39].

Furthermore, the regenerability and reusability from ABS poisoning were noticeable compared to catalysts with other metal oxides such as CeO_2 promoters, whose catalytic activities were high, but their abilities to regenerate were poor [51, 52]. V_2O_5-CeO_2/TiO_2 was not likely to be regenerated from blockages by ABS. For example, according to Chang et al. [52], the CeO_2 catalyst was easily deactivated by SO_2 poisoning and its catalytic activity was not recovered, even after regeneration. On the other

hand, the alumina mixture catalyst in the present system recovered its initial conversion every time and, moreover, it was deactivated less significantly than the conventional vanadium-based catalyst. Overall, the high sulfur resistance and reusability of 5VWTi were maintained by simple physical mixing with alumina, and the 5VWTi + 900cal Al catalyst would be also advantageous for large-scale utilization because of its affordable price compared to the zeolite mixture catalyst.

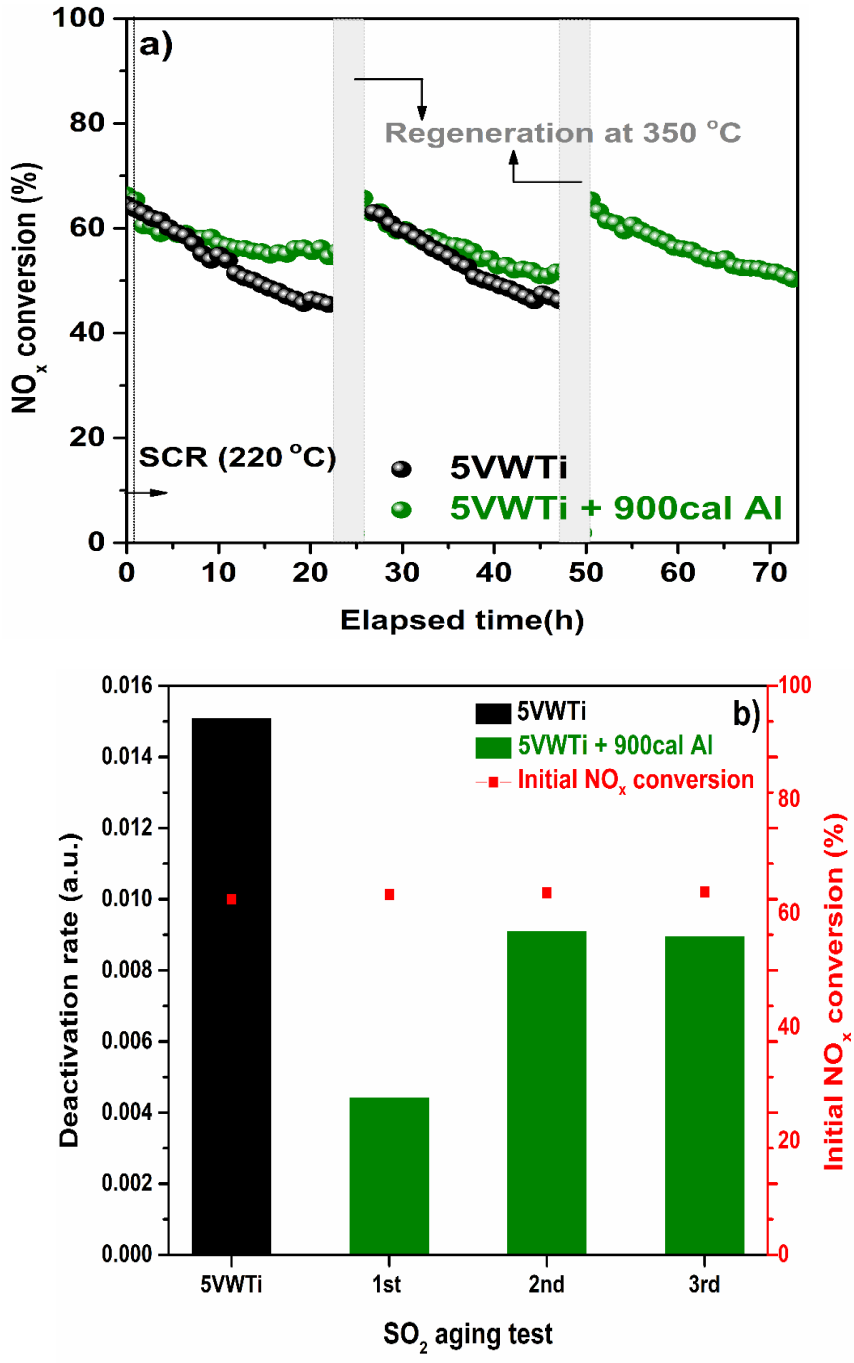

Fig. 2- 17. (a) Regeneration tests and (b) deactivation rates of the 5VWTi and 5VWTi + 900cal Al catalysts after three cycles of SO_2 aging and following thermal treatement.

(Unit: wt.%)

Catalyst	N	C	H	S
5VWTi + 900cal Al after 1st regeneration	n.d.	0.4	0.3	1.1
5VWTi + 900cal Al after 2nd regeneration	n.d.	0.0	0.3	1.6

Table 2- 3. Elemental analysis on 5VWTi + 900cal catalyst Al after each regeneration step at 350 ℃ for 2 h.

Catalyst	Deactivation rate
5VWTi	0.0150
5VWTi + 900cal Al after 1st regeneration	0.0044
5VWTi + 900cal Al after 2nd regeneration	0.0091
5VWTi + 900cal Al after 3rd regeneration	0.0090
5VWTi + 6 wt.% ABS/900cal Al	0.0090

Table 2- 4. Deactivation rates of 5VWTi + 900cal Al catalyst after each regeneration step at 350 ℃ for 2 h and 5VWTi + 6 wt.% ABS/Al after SO_2 aging, respectively.

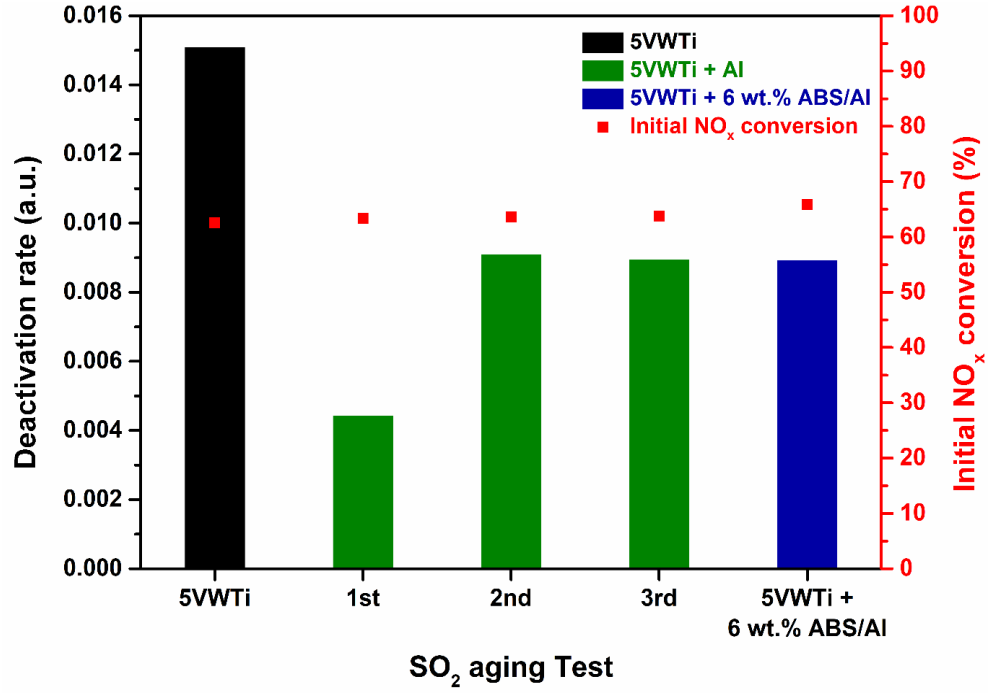

Fig. 2- 18. Deactivation rates of the 5VWTi, and 5VWTi + 6wt.% ABS/Al catalysts (6 wt.% of ABS pre-impregnated on 900cal Al) in comparison with deactivation rate of 5VWTi + Al catalyst after repeated SO_2 aging tests.

Chapter 3. Tailoring the Mechanochemical Interaction Between Vanadium Oxides and Zeolite for Sulfur-Resistant $DeNO_x$ Catalysts

3.1. Introduction

Mechanochemical methods, such as grinding two solids using a mortar or ball mill, have created new prospects in the fields of chemical synthesis and catalysis [53-57]. Further, these methods are attracting attention as sustainable synthetic techniques because they are more environmentally friendly than conventional solution-based chemistry. The profound effects of these facile methods increase the necessity for understanding and utilizing various type of mechanochemical interactions in detail [58-62]. This newly emerging synthetic technique could help ease the ongoing energy and environmental crisis [37, 63-69]. Our group recently reported that the mechanical mixing of Y-zeolite with a typical vanadium-based SCR catalyst (V_2O_5-WO_3/TiO_2 *aka* VWTi) is very effective in mitigating this low-temperature deactivation by SO_2 [37, 70, 71]. Crucially, the physical contact between the two materials enables the trapping of the deactivating substance (ABS) in the zeolite pores, thereby preventing the deactivation of the active vanadium catalyst. Further, we found that the ABS trapping ability of zeolite is proportional to its Al content [39].

Unfortunately, Al-rich zeolites ($Si:Al_2 < 6$) are difficult to use as ABS trapping materials because the activity of the vanadium catalyst is degraded after mixing with Al-rich zeolites. The observed degradation

caused by mechanical grinding is very unusual, and, to date, no studies have reported this type of interaction. Therefore, in this study, we investigated the origin of the mysterious catalyst deactivation resulting from mechanical grinding by comparing USY-zeolites having $Si:Al_2$ ratios of 6 and 12. Kinetic analysis and the results of characterization revealed that extra-framework Al species that are abundant in Al-rich Y-zeolite are responsible for the mechanochemically induced deactivation. Furthermore, we discovered that this deactivation can be effectively mitigated by introducing a thin carbon layer on the zeolite surface, which is thought to inhibit the migration of extra-framework Al species to catalytic active sites.

3.2. Experimental

3.2.1. Catalyst preparation

The V_2O_5/WO_3-TiO_2 catalyst containing 5 wt.% V_2O_5 (VWTi) was prepared by a conventional wet impregnation method. The resulting powder was calcined in an electronic furnace at 500 °C for 4 h. The VWTi + Y-zeolite hybrid catalyst was prepared by mixing the VWTi catalyst and hydrogen-form Y-zeolite FAU structure, $Si:Al_2$ = 5.1 or 12, Alfa Aesar) by grinding in a porcelain mortar under ambient conditions for 10 min. The ratios of VWTi to Y-zeolite were 2:1 in mass ratio. VWTi+Y-5.1 -without grinding was prepared by gentle handshaking of two materials in a vial. To prepare the Al-VWTi catalyst, the requisite quantity of $Al(NO_3)_3 \cdot 9H_2O$ was dissolved in distilled water and then deposited on the VWTi catalyst using the incipient wetness impregnation method.

Octadecyltrichlorosilane-coated Y-zeolite (OTSY) was carried out refer to the previously reported method [72]. To prepare a hydrocarbon-modified-H-Y-zeolite composite, which was used as for comparison to OTSY-zeolite, starch powder was used [72]. The amounts of carbon in OTSY-5.1 zeolite (2.8 wt.%) and starch-Y-5.1 (2.2 wt.%) were comparable, as determined by elemental analysis.

3.2.2. Reaction condition

The catalytic activities of the various catalysts for NH_3-SCR reaction were measured in a 0.25-inch tubular quartz reactor. All catalysts were pelletized and sieved to 180–250 μm to prevent pressure drop and to ensure data reproducibility. The simulated reaction feed contained 500 ppm NO, 600 ppm NH_3, 10% O_2, 5% CO_2, 10% H_2O, and 30 or 100 ppm SO_2 (when it was used) balanced with N_2. To simulate ABS deactivation in the presence of SO_2 and H_2O, the catalysts were exposed for either 22 or 44 h under the above reaction conditions to 30 or 100 ppm SO_2 at 180 or 220 °C. Note that the catalyst deactivation on the formation of ABS formation increases as the concentration of SO_2 increases and the reaction temperature decreases. When regenerating catalysts by decomposing ABS species, the catalysts were heated at 350 °C for 2 h under 10% O_2, 5% CO_2, and 10% H_2O balance with N_2.

3.2.3. Characterizations

Solid-state magic angle spinning (MAS) NMR spectra were obtained on a Bruker Avance III HD (Bruker, Germany) under ambient conditions (25 °C). The spectra were measured at 130 MHz at a spinning rate of 20 kHz using a 2.5-mm MAS probe; the pulse length was 1 μs, and the delay time was 0.2 s. Infrared (IR) spectra were obtained in a diffuse reflectance cell (Praying Mantis, Harrick) using a Fourier-transform infrared (FTIR) spectrometer (IS-50, Thermo Fisher Scientific).

For temperature-programmed oxidation (TPO), mass spectrometry (HIDEN Analytical QGA) was used for outlet gas analyses by using a secondary electron multiplier (SEM) detector. The particle size distributions were analyzed using dynamic light scattering spectrophotometry (DLS-7000, Otsuka Electronics, Japan). H_2 temperature-programmed reduction (H_2-TPR) was performed using a chemisorption analyzer (BEL-CAT, BEL Japan Inc.). For this, the catalyst (approximately 0.03 g) was loaded onto quartz wool in a U-shaped quartz reactor and exposed to 5% H_2/Ar gas at a ramping rate of 10 °C/min. The hydrogen consumption was monitored with a thermal conductivity detector (TCD) stabilized for 1 h before starting measurement.

3.3. Results and discussions

3.3.1. Effect of mixing Al-rich zeolite with the VWTi catalyst

The mechanical mixing and grinding of the VWTi catalyst and Y-zeolite produced well-mixed catalysts, as shown in the HR-TEM images in Fig. 3-1. The two different particles, i.e., zeolite and TiO_2, are easily distinguishable in the images as a result of their different sizes; zeolite has a size of several hundreds of nanometers, whereas the TiO_2 particles are small, measuring several tens of nanometers. Fig. 3-2 shows the trend in the catalytic activity that is typical of the deactivation of the VWTi catalyst at low temperatures (220 °C) in the presence of ABS. The initial NO_x conversion was 65%, but this gradually decreased to approximately 40% after 22 h. When the VWTi was mixed with Y-zeolite having a $Si:Al_2$ ratio of approximately 12, the initial activity was similar, but the ABS deactivation proceeded much more slowly as a result of the ABS trapping ability of the zeolite particles in the mixture. Interestingly, the Al-rich Y-zeolite ($Si:Al_2$ of approximately 5.1) showed totally different behavior when mixed with the VWTi catalyst. Although the initial activity dropped significantly from 65% to 45%, this initial activity was retained for 22 h without any decrease in the NO_x conversion. The superior sulfur resistance of the hybrid catalyst is attributed to the fact that Al-rich zeolite can more efficiently absorb ABS from VWTi surface compared to common zeolite. As shown by Fig. 3-3, the sizes of the particles of the Y-5.1 and Y-12 zeolites

are almost identical, meaning that there is no difference in physically contacted area between zeolite and VWTi particles. Thus, the only difference is the abundant acidic sites in the Al-rich zeolite that promote the migration of ABS.

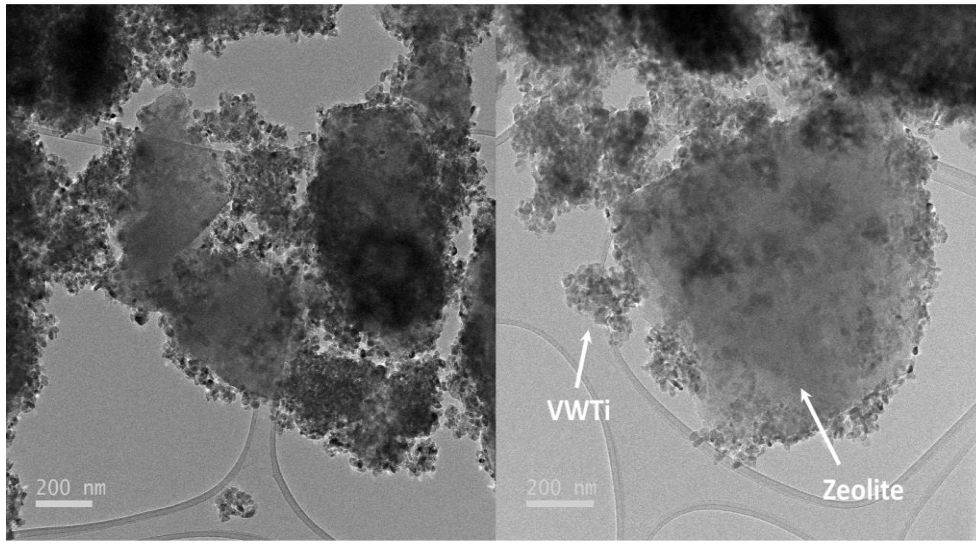

Fig. 3- 1. HR-TEM images of the mechanical mixture of VWTi catalyst and Y-zeolite. VWTi-to-Y-zeolite ratio was fixed to 2:1 with respect to mass.

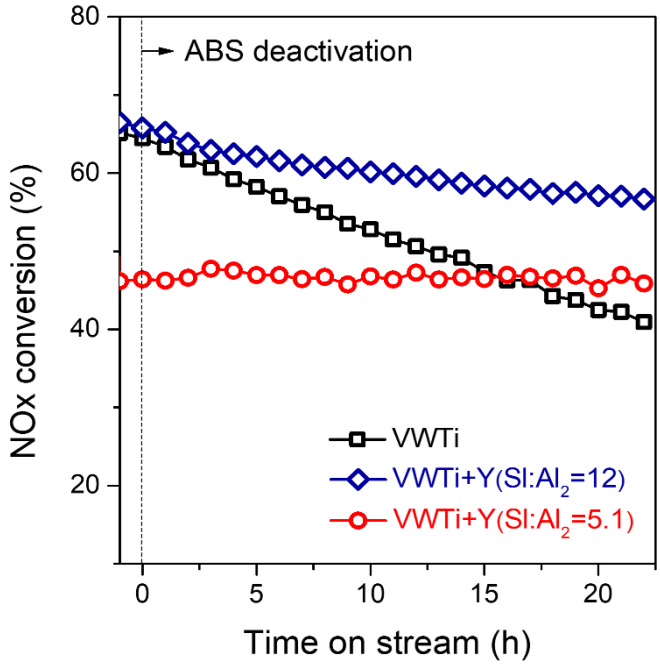

Fig. 3- 2. NH_3-SCR activities at 220 °C during simulated deactivation for 22 h via the formation of ABS in the VWTi + zeolite mixed catalysts.

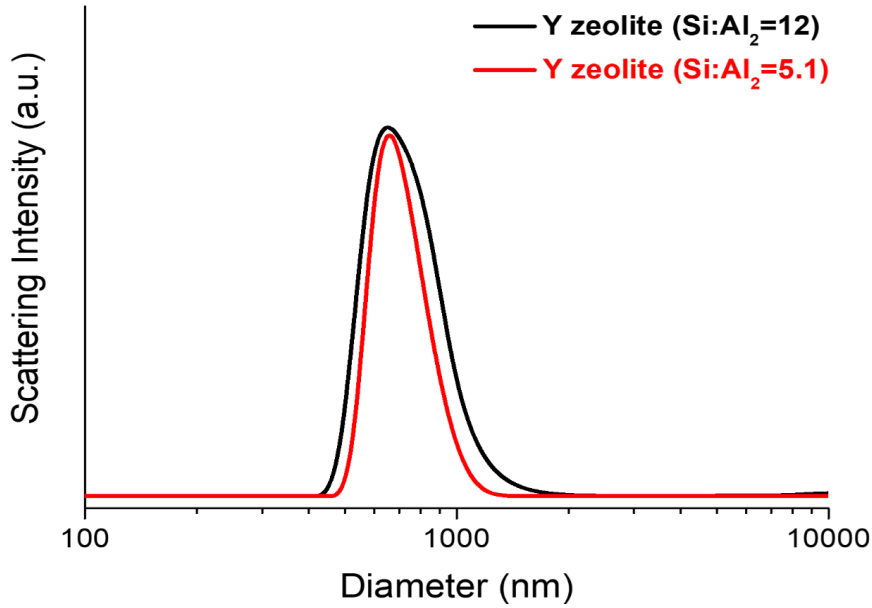

Fig. 3- 3. The size of the Y-zeolite with different Si:Al_2 ratio was analyzed using dynamic light scattering.

To identify the origin of the decrease in the initial activity of the VWTi + Y-5.1 catalyst, the steady-state activities of the catalysts were compared over a wide temperature range as shown in Fig. 3-4. Obviously, the mechanical mixing of Y-5.1 zeolite caused some degradation in the activity of the VWTi catalyst over the whole temperature range (150–250 °C), whereas the mixing of the Y-12 zeolite had little effect on the SCR performance. Furthermore, the VWTi-Y-zeolite mixing ratios were varied to determine whether the catalyst deactivation resulting from grinding was caused by the mixed Al-rich zeolite itself in Fig. 3-4(b). For the VWTi + Y-12 catalyst, the initial activity of the catalyst decreased slightly at a mass ratio of 64 to 1, but a certain degree of the initial catalytic activity was maintained, regardless of the VWTi-Y-zeolite mixing ratios. However, as more Y-zeolite-5.1 was added, the NO_x conversion gradually decreased, and the SO_2 resistance continuously increased.

Therefore, we asked ourselves, "why does the amount of Al-rich Y-zeolite mixed with VWTi have such a significant impact on the catalytic activity and ABS trapping ability at the same time?" The easiest answer is that both phenomena have the same cause. Thus, we deduce that the Al species in the zeolite, which provide sulfur resistance, are also the cause of the deterioration of the initial catalyst activity.

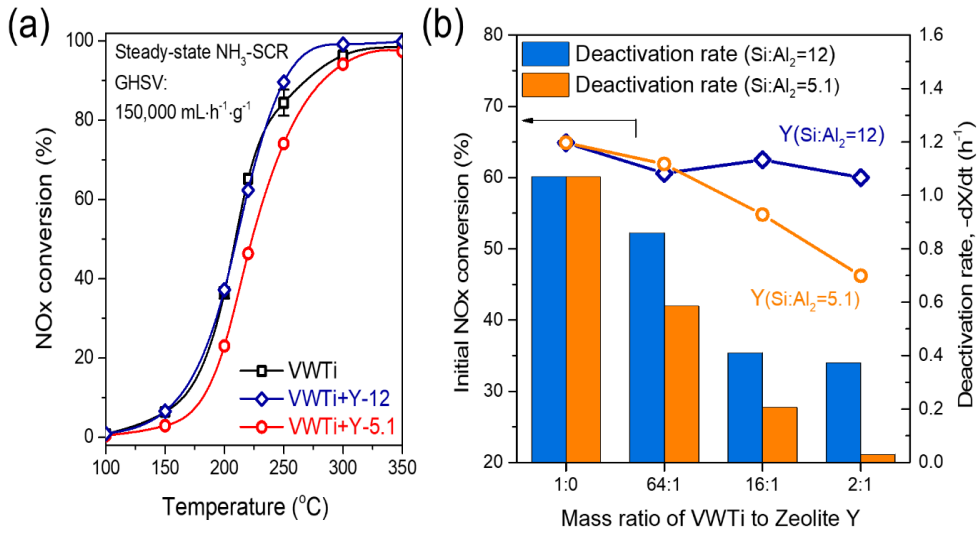

Fig. 3- 4. (a) Steady-state NO_x conversion as a function of temperature during the standard NH_3-SCR reaction. VWTi-to-Y-zeolite ratio was fixed to 2:1 with respect to mass. (b) Effect of the VWTi-to-Y-zeolite ratio ($Si:Al_2$ = 12, 5.1) on the initial catalytic activity and the deactivation rate.

3.3.2. Grinding induced Al redistribution in mechanical mixtures

To investigate the origin of the unusual catalytic deactivation after physical mixing, the physicochemical changes to the materials after grinding Al-rich Y-5.1 and VWTi were analyzed via various characterization methods. Even after 10 min of grinding, distinct changes were observed in the coordination environment of VWTi + Y-5.1 based on the ^{29}Si-, ^{27}Al-, and ^{51}V-solid-state NMR results in Fig. 3-5. The ^{29}Si-NMR spectra revealed a decrease in the intensity of the peak at -107 ppm, which corresponds to the tetrahedral coordinated framework of the Si-O groups [73], whereas the increase in the peaks at chemical shifts of -90 and -95 ppm can be attributed to Si-O groups surrounded by 3 or 2 Al in Fig. 3-5(a). At the same time, the ^{27}Al-NMR spectrum showed an increase in the peak corresponding to Al^{VI} in the extra-framework Al (0 ppm) and a slight decrease in the intensity of the Al^{V} peak corresponding to the extra-framework Al (EFAl) or a distorted tetrahedral peak (-30 ppm) [74], indicating a decrease in four-coordinated EFAl and an increase in six-coordinated EFAl species after grinding in Fig. 3-5(b) [75].

This change, which would seem counterintuitive, suggests that some of the EFAl species are converted back to framework Al species on grinding, even under ambient conditions. However, further investigation is required to confirm this phenomenon. Nevertheless, our results indicate that the application of mechanical force to the catalyst can induce the structural

rearrangement of framework-associated Al or the movement of EFAl species in the zeolite cage. These observations are consistent with the FT-IR results, which showed changes in the framework vibrations in Fig. 3-6. Specifically, the intensity of the Si-O-Si vibrations at 1179 cm^{-1} increased slightly, whereas the intensity of the Si-O-Al framework vibrations at 1048 cm^{-1} decreased slightly after grinding [76].

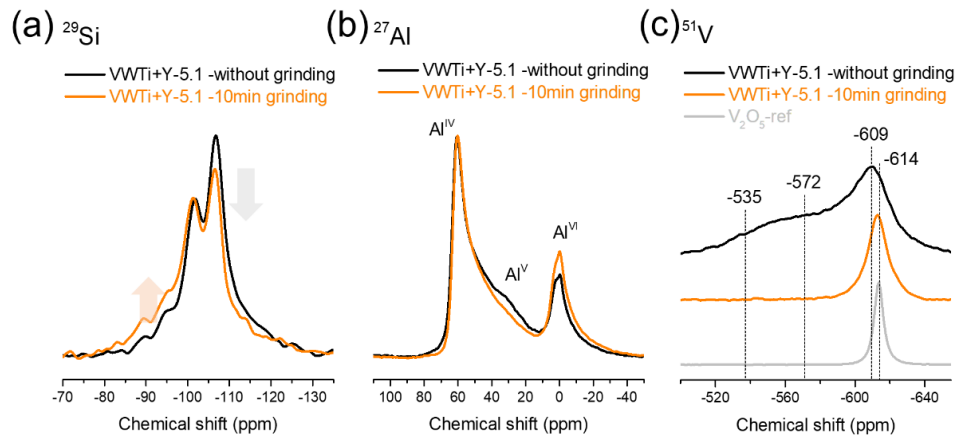

Fig. 3- 5. (a) Solid-state ^{29}Si, (b) ^{27}Al, and (c) ^{51}V NMR spectra of the mixed VWTi + Y-5.1 catalyst without grinding and after mechanical grinding.

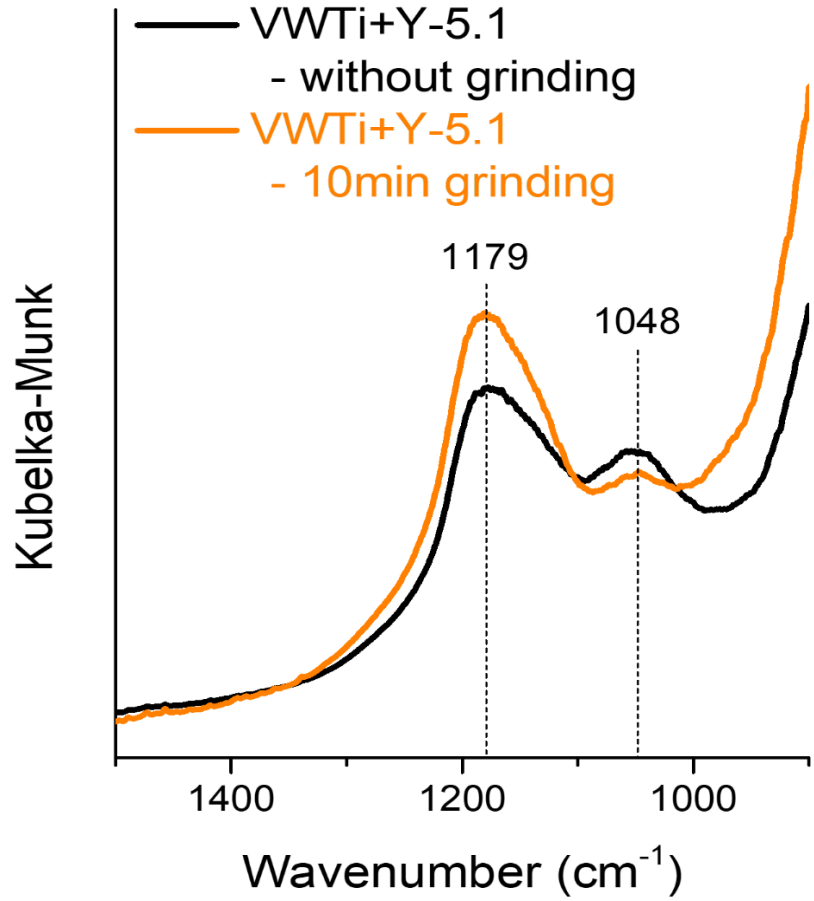

Fig. 3- 6. FTIR spectra of the mixed VWTi+Y-5.1 catalyst without grinding and after mechanical grinding.

Interestingly, mechanical grinding had a significant effect on the coordination environment of the vanadium species, as well as the Al species in Fig. 3-5(c). Specifically, the peaks of the highly dispersed isolated monomeric VO_x species (-535 and -572 ppm) on the TiO_2 surface almost disappeared after grinding, and only the peak at -614 ppm corresponding to oligomeric VO_x or nano-sized V_2O_5 remained after grinding [77]. The observation of the simultaneous decrease in the dispersed VO_x species and the change in the Al species in the zeolite structure strongly suggests that mechanical grinding induces interactions between V and Al species, possibly because of the diffusion of mobile Al species to isolated VO_x species on the TiO_2 surface. Additionally, the amount of NH_3 desorption at low temperatures decreased after grinding, whereas the number of acid sites at high temperatures increased, as shown in the NH_3 profiles in Fig. 3-7.

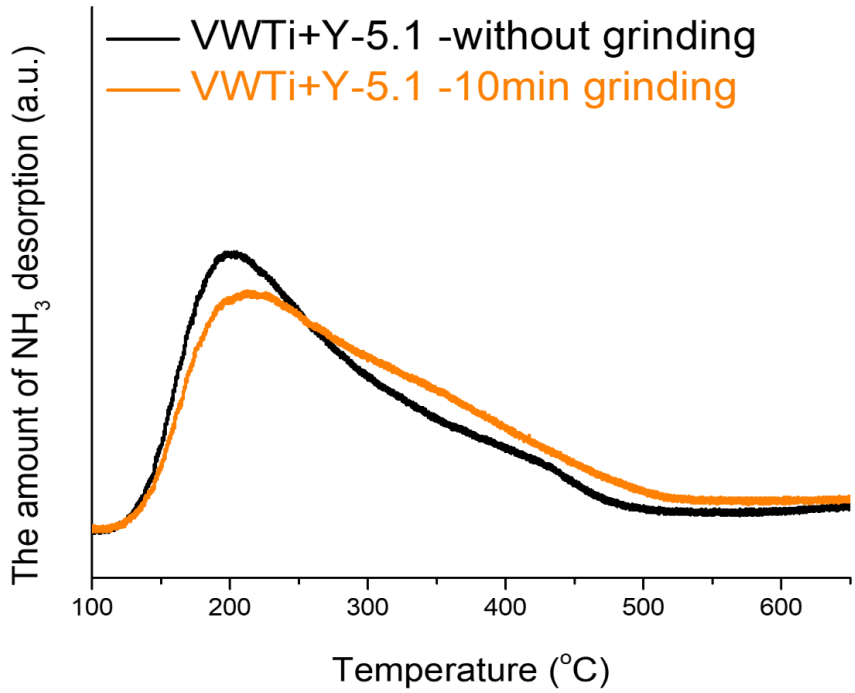

Fig. 3- 7. NH_3-TPD results over the Y-zeolite without grinding and after mechanical grinding.

TEM-EDS analysis showed that a portion of the VWTi particles contains a significant amount of Al after mechanical mixing in Fig. 3-8. These observations suggest the possibility of EFAl migration and subsequent interactions with the isolated V sites as a result of the grinding process. Note that a similar phenomenon in which mobile Al-OH species in zeolites can be incorporated into adjacent PdO nanoparticles has been reported recently [78].

The changes in the Al species resulting from the mechanical interactions of the VWTi-Al-rich Y-zeolite-5.1 also induced changes in the redox behavior of isolated V sites in Fig. 3-9(a). In the H_2-TPR profiles, the overall reduction peak at 370–620 °C, which was assigned to the reduction of dispersed VO_x and WO_x species, shifted to a higher temperature after grinding [79-81]. Note that the use of Y-zeolite-5.1 resulted in more pronounced changes in the reduction temperature in the mixed VWTi catalyst compared to that of Y-zeolite-12. Such a significant change in the reducibility of the isolated VO_x species can only be explained by chemical interaction with Al species, which inhibit the reduction of V-O-Ti by forming Al-O bonds. To confirm the potential effects of Al species on the reducibility of VO_x, we impregnated the $Al(NO_3)_3$ solution on the VWTi catalyst to simulate the migration of Al and observed the changes in the H_2-TPR results in Fig. 3-9(b). Interestingly, a similar trend was observed for the Al-impregnated VWTi catalysts in which the reduction peak below 450 °C

decreased, whereas the peak above 500 °C increased as more Al was impregnated. These results support our hypothesis that the diffused Al species originating from the zeolite affect the reducibility of the VO_x species on TiO_2 by grinding process.

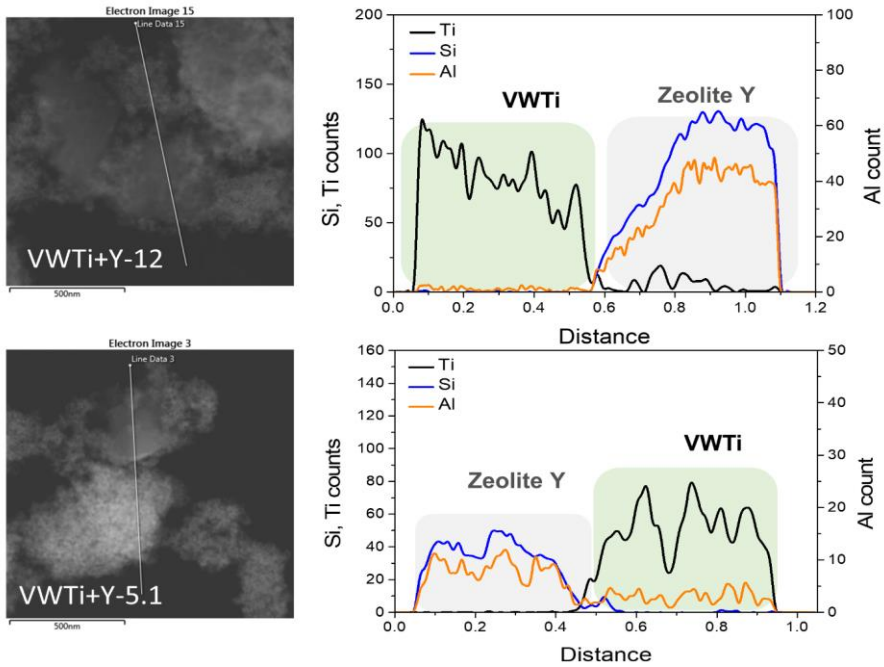

Fig. 3- 8. TEM image and EDS line scanning spectra for the mechanical mixtures of the VWTi + Y-12 and VWTi + Y-5.1 catalyst after grinding.

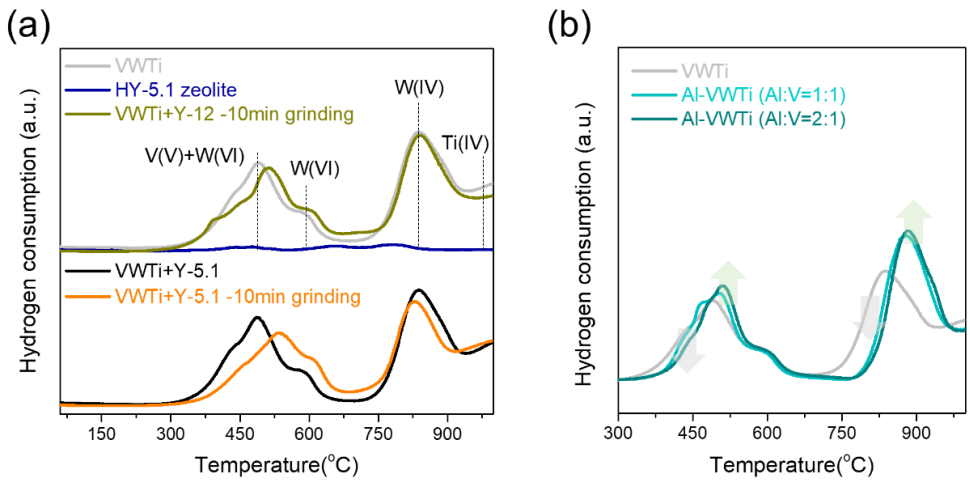

Fig. 3- 9. (a) H_2-TPR results comparing the effect of mechanical grinding on the mixed VWTi + Y-5.1 and VWTi + Y-12 catalysts. (b) H_2-TPR results for the Al-impregnated VWTi catalysts.

Next, kinetic analysis of the catalyst was performed to examine the effects of the VO_x-Al interaction on the reaction pathway in the SCR reaction in Fig. 3-10. The activation energy (E_a) of the VWTi catalyst with the wet feed was measured as approximately 60 kJ/mol under standard SCR conditions. However, after grinding with Y-zeolite-5.1, the E_a increased to approximately 69 kJ/mol. Similarly, under dry conditions, the E_a of VWTi was 52 kJ/mol, whereas that of VWTi + Y-5.1 increased to 64 kJ/mol, suggesting that the increase in E_a occurs regardless of the presence of water. The changes in the reaction kinetics, represented by an increase in the activation energy, can be explained only by the modulation of active sites of the reaction. Note that the E_a of the Al-impregnated VWTi catalyst was also higher (72 kJ/mol) than that of the VWTi catalyst, similar to the observations for the VWTi + Y-5.1 catalyst. The interaction between V and Al, thus, led to a higher E_a in SCR reaction, which is a major cause of catalytic deactivation after grinding. Recent papers have reported that surface VO_x species on TiO_2 are dynamic under reaction conditions, meaning that changes in the VO_x dispersion may also cause deactivation after grinding [79, 82-84]. To confirm this possibility, kinetic studies of VWTi catalysts with various V loadings were performed under wet conditions in Fig. 3-11, and the E_a was found to be 52–60 kJ/mol regardless of V loading, which is consistent with the literature [85, 86]. Therefore, the increase in E_a for the VWTi + Y-5.1 catalyst is attributed to the interaction with Al species rather than the change in V dispersion.

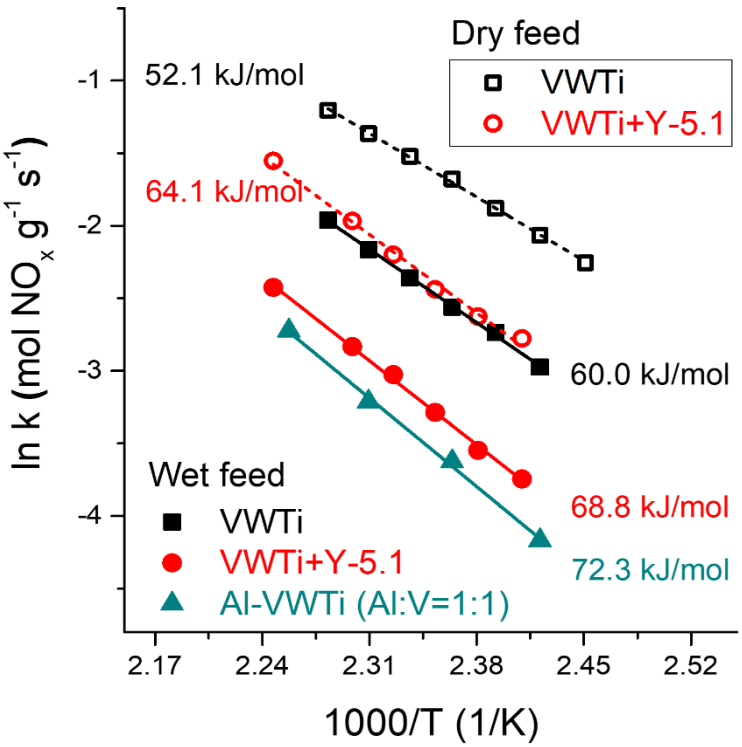

Fig. 3- 10. Kinetic analysis of the VWTi and the mixed catalysts under dry and wet reaction conditions.

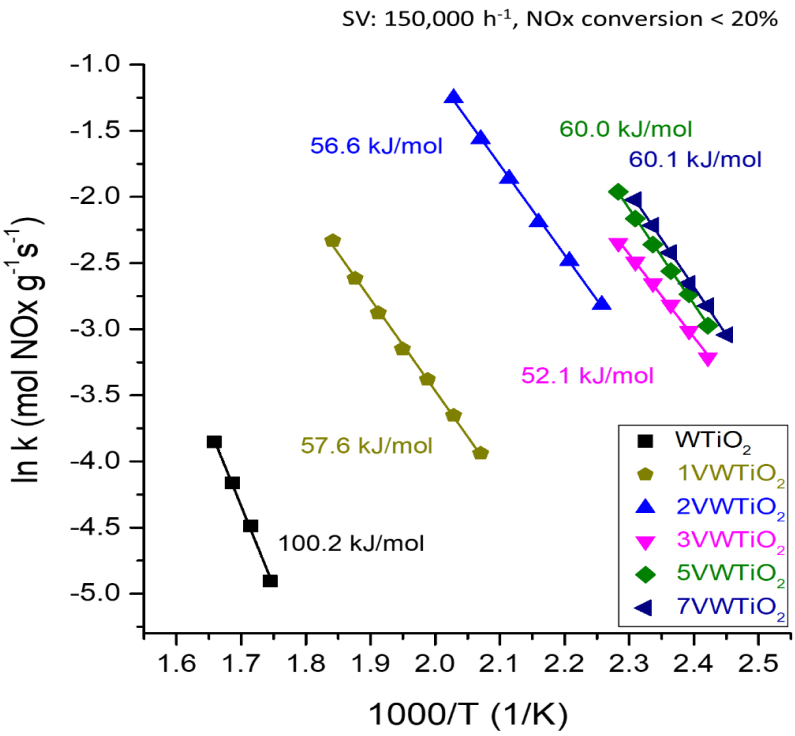

Fig. 3- 11. Kinetic analysis over the VWTi catalysts with various V_2O_5 loadings from 1 to 7 wt.%.

3.3.3. Regulating Al diffusion using a carbon barrier surrounding zeolite

Therefore, a novel strategy is required to prevent the catalytic deactivation arising from the chemical interaction between V and Al formed by grinding while retaining a high SO_2 resistance. Thus, we suggest the introduction of a carbon layer as a physical barrier on the external surface of zeolite particles to suppress the diffusion of EFAl species during mechanical grinding [72]. Before grinding, Y-zeolite was coated with OTS, which formed bonds with the hydroxyl groups in the toluene solvent by forming HCl in Fig. 3-12. The results of characterization confirmed the successful formation of a carbon layer on Y-zeolite in Figs. 3-13–3-15, and most of the carbon layer was removed as CO_2 and water after oxidation at 500 °C without change to the zeolite structure. The carbon-coated Y-zeolite (OTSY) was then ground with VWTi, producing VWTi + OTSY-5.1.

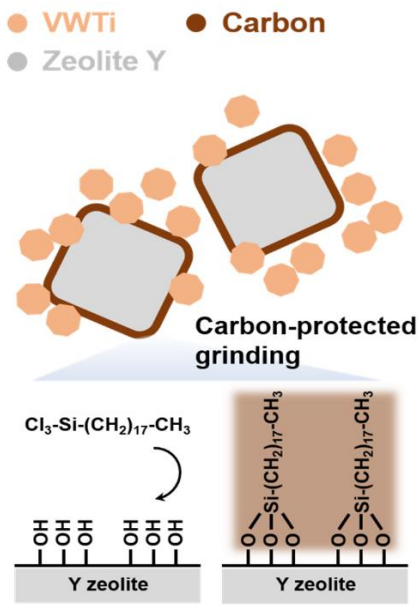

Fig. 3- 12. Schematic of the grinding method using a protective carbon layer.

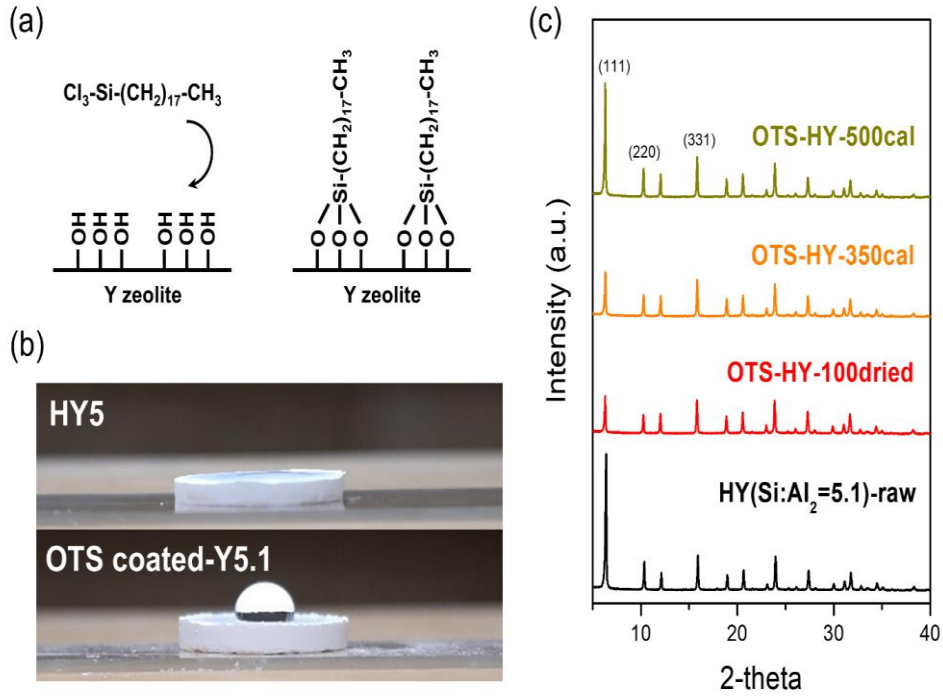

Fig. 3- 13. (a) Scheme of organosilane (octadecyltrichlorosilnae, OTS) coating on the external surface of Y-zeolite. (b) Water droplet on the zeolite pellet with and without organosilane-monolayer. (c) XRD pattern of HY zeolite, OTS coated Y-zeolite, and its calcined forms (350 and 500 °C).

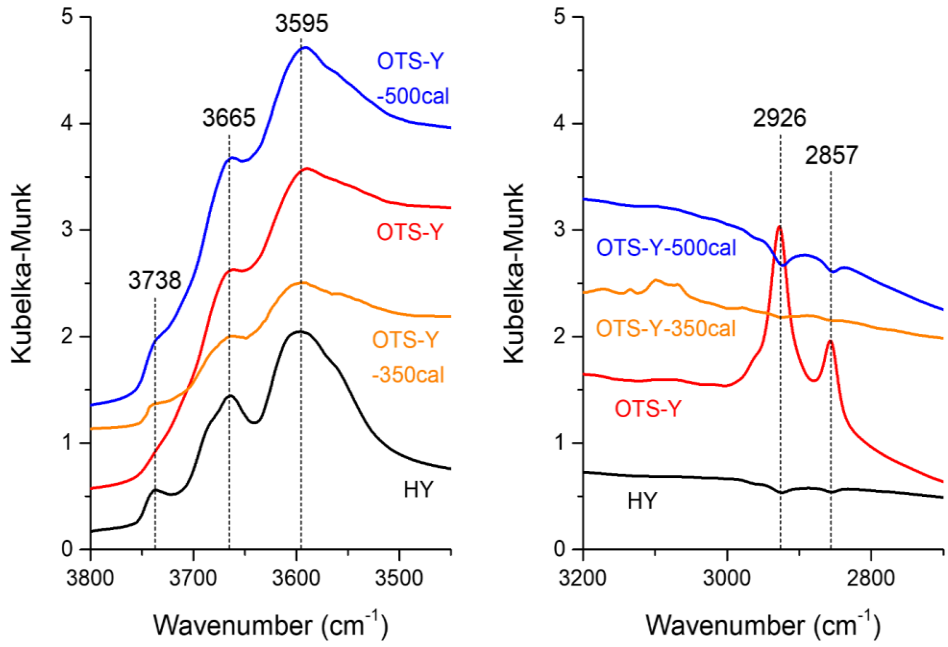

Fig. 3- 14. FT-IR spectra for HY zeolite, OTS-Y zeolite, OTS-Y zeolite-350cal, and OTS-Y zeolite-500cal sample.

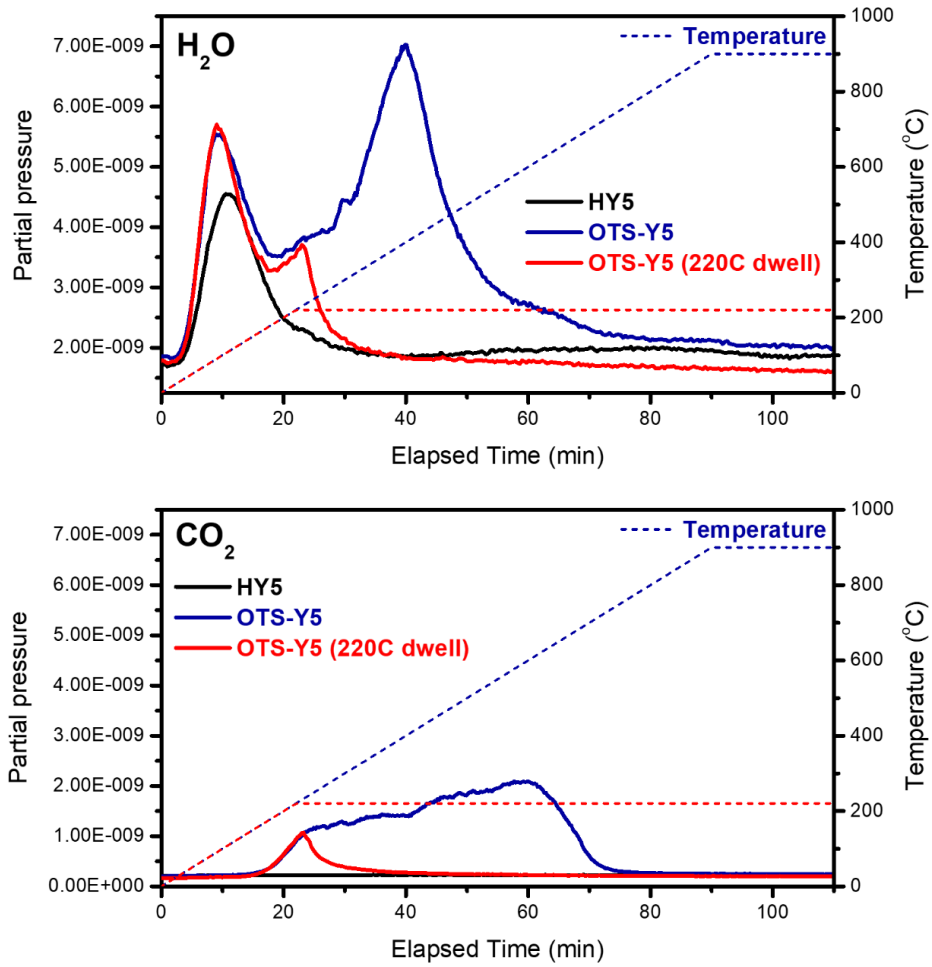

Fig. 3- 15. Temperature programmed oxidation to 900 °C at a ramping rate of 10 °C/min for OTS-Y-5.1 zeolite under 10% O_2/N_2 (blue). The signals of H_2O and CO_2 were monitored by mass spectrometer. For comparison, temperature was increased to 220 °C and dwelled at same temperature (red).

Interestingly, the mixed VWTi + zeolite catalyst protected with a carbon layer resulted in similar ^{51}V NMR peak intensities before and after grinding in Fig. 3-16(a). In addition, the H_2-TPR profiles also showed no decrease in the reducibility of VWTi after grinding in Fig. 3-16(b). These results indicate that isolated VO_x is preserved without the interaction of Al species.

Compared to the VWTi + Y-5.1 catalyst, VWTi + OTSY-5.1 retained its initial catalytic activity without any deactivation from 100 to 300 °C (Fig. 3-17). This clearly shows that thin carbon layers on the external surfaces of zeolite particles effectively act as a physical barrier as intended and prevent the diffusion of Al species, thereby protecting the active isolated VO_x sites on the TiO_2 surface. After conducting the SCR reaction over this catalyst up to 500 °C, the reactor was cooled to room temperature and retested under the same conditions (2^{nd} run in Fig. 3-17). In the 2^{nd} SCR test, there should be direct contact between the VWTi and zeolite particles because most of the carbon layer is removed by oxidation as shown in Fig. 3-14. The elemental analysis of the OTSY-5.1 catalyst showed only a small amount of the carbon layer remaining after oxidation at 500 °C as listed in Table 3-1. Elemental analysis (CNHS) of the carbon-coated Y-zeolite with Si: Al_2 =5.1 (OTSY-5.1) before and after calcination at 350 °C and 500 °C for 4 h were denoted as OTSY-5.1-350 cal and OTSY-5.1-500 cal, respectively. Also, elemental analysis of the physically mixed 5VWTi and carbon layer protected Y-zeolite-5.1 after the 1st SO_2 aging (5VWTi + OTSY-5.1-S) and the physically mixed 5VWTi and the calcined carbon-

coated Y-zeolite at 350 °C and 500 °C for 4 h after the 1st SO_2 aging test (5VWTi + SY-5.1-350 cal-S and 5VWTi +SY-5.1-500cal-S, respectively) were acquired. Interestingly, the SCR activity was totally maintained without any change in the 2nd SCR test, even though there was direct contact between zeolite and VWTi particles, indicating that chemical deactivation by mobile EFAl species does not occur without the mechanical grinding process. This observation proves our hypothesis that the migration of Al species, mostly EFAl, to adjacent particles is caused by mechanical force rather than differences in the chemical potential. For comparison, we also prepared a VWTi + SY-5.1 catalyst, in which the carbon-coated OTSY-5.1 was pre-oxidized at 500 °C to make SY-5.1, to observe what happens if the carbon layer is removed before grinding. In this case, as expected, a decrease in SCR activity was observed again, which is similar to the observations for the VWTi + Y-5.1 as displayed in Fig. 3-17. This indicates that the remaining silane groups on the zeolite after oxidation cannot prevent the mechanochemical interaction between VO_x and Al species. In other words, a thin carbon layer on the zeolite surface that prevents direct contact between V and zeolite must be present.

Sample	Nitrogen[a]	Carbon[a]	Hydrogen[a]	Sulphur[a]
HY-5.1	n.d	0.0	0.1	n.d
OTSY-5.1	n.d	2.9	2.6	n.d
OTSY-5.1-350 cal	n.d	1.4	2.1	n.d
OTSY-5.1-500 cal	n.d	0.1	2.3	n.d
5VWTi + OTSY-5.1-S	0.8	0.5	0.9	0.4
5VWTi + SY-5.1-350 cal-S	1.0	0.4	0.7	0.5
5VWTi + SY-5.1-500 cal-S	0.8	0.1	0.9	0.3

a : wt.%, obtained from Elemental analysis (CNHS).

Table 3- 1. Elemental analysis (CNHS) of the carbon-coated Y-zeolite with Si: Al_2 =5.1 (OTSY-5.1) before and after calcination at 350 °C and 500 °C for 4 h and the physically mixed 5VWTi and carbon layer protected Y-zeolite-5.1 after the 1st SO_2 aging and the physically mixed 5VWTi and the calcined carbon-coated Y-zeolite at 350 °C and 500 °C for 4 h after the 1st SO_2 aging test.

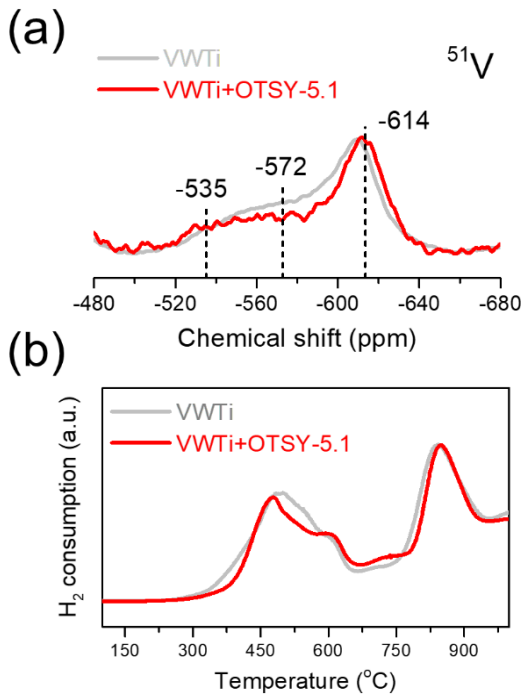

Fig. 3- 16. (a) ^{51}V solid-state NMR spectra and (b) H_2-TPR results for VWTi + OTSY-5.1 catalyst.

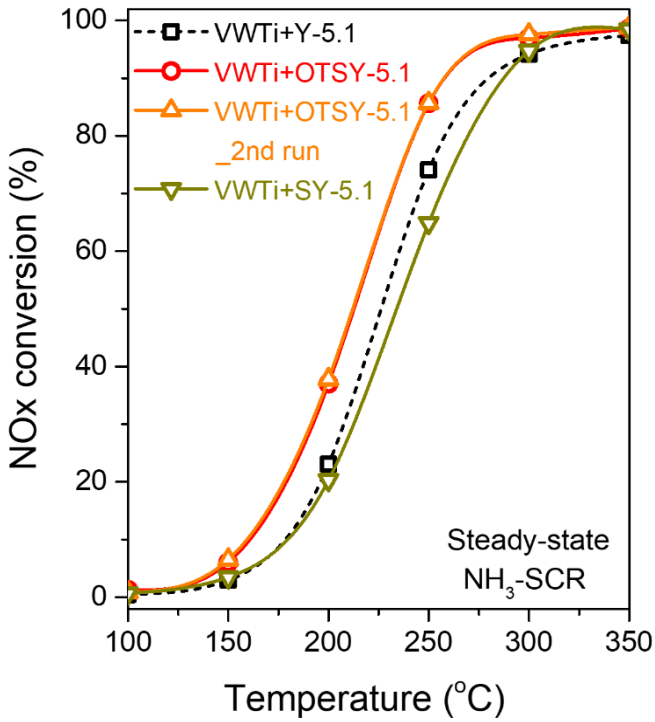

Fig. 3- 17. Steady-state NO_x conversions as a function of temperature during the standard NH_3-SCR reaction for the VWTi + OTSY-5.1 catalyst and its calcined form (VWTi + SY-5.1).

Finally, we tested the longevities of the prepared catalysts under accelerated deactivation condition with 10% H_2O and 100 ppm SO_2 (GHSV of approximately 150,000 $mL \cdot g^{-1} \cdot h^{-1}$). The VWTi + OTSY-5.1 catalyst retained its initial catalytic activity without any chemical deactivation arising from EFAl species while successfully maintaining a high SO_2 resistance without any physical deactivation with ABS for 44 h operation as shown in Fig. 3-18(a). The catalysts were regenerated at 350 °C from 22 to 25 h during operation. This performance is superior compared to conventional VWTi and Mn-based catalysts and, thus, can be utilized in combustion facilities with sulfur-containing exhaust gas. Meanwhile, it has been reported that low temperatures (below 200 °C) can further accelerate ABS deactivation [37, 87]. This is because the vapor pressure of ABS drops substantially as the temperature decreases according to the Clausius–Clapeyron equation. Thus, the catalyst was also tested at a much lower temperature (180 °C), where the condensation of ABS in the catalyst pores occurred more easily as displayed in Fig. 3-18(b). The conventional VWTi catalyst rapidly lost its activity in 5 h under these conditions and the activity was lower still (below 20%) when temperature was increased to 220 °C because condensed ABS is hard to decompose at this temperature. In contrast, the VWTi + OTSY-5.1 catalyst retained its activity with very little deactivation for 22 h, and the activity was still higher (approximately 60%) when the temperature was recovered to 220 °C. It was also confirmed that further low-temperature exposure for 44 h did not completely deactivate the

catalyst. The catalysts were heated to 220 °C after 22 and 48 h to monitor the deactivation progress. These results are remarkable and indicate that this strategy can prevent the low-temperature events currently occurring during real SCR operation.

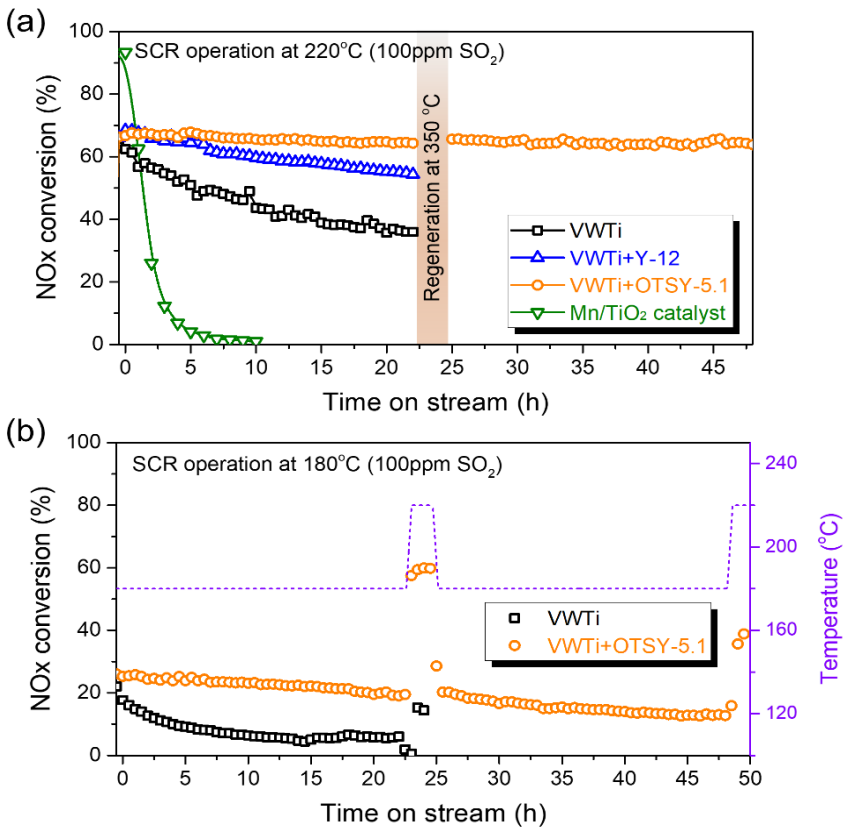

Fig. 3- 18. (a) NO_x conversion in the NH_3-SCR reaction at 220 °C during accelerated deactivation for 44 h by forming ABS on the catalysts. (b) Simulated deactivation at 180 °C for 44 h by forming ABS on VWTi and VWTi + OTSY-5.1 catalysts.

Our further curiosity on this phenomenon is that whether bulk carbon has a similar effect to that of thin carbon layers prepared from organosilane. Therefore, instead of using silane, we deposited a bulk carbon compound, i.e., colloidal starch in aqueous solution, on zeolite particles and mixed it with the VWTi catalyst. Starch-Y-5.1 zeolite composite material was prepared by impregnating zeolite particle on the colloidal starch solution in boiling water. The amount of carbon in OTS-Y-5.1 zeolite (2.8 wt.%) and Starch-Y-5.1 (2.2 wt.%) was comparable based on Elemental analysis in Table 3-1. In this case, unfortunately, ABS deactivation occurred (VWTi + starch-Y-5.1 in Fig. 3-19). Our interpretation of this result is that the long colloidal starch ligands induce zeolite agglomeration, thereby inhibiting sufficient VWTi–zeolite contact for ABS trapping, unlike the OTS layer that only covers the external surface of zeolite. This shows that the carbon layer must be carefully introduced without interrupting the essential contact between VWTi and zeolite for efficient ABS trapping. In summary, the VWTi + OTSY-5.1 catalyst with tailored mechanochemical interactions resulted in superior SO_2 resistance and moderate SCR activity concurrently.

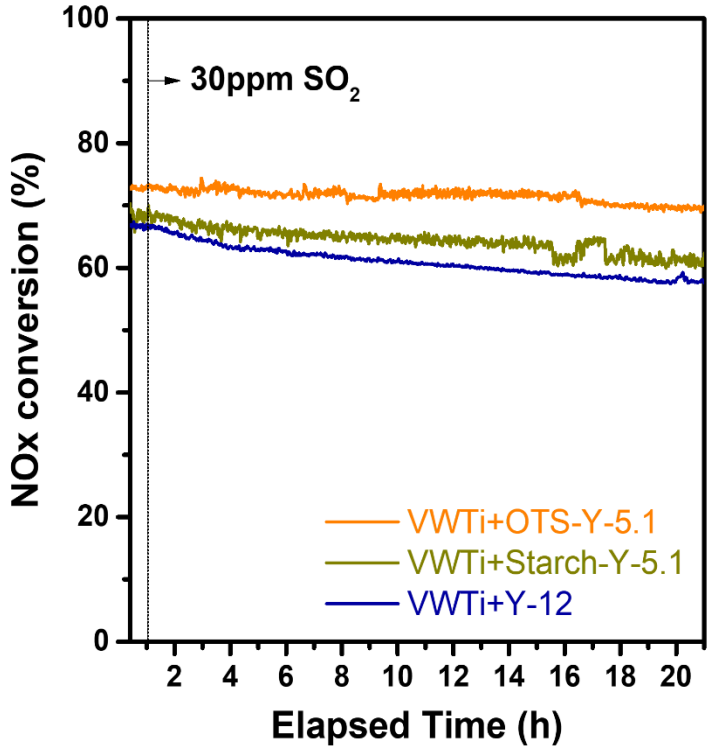

Fig. 3- 19. NO_x conversions comparison of OTS-Y-5.1 and starch-Y-5.1 zeolite composite material at 220 ^oC during simulated deactivation for 22 h.

Based on our characterization results, we focus on the chemical interaction between V and Al, which most likely comprise V-O-Al bonds, induced by the mechanical mixing of VWTi and Y-zeolite. Some assumptions about these chemical interactions can be made. First, when the amount of the mixed Y-zeolite was controlled as shown in Fig. 3-4(b), more zeolite was added, and a larger degradation of the initial performance was obtained. However, this phenomenon was not observed with Y-zeolite ($Si/Al_2 = 12$), which contains less Al. Thus, we can easily assume that the degraded activity after the mechanical mixing is strongly related to the amount of Al, especially with Al-rich zeolite ($Si/Al_2 = 5.1$). The AlO_x species in zeolite can be divided into framework Al and extra-framework Al. The framework Al species are strongly bound to Si by strong chemical bonds, whereas the extra-framework Al species in the zeolite cage are mobile and, thus, most likely related to the loss in catalytic activity.

On the other hand, it is well known that the deactivation of SCR catalysts is caused by a decrease in acid sites or decreased reducibility. If the presence of Al simply reduced the amount of acid sites, such as the blockage of acid sites, the rate-determining step, the reduction of vanadium oxide, would still proceed similarly, and no change in activation energy should be observed. However, the activation energy significantly increased after deactivation by Al during mechanical mixing in Fig. 3-10. This means that reducibility of vanadium oxide is decreased by the presence of Al. In addition, the NMR spectra indicate the structural rearrangement of V

species and Al species in zeolite after mechanical mixing in Fig. 3-5. From these data, it can be inferred that unexpected chemical interactions are induced during mechanical mixing, thus decreasing the reducibility of vanadium oxide. The shift in the V reduction peak to higher temperatures in the H_2-TPR results also demonstrates the reduced redox ability of V as shown in Fig. 3-9.

Thus, how can EFAl move and form such chemical interactions with V? According to previous research, extra-framework Al species, such as $Al(OH)_3$, are bound to hydroxyl groups, which become mobile in the zeolite cage in the presence of moisture. $Al(OH)_3$ solution is impregnated on VWTi catalyst to simulate the chemical interaction formed between extra-framework Al and V in Fig. 3-9(b). With impregnation of $Al(OH)_3$, the reduction peak of V shifted to higher temperatures, indicating a decrease in redox ability, and the activation energy was increased in Fig. 3-10. From these results, we can conclude that some chemical interactions between V and Al occur during mechanical mixing, leading to the decreased reducibility of the V-based catalyst. The simple physical blockage of V sites by nearby Al could have also occurred, which would have reduced the activity, but it is difficult to find conclusive evidence for this hypothesis.

To explain why we used the carbon coating strategy in this study, we first need to explain how physically mixed zeolite suppresses the deactivation of the V-based catalyst. As mentioned in our previous study

[39], V-based catalysts oxidize SO_2 to SO_3 rather than chemically deactivated by SO_2. However, SO_3 can produce ABS in the presence of H_2O and NH_3 at low temperatures. The formed ABS can physically block vanadium active sties, causing the physical deactivation of the V catalyst. However, we found that physical mixing with zeolite can prevent the deactivation of the V catalyst. ABS formed on V active sites migrates to zeolite sites in V catalyst physically mixed with zeolite, trapping ABS on zeolite sites [39]. This novel strategy enables to protect the V active sites, resulting in the superior sulfur resistance of the V catalyst. Among the various zeolites, we found that zeolites having large pores and a high proportion of Al achieves high ABS trapping ability because ABS formed on V sites strongly interacts with Al sites. Thus, Al-rich zeolite achieves higher sulfur resistance.

In this study, we demonstrate the chemical deactivation induced when Al-rich zeolite is mixed with a V-based catalyst and suggest the use of a carbon coating as a novel strategy to resolve this problem. The thin carbon layer on the surface of Al-rich zeolite can inhibit the chemical interaction between V and Al during the mechanical mixing, thus suppressing degeneration of activity without affecting its high ABS trapping ability. In summary, the surface modification of the Al-rich zeolite allows us to suppress the chemical and physical poisoning in V-based catalysts physically mixed with zeolite simultaneously.

Chapter 4. Understanding the ball milling effects over ball milled V_2O_5/WO_3-TiO_2 with zeolite Y for selective catalytic reduction of NO_x with NH_3.

4.1. Introduction

The mechanical mixing would include two different ways of mixing, hand mixing and ball milling of two or more materials. The mechanical mixing has been recognized and respect to these advantages, the newly rising method, especially ball milling, has been highlighted for its advantages to design or scale up the NH_3-SCR catalysts in industrial fields [88-90]. However, unlike the conventional methods that have been studied for past decades, many parts of synthesis via mechanical mixing are still ambiguous and further study are still necessary for practical applications, especially regulating parameters and possibility of unexpected interaction between the mixed materials [91-93].

Previous studies have studied over vanadium oxide-based catalysts for NH_3-SCR in stationary sources due to its higher thermal stability and sulfur stability at high temperature [70, 94]. Besides, we have found some breakthrough catalysts synthesized by mechanical mixing in our previous studies [71, 95]. From our previous studies, we found that simple hybrid catalyst, mechanically mixed vanadium oxide-based catalysts (5 wt.% V_2O_5/WO_3-TiO_2) with zeolite Y, can maintain high SCR activity and increase sulfur resistance of V catalyst. Although the mixed catalyst usually

brings positive consequences, the mechanical mixing can also provoke unexpected results [96]. From our previous study, after V based catalyst was mixed with Al-rich zeolite Y, the chemical interaction between VOx species and diffused AlOx species in Al-rich zeolite was formed, resulting in increase of activation energy, while maintaining high stability to sulfur.

Hence, the catalyst synthesized via mechanical mixing method have full of potentials, but further study on the new synthesis method to regulate valuables. In addition, this study focuses on investigating ball milled 5 wt.% V_2O_5/WO_3-TiO_2 catalyst and zeolite Y (Si:Al_2= 12), catalyst synthesized by ball milling to simulate ball milling synthesis method as many industrial fields apply. The hybrid catalysts of V_2O_5/WO_3-TiO_2 with zeolite Y synthesized by ball milling was studied on how the ball milling process affected on catalytic properties and performance.

4.2. Experimental

4.2.1. Catalyst preparation

The 5 wt.% V_2O_5/WO_3-TiO_2 catalyst was prepared by a wet impregnation method and was simply denoted as VWTi. Hydrogen form zeolite Y with $Si:Al_2$ = 12 (Alfa Aesar) were used with the synthesized VWTi. The samples were synthesized by hand mixing (mechanical mixing) or ball milling with the mass ratios of 2:1 (VWTi to zeolite Y). Hand mixed samples were ground in a porcelain mortar under ambient conditions for 10 min and labeled as VWTi + Y12 hand mixing while the ball milled samples were prepared by ball mill grinding machine (Mixer Mill MM400) with transient frequency of 10 Hz, 20 Hz, and 30 Hz for 10 min. The prepared samples were denoted as VWTi + Y12 (x)Hz 10 min B.M where x stands for frequency for 10 min of ball milling. Also, the ball milled samples were prepared for different time of ball milling, 10 min, 20 min, and 30 min with fixed frequency, which were denoted as VWTi + Y 5.1 or Y12 20 Hz (y)min B.M. The y stands for time of ball milling with the fixed frequency.

4.2.2. Reaction condition

The catalytic NH_3-SCR activity were performed in a 0.25-inch tubular quartz reactor. The SCR reaction data were conducted under the feed containing 500 ppm NO, 600 ppm NH_3, 10% O_2, 5% CO_2, 10% H_2O balanced with N_2 [96]. To test sulfur stability, SCR reaction feed contained with 30 ppm SO_2 (when it was used) balanced with N_2 at 220 ℃ for 22 h.

4.2.3. Characterizations

Corrected transmission electron microscope (Cs-TEM) image and line energy dispersive X-ray spectroscopy (line-EDS) scans of samples were collected in tunneling electron microscopy (TEM) mode. For reduction ability of samples, H_2-temperature-programmed reduction (H_2-TPR) was acquired with 5% H_2/Ar gas at a ramping rate of 10 °C/min. Powder X-ray diffraction (XRD) of all samples was obtained using a Bruker, D8 Advance model with a Cu Kα detector. Diffuse Reflectance Infrared Fourier Transform Spectroscopy (DRIFTS) spectra were obtained to simulate SCR reaction.

4.3. Results and discussion

4.3.1. Catalytic activity tests over the ball milled 5 wt.% V_2O_5/WO_3-TiO_2 catalyst with zeolite Y(Si:Al_2= 12)

Catalytic activity of 5 wt.% V_2O_5 (VWTi) and zeolite Y (Si:Al_2 = 12) with different frequency and time of ball milling were obtained and compared with the hybrid catalyst synthesized by hand mixing (VWTi + Y12 hand mixing) as shown in Fig. 4-1(a). The VWTi + Y12 hand mixing catalyst obtained approximately 65% of NOx conversion at low temperature of 220 ℃ while ball milled VWTi + Y12 catalysts with 10 Hz and 20 Hz for 10 min obtained the improved NOx conversion of approximately 80 %. On the other hand, only approximately 54% of catalytic activity at 220 ℃ was conducted when the VWTi + Y12 B.M was synthesized with 30 Hz frequency. Interestingly, the catalytic activity of VWTi + Y12 B.M with frequency of 10 Hz and 20 Hz were almost identical to each other, which showed that these two different ball milling frequencies did not affect the catalytic activity of the synthesized catalysts. Besides, the activity of VWTi + Y12 30 Hz 10 min B.M. catalyst degenerated, meaning that such high frequency can affect the catalytic activity.

Furthermore, when the ball milled VWTi + Y12 catalyst with increasing ball milling time with the fixed frequency of 20 Hz, every synthesized catalyst achieved the enhanced activity of VWTi + Y12 catalysts compared to the hand mixed sample. However, as ball milling time increased up to 30 min, the activity tended to decrease and approximately

65 % of catalytic activity was obtained, which is similar to activity of hand mixed catalyst as shown in Fig. 4-1(b). The results showed that the improved catalytic ability was achieved up to certain degree, but it become comprised as ball milling process took longer.

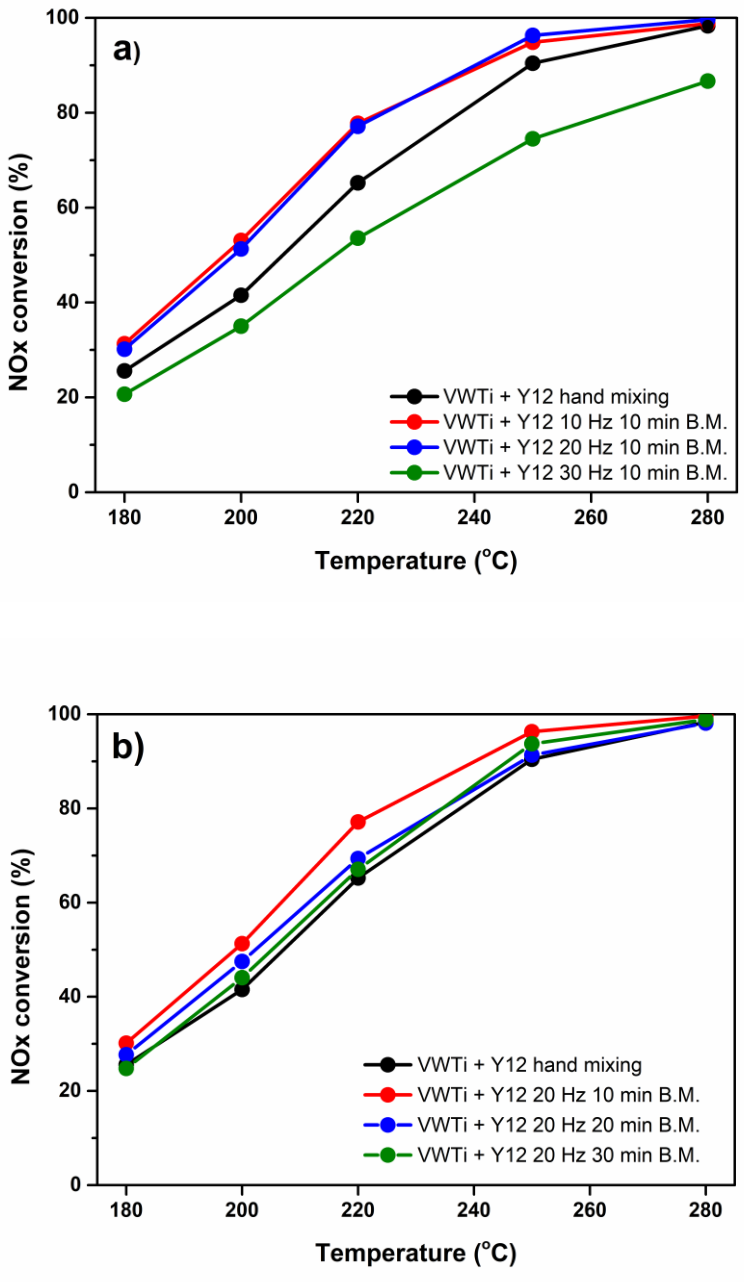

Fig. 4- 1. Catalytic activity of physically mixed V_2O_5/WO_3-TiO_2 catalyst with zeolite Y12 and ball milled V_2O_5/WO_3-TiO_2 catalyst with zeolite Y12 with different (a) frequency and (b) time.

NH_3-SCR catalysts often require having high sulfur tolerance, maintaining high NOx removal ability. We found that the sulfur stability of the VWTi + Y12 catalyst was also different by mixing methods as shown in Fig. 4-2. Although the hybrid catalyst designed by hand mixing still maintained its superior NOx conversion during SO_2 aging test at 220 ℃ for 22 h, VWTi + Y12-B.M. catalyst tended to have even higher sulfur resistance at the low temperature for 22 h. VWTi + Y12-B.M. synthesized by 20 Hz for 10 min achieved the initial activity of 80% and its deactivation rate was only 0.0005 as shown in Fig. 4-2(b), which was hardly deactivated. The VWTi + Y12 hand mixing catalyst still maintained its high NOx conversion during SO_2 aging, but it deactivated slightly more, obtaining deactivation rate of 0.0061. When the ball milling time increased up to 30 min, its initial activity at 220 ℃ decreased by approximately 12.5 %, but its high sulfur resistance maintained with slightly increased deactivation rate of 0.001. From the SO_2 aging tests, it was found that ball milling synthesis can increase the sulfur resistance of the hybrid system.

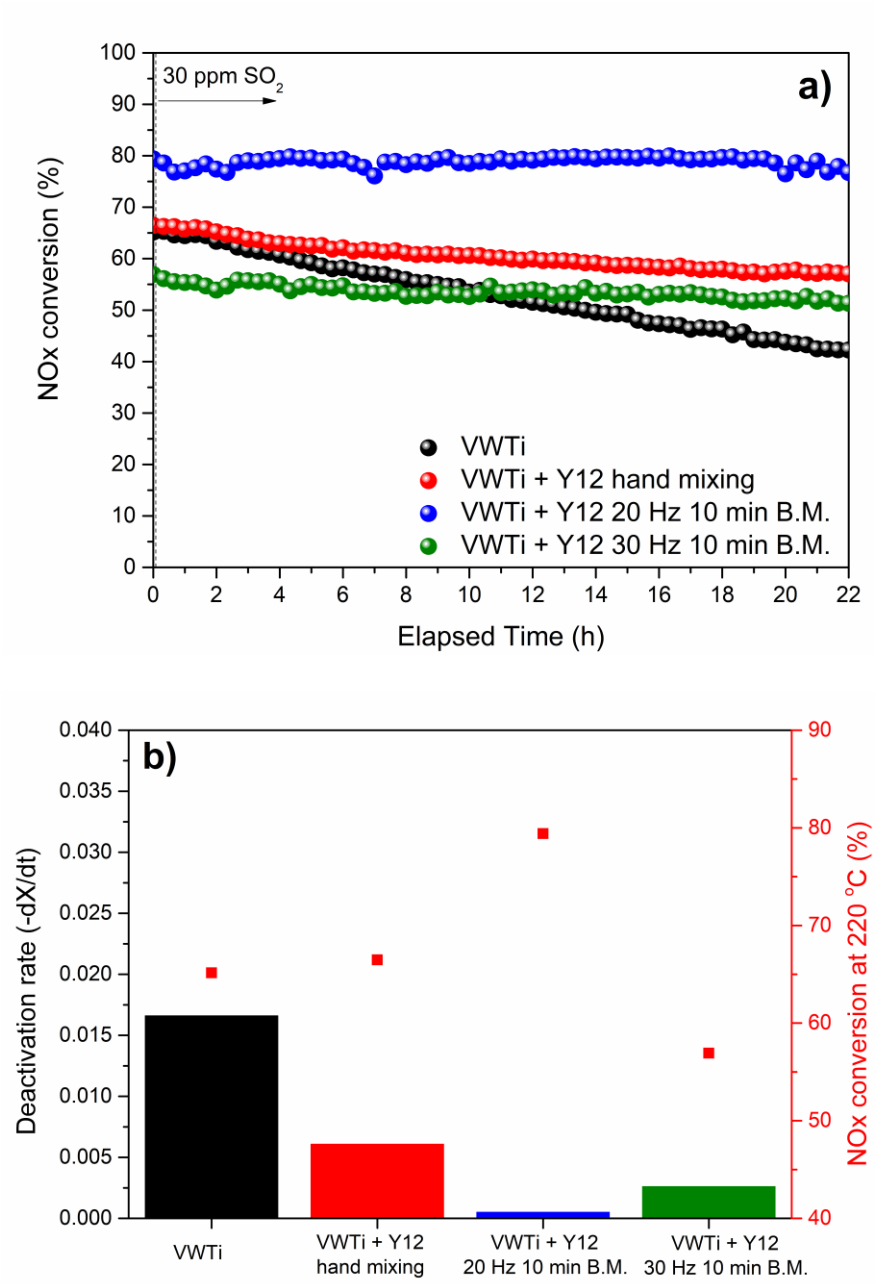

Fig. 4- 2. (a) NO_x conversion profiles of the VWTi and VWTi + Y12 B.M. catalysts with different frequency during SO_2 aging at 220 ^oC and (b) deactivation rates of the samples after SO_2 aging.

In order to investigate the ball milling effect on the samples, textural properties of the samples were observed. XRD results in Fig. 4-3 demonstrates that crystalline structure of VWTi and zeolite changed a bit during the ball milling process, but only insignificant increased peak of anatase TiO_2 were observed while the peaks usually denoted as faujasite were hardly changed. The XRD results with longer time of ball milling are similar. In addition, N_2 adsorption and desorption results displayed the changes in surface area and the pore volume of the catalyst as shown in Table 4-1. The surface area and pore volume of the catalyst mixed by ball milling increased a bit with increasing frequency of ball milling up to 20 Hz, but they eventually became smaller with 30 Hz of ball milling, 220 m^2/g and 0.377 cm^3/g. Increasing ball milling time brings more drastic changes in these properties. As the ball milling time increased, surface area and pore volume of samples decreased. When it was exposed to ball milling with 20 Hz for 30 min, its properties are almost identical to those of VWTi + Y12 30 Hz 10min B.M. catalyst. From the results, it was assumed that some textural properties would be affected by synthesis method.

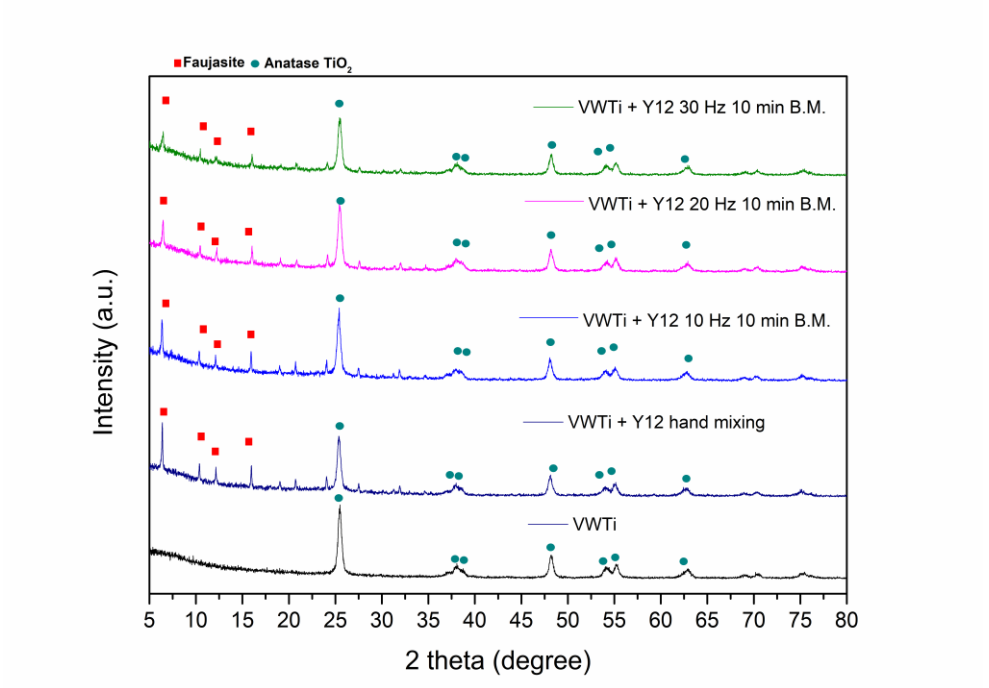

Fig. 4- 3. X-ray diffraction (XRD) results of ball milled V_2O_5/WO_3-TiO_2 catalyst with zeolite Y12 with different frequency.

	Surface area (m^2/g)	**Pore volume (cm^3/g)**
VWTi + Y 12 hand mixing	259	0.410
VWTi + Y 12 10 Hz 10 min B.M.	265	0.413
VWTi + Y 12 20 Hz 10 min B.M.	267	0.495
VWTi + Y 12 20 Hz 20 min B.M.	227	0.374
VWTi + Y 12 20 Hz 30 min B.M.	219	0.361
VWTi + Y 12 30 Hz 10 min B.M.	220	0.377

Table 4- 1. Surface areas and pore size distributions of VWTi + Y12 catalyst synthesized by hand mixing and ball milling.

H_2-TPR profiles in Fig. 4-4 also indicated that reduction ability of the catalyst changed by synthesis method. The reduction peak of V in the hand mixed catalyst appeared at approximately 440 ℃ and 570 ℃ ascribed as reduction of V and W, respectively, in VWTi + Y12 hand mixing catalyst. The peak at high temperature above 700 ℃ is often denoted as reduction of TiO_2. On the other hand, these reduction peaks of V and W in every VWTi + Y12 B.M. catalysts were shifted to higher temperatures, 500 ℃ and 590 ℃, respectively, which would demonstrate a formation of strong metal support interaction during ball milling process compared to that of hand mixed sample. The shift of reduction peaks to higher temperatures were also observed in every VWTi + Y12 B.M. catalysts with different ball milling time. The results of characterizations showed that the mechanical forces applied differently by hand mixing and ball milling, and it also influenced properties changes in the catalyst. However, the decreased reduction ability after the ball milling and the enhanced activity were not in coordination and it may not play the main role for decreased activity as the ball milling frequency and time increased.

The decreased activity could be elucidated from the corrected transmission electron microscope (Cs-TEM) image and line energy dispersive X-ray spectroscopy (line-EDS) scans of VWTi + Y12 30Hz 10 min B.M. catalyst as shown in Fig. 4-5. The designed system of hybrid VWTi + Y12 catalyst were to have the essential physical contact for migration of ABS from VWTi domain to zeolite domain, but it seemed to be

interrupted by ball milling process. The VWTi catalyst and zeolite Y12 were overlapped too much, leading to existence of V on zeolite site and Al on VWTi site. The overlapped existence may have caused the chemical interaction between VOx and AlOx and shift of the reduction to higher temperatures would be occurred.

The ball milling process tended to affect the particle size as well respect to the Scanning Electron Microscopy (SEM) images of VWTi catalysts and zeolite Y12 in Fig. 4-6 and Fig. 4-7, respectively. In case of VWTi catalyst, the particle size of VWTi increased as the ball milling frequency increased. The VWTi particle tended to agglomerate as the ball milling process performed at larger frequency while the particle size of zeolite Y12 seemed to decrease with increasing frequency. Up to frequency of 10 Hz, its particle size maintained, but shatters of zeolite Y were observed as the frequency increased to 20 Hz and 30 Hz. The agglomeration of VWTi and shattered zeolite Y would have affected the surface VOx population and acidity of the VWTi + Y12 catalysts.

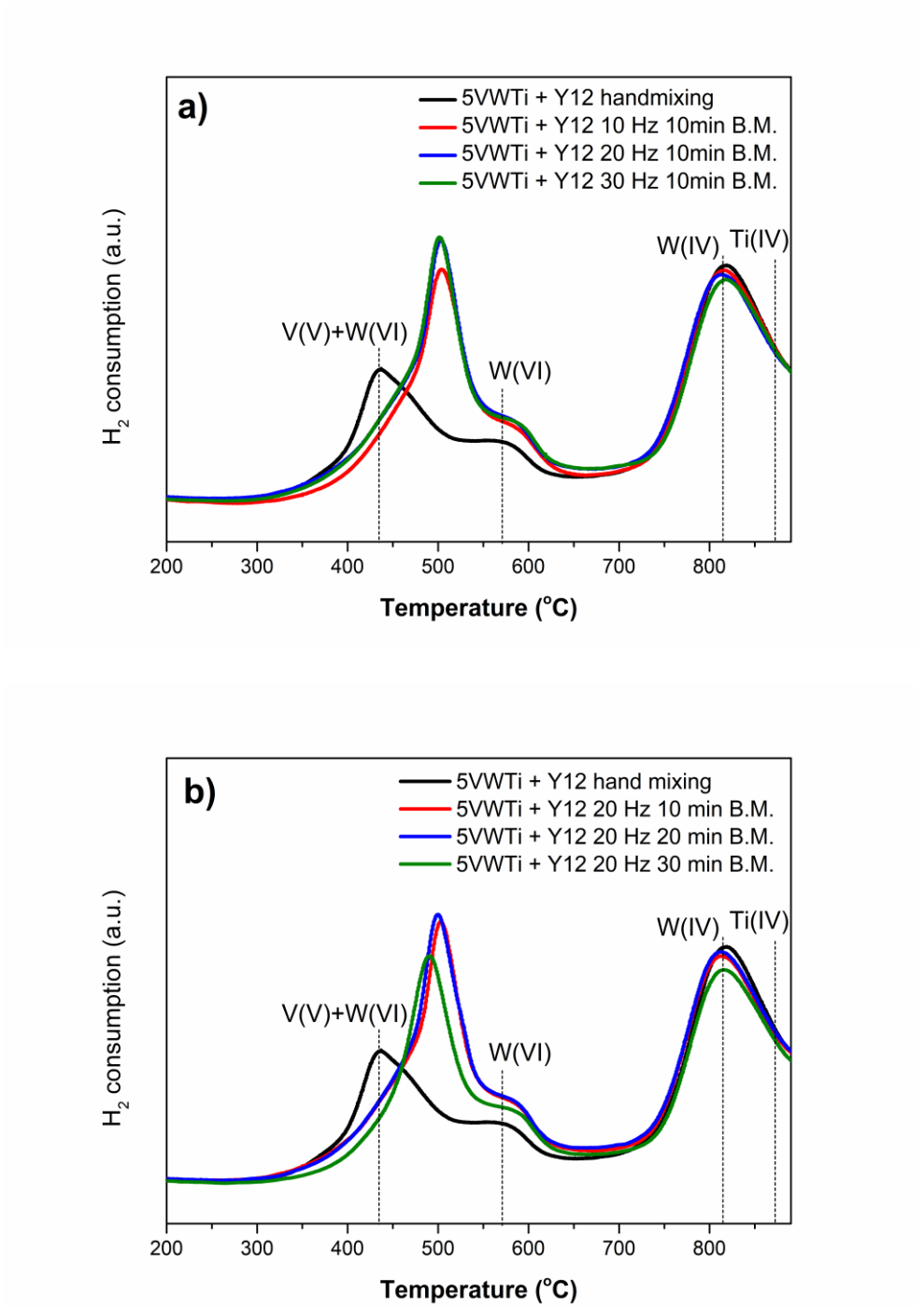

Fig. 4- 4. H_2-TPR results of VWTi + Y12 -B.M. catalysts with (a) different frequency and (b) time.

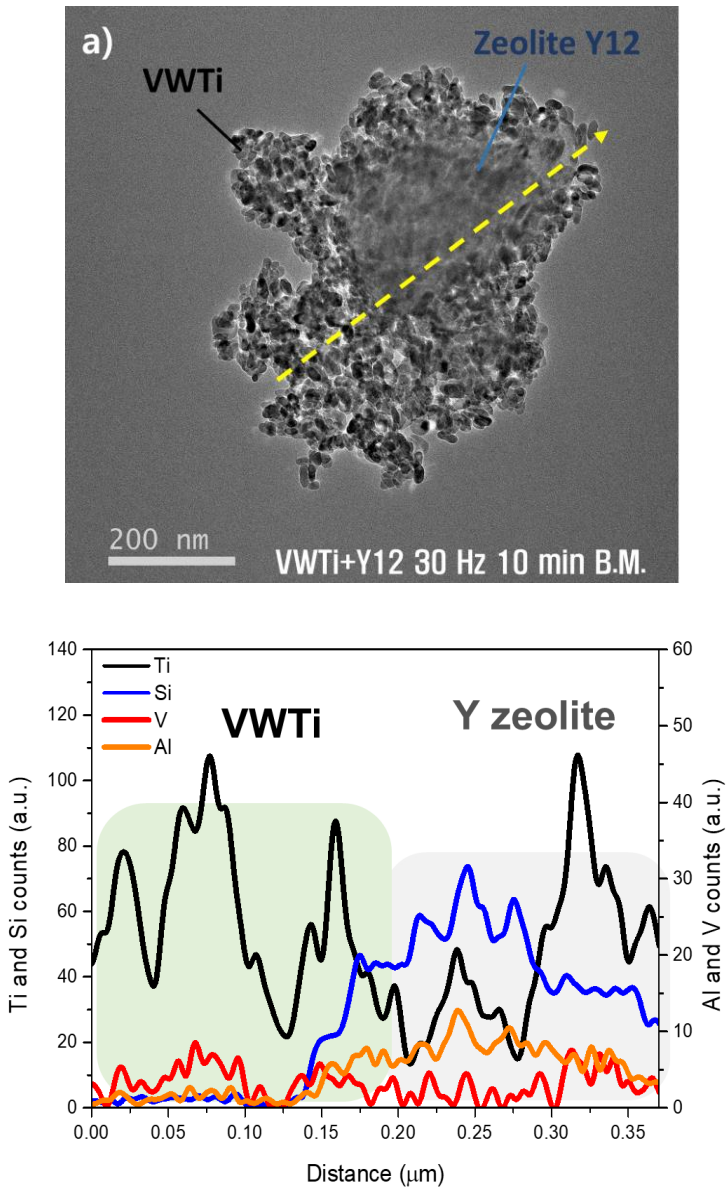

Fig. 4- 5. (a) Corrected transmission electron microscope (Cs-TEM) image and (b) line energy dispersive X-ray spectroscopy (line-EDS) scans of VWTi + Y12 30Hz 10 min B.M. catalyst.

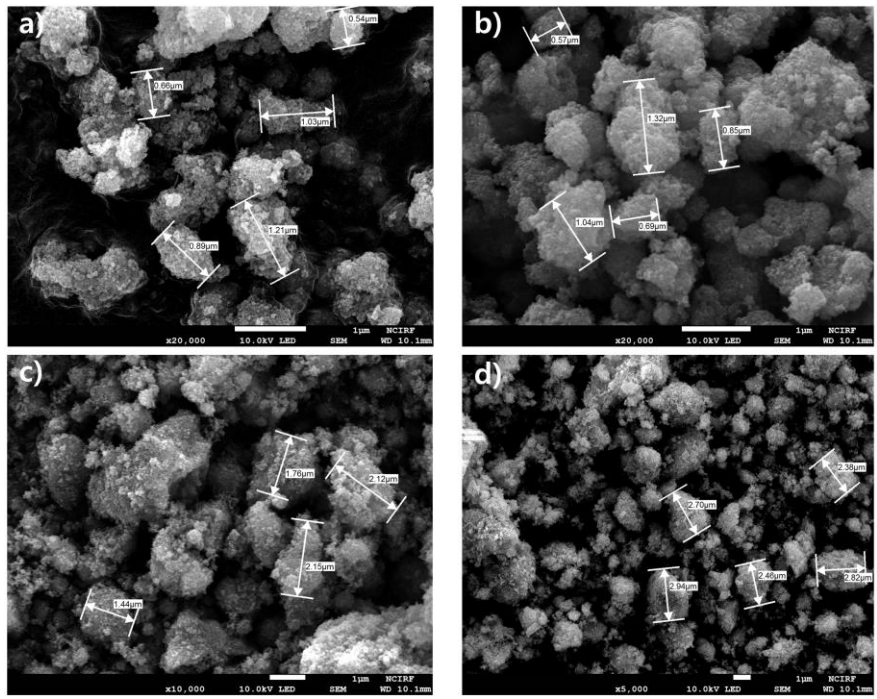

Fig. 4- 6. SEM images of (a) VWTi, (b) VWTi 10 Hz 10min B.M., (c) VWTi 20 Hz 10min B.M., and (d) VWTi 30 Hz 10min B.M. catalysts.

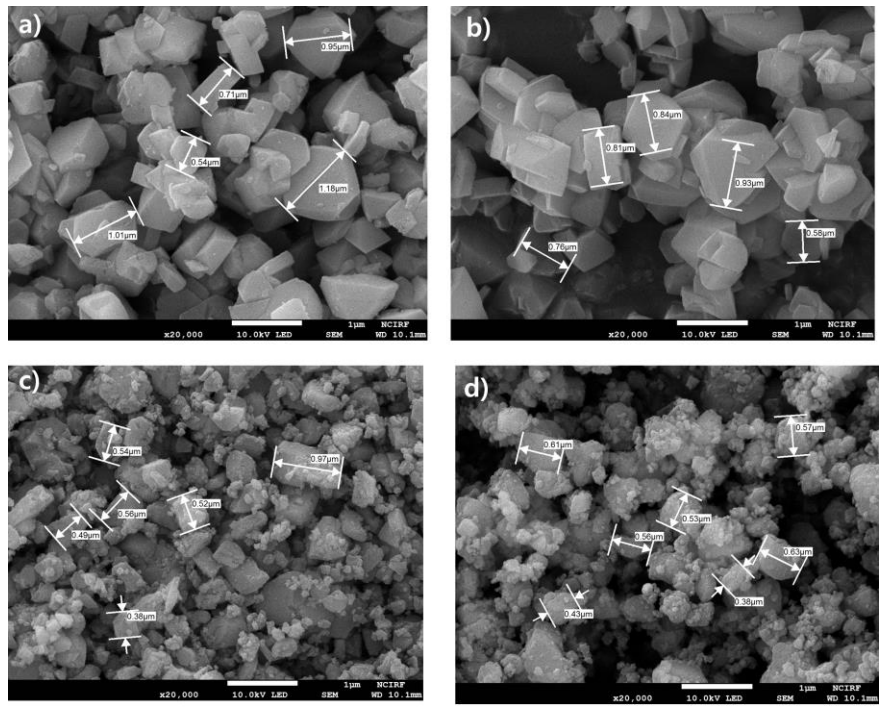

Fig. 4- 7. SEM images of (a) zeolite Y12 (b) zeolite Y12 10 Hz 10min B.M., (c) zeolite Y12 20 Hz 10min B.M., and (d) zeolite Y12 30 Hz 10min B.M. catalysts.

From the NH_3-TPD profiles in Fig. 4-8, acidity significantly increased after ball milling of VWTi catalyst and Y12 catalyst was observed compared to the hand mixed catalyst. The peak below 300 ℃ and the peak below 400 ℃ can be ascribed to weak acid sites and medium acid sites, respectively. The peak appeared above 400 ℃ would be denoted as strong acid sites. The increased acidity would give a rise to enhance catalytic activity. Diffuse Reflectance Infrared Fourier Transform Spectroscopy (DRIFTS) results were also collected for hand mixed catalyst and ball milled catalysts as shown in Fig. 4-9. Two significant peaks appeared at approximately 1185 cm^{-1} and at approximately 1432 cm^{-1}, which are ascribed the NH_3 adsorbed on Bronsted acid sites and NH_3 onto Lewis acid sites, respectively [84, 97]. Every VWTi + Y12 catalysts tended to have abundant amount of NH_3 adsorbed onto Lewis acid site, which would be originated from the mixed zeolite Y, while the NH_3 onto Bronsted acid site would be originated from VWTi catalyst. It was noteworthy that the peak at 1185 cm^{-1} hardly changed throughout the reaction while the peak at 1432 cm^{-1} decreased as the reaction continued in every sample, meaning that the mixed zeolite Y12 did not significantly participate in the reaction. For fair comparison, the ratio of the NH_3 adsorbed on Bronsted acid sites and NH_3 onto Lewis acid sites (B/L ratio) was obtained as shown in Fig. 4-10. B/L ratio of each sample was normalized by its initial value as 1. The decrease of B/L ratio demonstrated that consumption of adsorbed NH_3 under the NO + O_2 reaction flow as it was simulated the SCR reaction. From the result, it

was found that the NH_3 ratio decreased faster with the ball milled catalysts, which would reflect more participation of NH_3 adsorbed on Bronsted acid sites that that onto Lewis acid sites in ball milled catalysts, leading to higher reactivity. The decreasing ratio among the ball milled catalysts is also in accordance with the increased activity as shown in Fig. 4-1.

According to Raman spectra as displayed in Fig. 4-11, as the frequency of ball milling increased, the broad peak around 930-940 cm^{-1} increased while the peak appearing at 1020-1044 cm^{-1} tended to decrease, which are ascribed as polymeric vanadyl group and monomeric vanadyl group, respectively [97]. From the Raman spectra, it was found that the population of surface polymeric VOx species increased while the monomeric VOx species decreased. The increase of acidity as displayed in Fig. 4-9 could be induced by changing surface vanadyl group populations. According to previous studies, the polymeric vanadyl group contributes to increasing redox ability and acidity, especially strong acid sites and lead to improved SCR activity [98, 99]. However, the peak at 994 cm^{-1}, which is often denoted as crystalline V_2O_5, clearly increased, especially in ball milled VWTi with 30 Hz. The existence of crystalline V_2O_5 would interrupt the redox ability of vanadium oxide, resulting in degenerated activity. The increased population of polymeric vanadyl group would induce the enhanced activity of VWTi + Y12 B.M. catalysts, but ball milling at 30 Hz would have brought negative effect on the reaction.

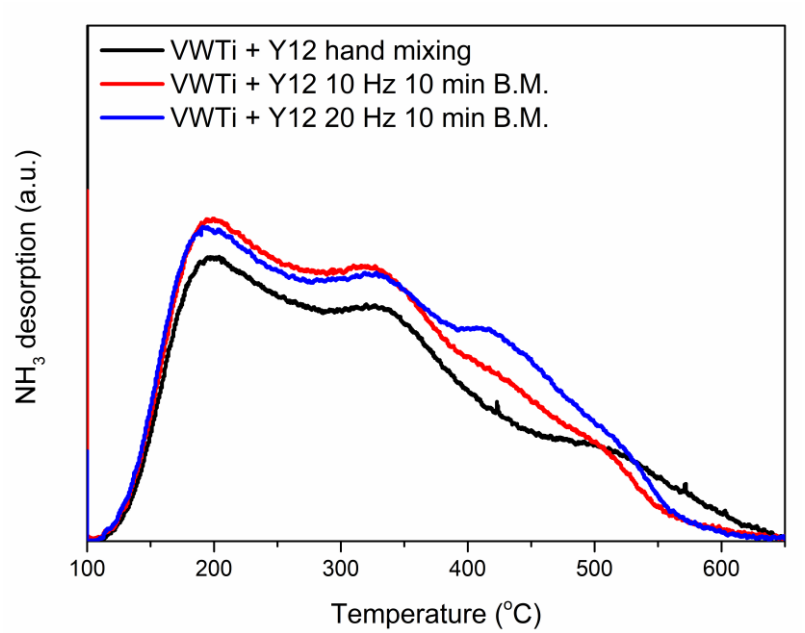

Fig. 4- 8. NH_3-temperature programmed desorption profiles of VWTi + Y 12 hand mixing and VWTi + Y12 B.M. catalysts.

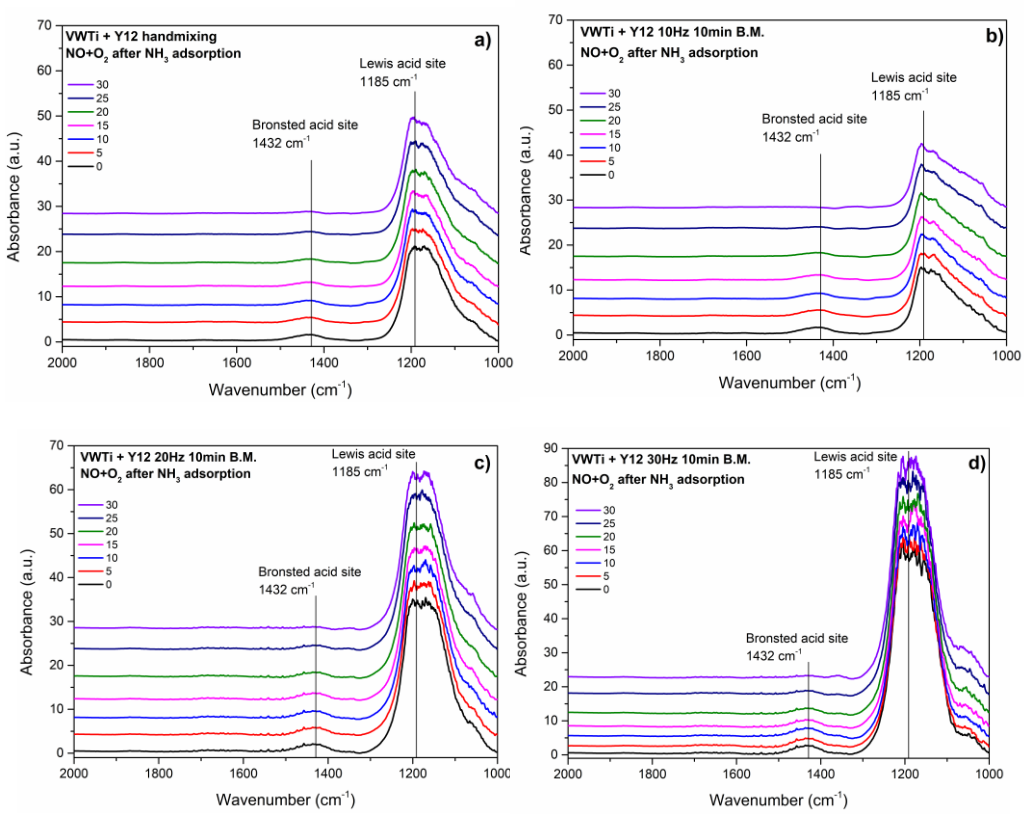

Fig. 4- 9. Diffuse Reflectance Infrared Fourier Transform Spectroscopy (DRIFTS) of (a) VWTi + Y12 -hand mixing, (b) VWTi+ Y12 – 10 Hz 10 Min B.M., (c) VWTi+ Y12 – 10 Hz 10 Min B.M., and (d) VWTi+ Y12 – 10 Hz 10 Min B.M. catalysts under $NO+O_2$ flow after NH_3 adsorption for 1 h.

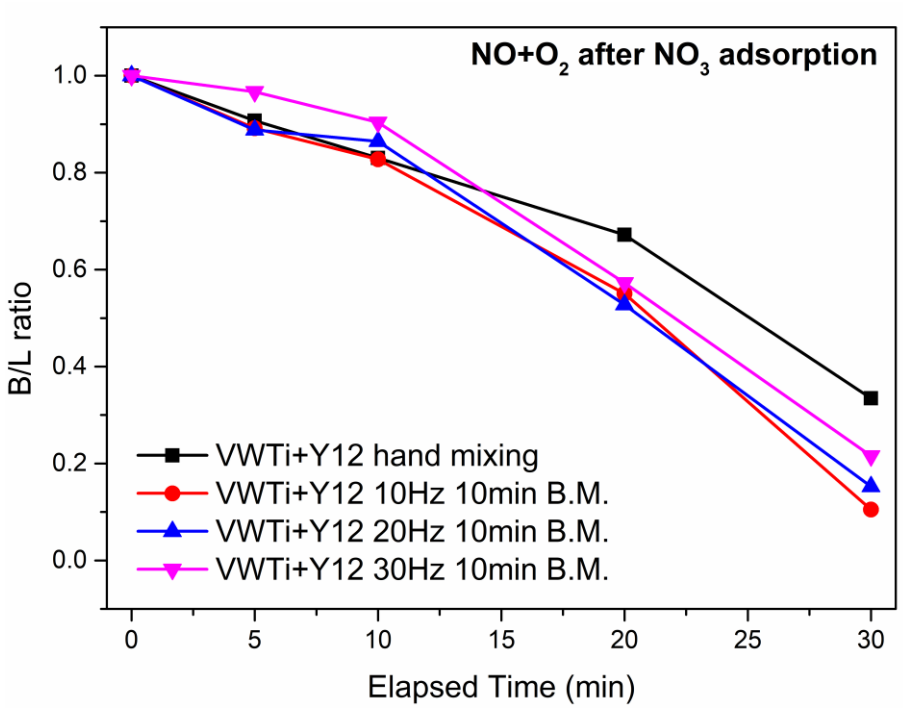

Fig. 4- 10. Ratio of NH_3 adsorbed onto Bronsted acid sites over that onto Lewis acid sites (B/L Ratio) under $NO+O_2$ flow after NH_3 adsorption.

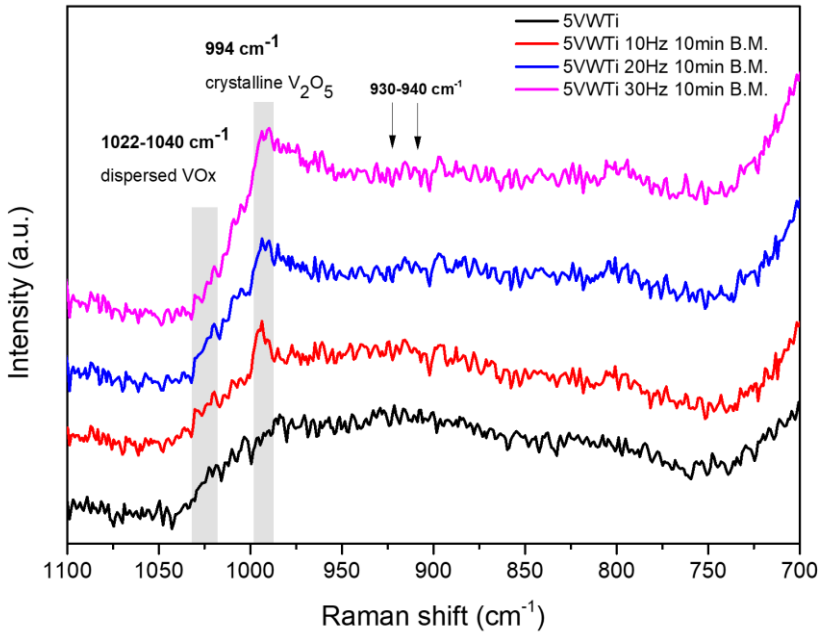

Fig. 4- 11. Raman spectra of ball milled VWTi catalysts.

4.3.2. Optimizing the ball milling process of 5 wt.% V_2O_5/WO_3-TiO_2 catalyst with zeolite Y

The ball milled catalysts achieved high catalytic activity and sulfur resistance. However, harsh ball milling condition can result in negative effects and inhibited the originally designed mechanical mixing system, interrupting the essential contact between VWTi and zeolite for ABS migration. To mitigate the inhibition, the ball milled catalysts were prepared under various milling conditions. Firstly, two materials, VWTi and zeolite Y12, were ball milled without grinding ball at three different frequencies. As shown in the Fig. 4-12, the ball milled samples without grinding ball obtained the significantly decreased activity at every frequency. In addition, NOx conversion during SO_2 aging test with 30 ppm SO_2 containing reaction flow decreased and the deactivation rate was similar to the hand mixed sample as shown in Fig. 4-13. H_2-TPR profiles in Fig. 4-14 indicated that the intensity of reduction peaks of V and W decreased in ball milled samples without ball, which would demonstrate the decrease of reduction property. The crystallinity of VWTi and zeolite Y12 mixture also decreased after ball milling process without grinding ball as demonstrated in Fig. 4-15.

From the Cs-TEM images and line EDS results in Fig. 4-16, it was found that the sample prepared by ball milling without ball maintained the essential contact between two materials, which is originally designed system for ABS trapping. The maintained physical contact would reflect the similar deactivation rate with VWTi + Y12 hand mixing catalyst during the

exposure to sulfur. From the activity tests and characterizations, the mixture should be prepared by ball milling with grinding ball, which seems more beneficial for increasing catalytic activity, and chemical interaction should exist up to some extent while maintaining the physical contact for ABS trapping.

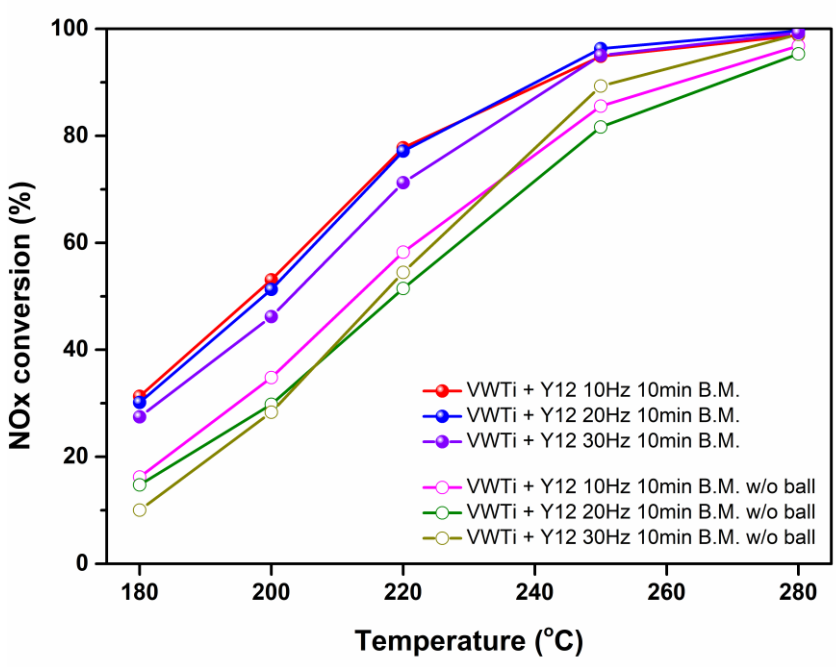

Fig. 4- 12. Catalytic activity of ball milled V_2O_5/WO_3-TiO_2 catalyst with zeolite Y12 without(w/o) grinding ball.

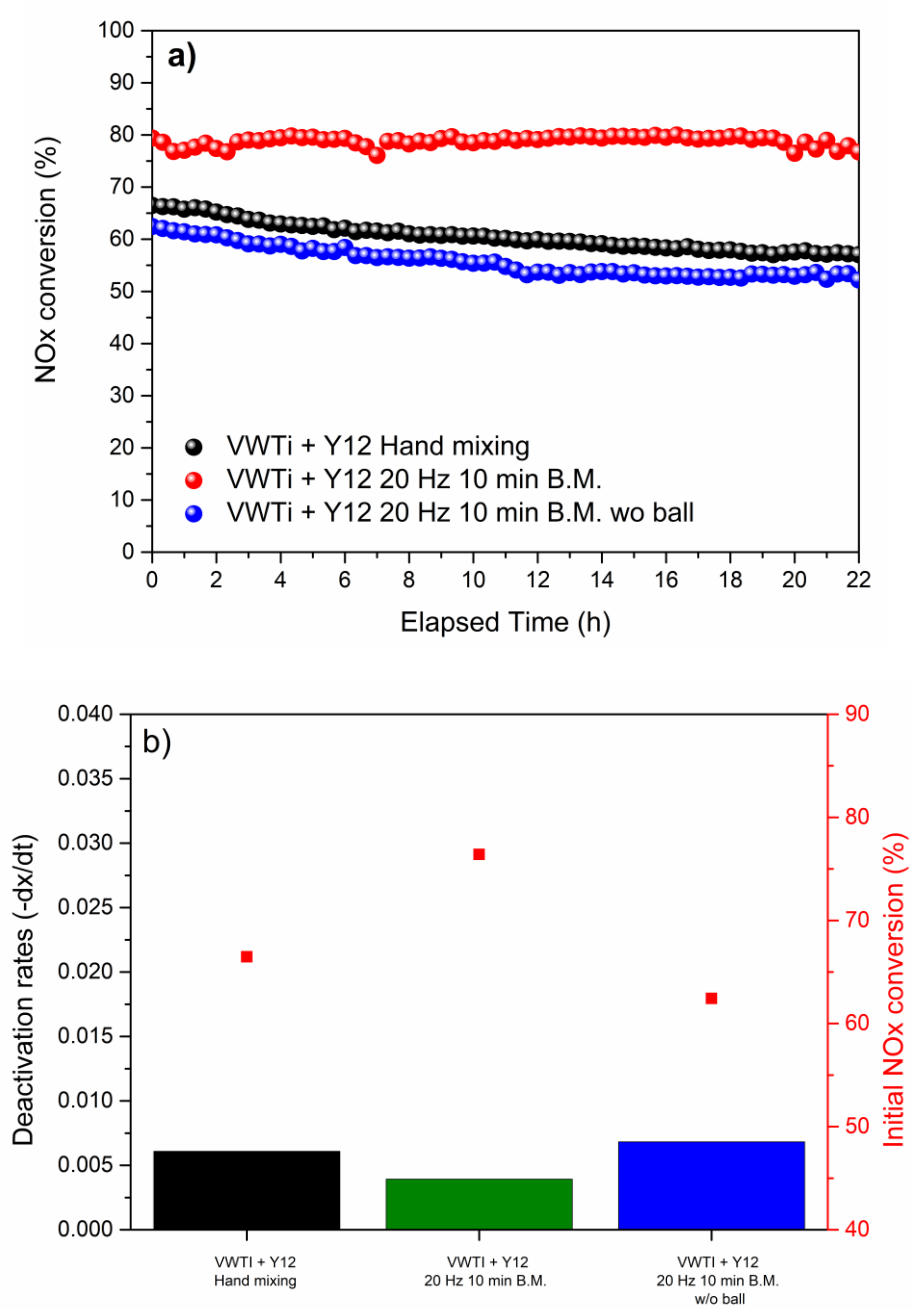

Fig. 4- 13. (a) NO_x conversion profiles of the VWTi + Y12 B.M. catalysts without grinding ball during SO_2 aging at 220 ^oC and (b) deactivation rates of the samples after SO_2 aging.

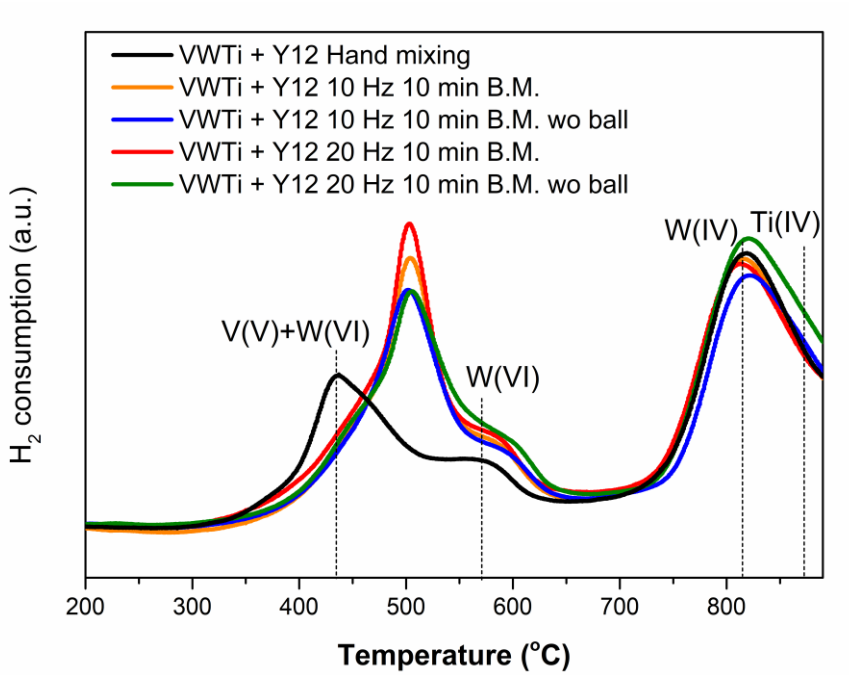

Fig. 4- 14. H_2-TPR results of VWTi + Y12 -B.M. catalysts with and without grinding ball.

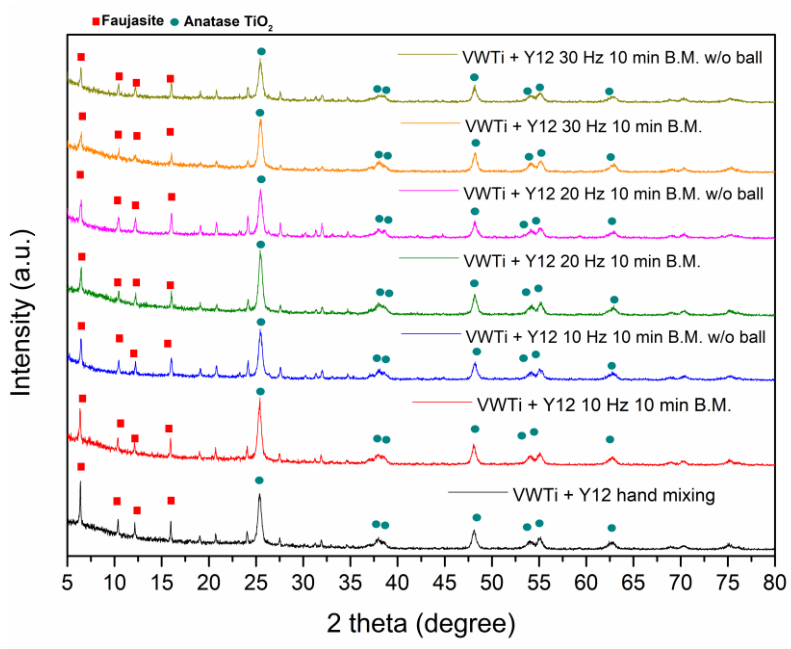

Fig. 4- 15. XRD results of ball milled VWTi + Y512 with and without grinding ball.

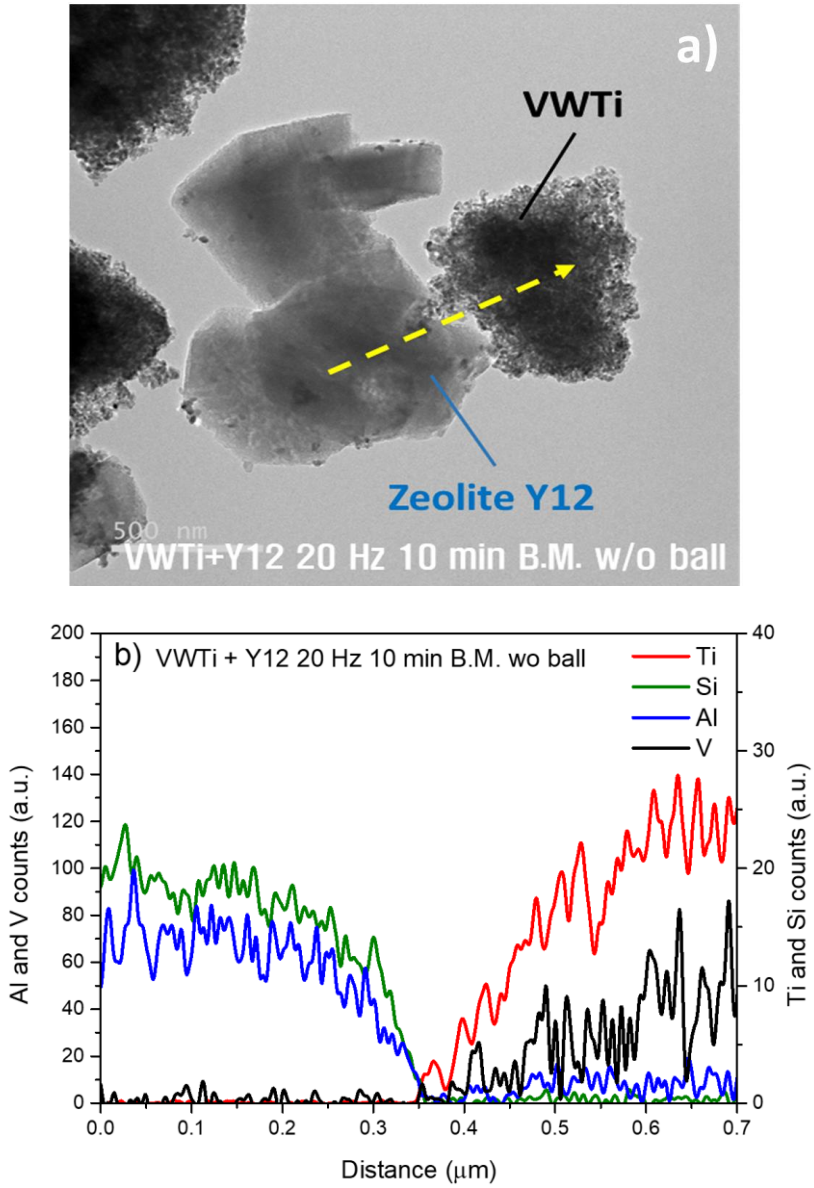

Fig. 4- 16. (a) Corrected transmission electron microscope (Cs-TEM) image and (b) line energy dispersive X-ray spectroscopy (line-EDS) scans of VWTi + Y12 20Hz 10 min B.M. w/o ball catalyst.

Furthermore, ball milling volume and size of grinding ball also affected the catalytic activity of the mixture as shown in Fig. 4-17. The frequency of ball milling process was fixed as 20 Hz for 10 min. Although the same volume of ball milling was used, the catalytic activity was different depending on the size of grinding ball. The ball milled sample in 10 ml of ball milling container with 12 mm ball obtained approximately 80 % of NOx conversion at 220 ℃ while that with 15 mm ball acquired approximately 60 % at 220 ℃. Similar results were obtained with the samples prepared in 25 ml of ball milling container. The sample prepared with smaller size of grinding ball achieved approximately 90 % at 250 ℃ while the sample synthesized with larger size of ball acquired approximately 70 % at 250 ℃.

According to the H_2-TPR results in Fig. 4-18, the reduction of V and W in every ball milled samples with different volume of ball milling container and different size of grinding balls still occurred at similar temperature ranges. However, slightly decreased intensity of reduction was observed with larger volume of container, which would demonstrate the slight decrease in redox ability. From the results, the highest catalytic activity was obtained when the VWTi + Y12 -B.M. sample was prepared in 10 ml of ball milling container with small size of ball at the fixed frequency.

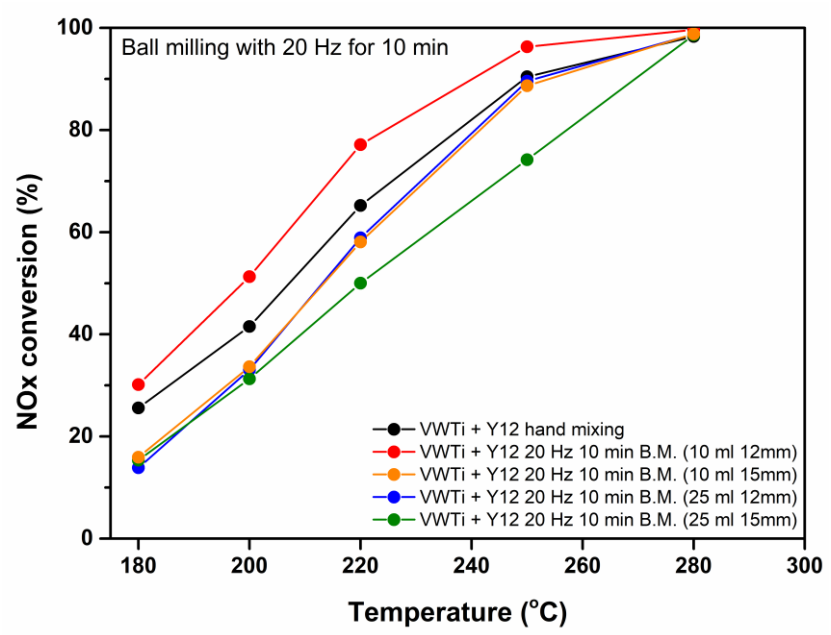

Fig. 4- 17. Catalytic activity of ball milled V_2O_5/WO_3-TiO_2 catalyst with zeolite Y12 with different ball milling volume and ball size.

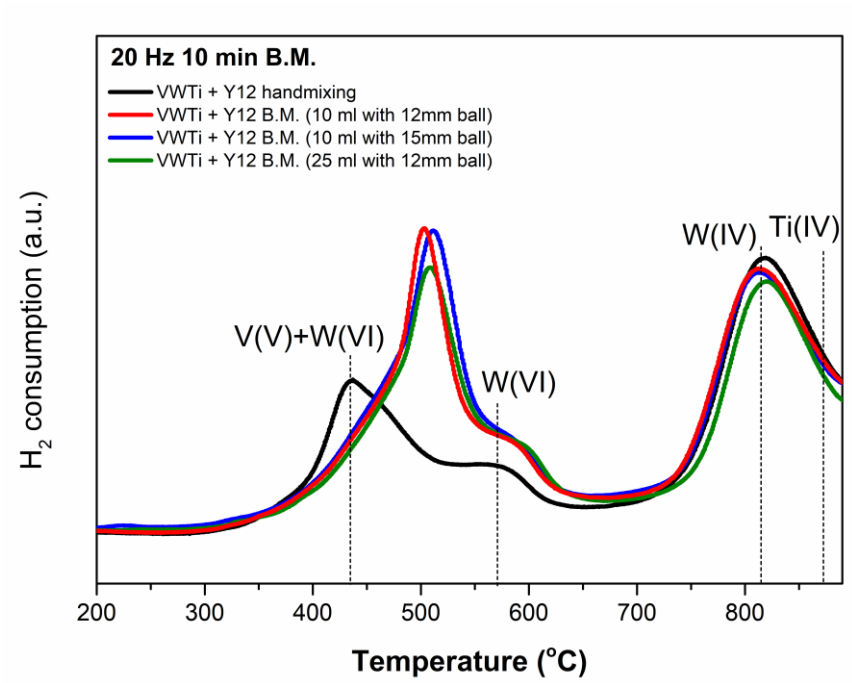

Fig. 4- 18. H_2-TPR results of VWTi + Y12 -B.M. catalysts with different ball milling volume and ball size.

Chapter 5. Conclusions and summary

In this research, the physically mixed 5 wt.% V_2O_5/WO_3-TiO_2 catalyst with alumina calcined at 900 ℃ (5VWTi+ 900 cal Al) demonstrated the ability to enhance SO_2 resistance, achieving a lower deactivation rate compared to that of the traditional 5VWTi catalyst. By combining the reaction tests and the characterization results, the physically mixed alumina catalyst trapped the ABS migrating from vanadia sites through the physical contact between vanadia and alumina by absorbing sulfur species. In addition, alumina itself did not participate in enhancing its catalytic activity, but it contributed to absorbing sulfur only when close physical contact was made by mechanical mixing with vanadia. Moreover, the physically mixed alumina catalyst recovered its initial catalytic activity even after repetitive exposure to SO_2. In summary, the physically mixed 5VWTi catalyst with alumina could preclude vanadia catalyst deactivation, maintaining superior sulfur resistance and NO_x removal ability at the same time.

Secondly, this study also demonstrated that the physically mixed V_2O_5/WO_3-TiO_2 catalyst and Al-rich zeolite Y accomplished superior sulfur resistance at low temperature, but degradation of activity simultaneously. This research identified the origin of the chemical deactivation derived from the mechanochemical interaction in physically mixed V_2O_5/WO_3-TiO_2 catalyst and Al-rich zeolite Y. The AlOx moieties of zeolite in a mixed catalytic system formed chemical bond with VOx species, V-O-Al, during

grinding and induced decreased reducibility of V active sites, which were confirmed by kinetic study and H_2-TPR results. Various characterization indicated the diffused AlO_x to vanadia sites and changes in Al and V coordination. To resolve the chemical deactivation, thin carbon layers on zeolite particles readily inhibit the migration of EFAl before mechanochemical grinding process without interrupting the essential physical contact with VWTi. The mixed V_2O_5/WO_3-TiO_2 catalyst with the carbon layered zeolite enabled suppressing physical and chemical deactivation and led to high catalytic activity and superior SO_2 resistance simultaneously.

Furthermore, the ball milled V_2O_5/WO_3-TiO_2 catalyst and zeolite Y catalysts were prepared to investigate the ball milling effect over catalytic activity and sulfur resistance for the designed system. Enhanced activity and sulfur resistance of ball milled catalyst were achieved compared to that of hand mixed samples due to the increased acidity and faster consumption of NH_3 adsorbed onto Bronsted acid sites. However, regulating the synthesis parameters was still necessary to maintain the designed the system and the enhanced activity and sulfur resistance simultaneously. Otherwise, the essential physical contact was inhibited, and degradation of activity occurred during ball milling process. The research demonstrated that the synthesis method of mixing two materials could influence the property of the VWTi catalyst, which led to reactivity of the samples.

In summary, the present research provided some ways to modify

vanadium oxide based cataslysts via physical mixing with alumina or zeolite Y to enhance sulfur resistance at low temperatures. The suggested ways can be potential suggestions for preventing air pollutant emission, NOx, which could be practically utilized in industrial fields.

Bibliography

[1] U.S.E.P. Agency, What is Particle Pollution?, United States Environmental Protection Agency, EPA, 2019.
[2] J.L. Domingo, J. Rovira, Effects of air pollutants on the transmission and severity of respiratory viral infections, Environmental research, 187 (2020) 109650.
[3] F. Dutheil, J.S. Baker, V. Navel, COVID-19 as a factor influencing air pollution?, Environmental pollution, 263 (2020) 114466.
[4] D. Sofia, F. Gioiella, N. Lotrecchiano, A. Giuliano, Mitigation strategies for reducing air pollution, Environmental Science and Pollution Research, 27 (2020) 19226-19235.
[5] A.q.i. Asia, Asia Development Bank, 2022.
[6] Greenpeace, World's most polluted cities (historical data 2017-2022), AirVisual, 2022.
[7] H.-S. Kim, S. Kasipandi, J. Kim, S.-H. Kang, J.-H. Kim, J.-H. Ryu, J.-W. Bae, Current catalyst technology of selective catalytic reduction (SCR) for NO_x removal in South Korea, Catalysts, 10 (2020) 52.
[8] Y. Guan, Y. Liu, Q. Lv, B. Wang, D. Che, Review on the selective catalytic reduction of NO_x with H_2 by using novel catalysts, J. Environ. Chem. Eng., 9 (2021) 106770.
[9] T. Andana, K.G. Rappe, F. Gao, J. Szanyi, X. Pereira-Hernandez, Y. Wang, Recent advances in hybrid metal oxide–zeolite catalysts for low-temperature selective catalytic reduction of NOx by ammonia, Appl. Catal. B: Environ., 291 (2021) 120054.
[10] F. Birkhold, U. Meingast, P. Wassermann, O. Deutschmann, Modeling and simulation of the injection of urea-water-solution for automotive SCR $DeNO_x$-systems, Appl. Catal. B: Environ., 70 (2007) 119-127.
[11] P. Forzatti, Present status and perspectives in de-NO_x SCR catalysis, Appl. Catal. A: Gen., 222 (2001) 221-236.
[12] P.L. Gabrielsson, Urea-SCR in automotive applications, Top Catal, 28 (2004) 177-184.
[13] M. Koebel, M. Elsener, M. Kleemann, Urea-SCR: a promising technique to reduce NO_x emissions from automotive diesel engines, Catal. Today, 59 (2000) 335-345.
[14] N. Akter, X. Chen, J. Parise, J.A. Boscoboinik, T. Kim, Effects of copper loading on NH_3-SCR and NO oxidation over Cu impregnated CHA zeolite, Korean J Chem Eng, 35 (2018) 89-98.
[15] A. Marberger, D. Ferri, M. Elsener, O. Kröcher, The Significance of Lewis Acid Sites for the Selective Catalytic Reduction of Nitric Oxide on Vanadium-Based Catalysts, Angew. Chem. Int. Ed., 55 (2016) 11989-11994.
[16] I.E. Wachs, B.M. Weckhuysen, Structure and reactivity of surface vanadium oxide species on oxide supports, Appl. Catal. A: Gen., 157 (1997) 67-90.
[17] M. Zhu, J.-K. Lai, U. Tumuluri, M.E. Ford, Z. Wu, I.E. Wachs, Reaction Pathways and Kinetics for Selective Catalytic Reduction (SCR) of Acidic NOx Emissions from Power Plants with NH_3, ACS Catal., (2017).
[18] E. Tronconi, I. Nova, C. Ciardelli, D. Chatterjee, M. Weibel, Redox features in the catalytic mechanism of the “standard” and “fast” NH_3-SCR of NO_x over a V-based catalyst investigated by dynamic methods, J. Catal., 245 (2007) 1-10.
[19] X. Gao, Y. Jiang, Y. Fu, Y. Zhong, Z. Luo, K. Cen, Preparation and characterization of CeO_2/TiO_2 catalysts for selective catalytic reduction of NO with NH_3, Catal. Commun., 11 (2010) 465-469.
[20] P.R. Ettireddy, N. Ettireddy, S. Mamedov, P. Boolchand, P.G. Smirniotis, Surface characterization studies of TiO_2 supported manganese oxide catalysts for low temperature SCR of NO with NH_3, Appl. Catal. B: Environ., 76 (2007) 123-134.
[21] J. Pasel, P. Käßner, B. Montanari, M. Gazzano, A. Vaccari, W. Makowski, T. Lojewski, R. Dziembaj, H. Papp, Transition metal oxides supported on active carbons as low temperature catalysts for the selective catalytic reduction (SCR) of NO with NH_3, Appl. Catal. B: Environ., 18 (1998) 199-213.
[22] J. Xu, X. Zhang, Y. Sun, H. Long, Z. Zheng, Improvement of low-temperature NH_3-SCR catalytic activity over Mn-Ce oxide catalysts supported on sewage sludge char

activated with KOH and H_3PO_4, Korean J Chem Eng, 37 (2020) 2152-2160.
[23] A. Burkardt, W. Weisweiler, J. van den Tillaart, A. Schäfer-Sindlinger, E. Lox, Influence of the V_2O_5 loading on the structure and activity of V_2O_5/TiO_2 SCR catalysts for vehicle application, Top Catal, 16 (2001) 369-375.
[24] M. D. Amiridis, J. P. Solar, Selective Catalytic Reduction of Nitric Oxide by Ammonia over V_2O_5/TiO_2, $V_2O_5/TiO_2/SiO_2$, and $V_2O_5–WO_3/TiO_2$ Catalysts: Effect of Vanadia Content on the Activation Energy, Ind. Eng. Chem. Res., 35 (1996) 978-981.
[25] S. Youn, I. Song, D.H. Kim, Roles of promoters in V_2O_5/TiO_2 catalysts for selective catalytic reduction of NOx with NH_3: Effect of order of impregnation, J. Nanosci. Nanotechnol, 16 (2016) 4350-4356.
[26] D.W. Kwon, K.H. Park, S.C. Hong, Enhancement of SCR activity and SO_2 resistance on VO_x/TiO_2 catalyst by addition of molybdenum, Chem. Eng. J., 284 (2016) 315-324.
[27] W. Cha, S.H. Ehrman, J. Jurng, CeO_2 added V_2O_5/TiO_2 catalyst prepared by chemical vapor condensation (CVC) and impregnation method for enhanced NH_3-SCR of NOx at low temperature, J. Environ. Chem. Eng., 4 (2016) 556-563.
[28] J.-K. Lai, I.E. Wachs, A perspective on the selective catalytic reduction (SCR) of NO with NH_3 by supported $V_2O_5–WO_3/TiO_2$ catalysts, ACS Catal., 8 (2018) 6537-6551.
[29] L. Chen, J. Li, M. Ge, Promotional effect of Ce-doped V_2O_5-WO_3/TiO_2 with low vanadium loadings for selective catalytic reduction of NO_x by NH_3, J. Phys. Chem. C, 113 (2009) 21177-21184.
[30] M. Zhu, J.-K. Lai, U. Tumuluri, Z. Wu, I.E. Wachs, Nature of active sites and surface intermediates during SCR of NO with NH_3 by supported $V_2O_5–WO_3/TiO_2$ catalysts, J. Am. Chem. Soc., 139 (2017) 15624-15627.
[31] M.D. Amiridis, I.E. Wachs, G. Deo, J.-M. Jehng, Reactivity of V_2O_5catalysts for the selective catalytic reduction of NO by NH_3: Influence of vanadia loading, H_2O, and SO_2, J. Catal., 161 (1996) 247-253.
[32] A. Marberger, M. Elsener, D. Ferri, O. Kröcher, VO_x surface coverage optimization of V_2O_5/WO_3-TiO_2 SCR catalysts by variation of the V loading and by aging, Catalysts, 5 (2015) 1704-1720.
[33] Z. Liu, Y. Li, T. Zhu, H. Su, J. Zhu, Selective catalytic reduction of NO_x by NH_3 over Mn-promoted V_2O_5/TiO_2 catalyst, Ind. Eng. Chem. Res., 53 (2014) 12964-12970.
[34] M. Qing, S. Su, L. Wang, L. Liu, K. Xu, L. He, X. Jun, S. Hu, Y. Wang, J. Xiang, Getting insight into the oxidation of SO_2 to SO_3 over V_2O_5-WO_3/TiO_2 catalysts: Reaction mechanism and effects of NO and NH_3, Chem. Eng. J., 361 (2019) 1215-1224.
[35] H. Kamata, H. Ohara, K. Takahashi, A. Yukimura, Y. Seo, SO_2 oxidation over the V_2O_5/TiO_2 SCR catalyst, Catal. Lett, 73 (2001) 79-83.
[36] Y. Chen, C. Li, J. Chen, X. Tang, Self-prevention of well-defined-facet Fe_2O_3/MoO_3 against deposition of ammonium bisulfate in low-temperature NH_3–SCR, Environ. Sci. Technol., 52 (2018) 11796-11802.
[37] K. Guo, J. Ji, W. Song, J. Sun, C. Tang, L. Dong, Conquering ammonium bisulfate poison over low temperature NH_3-SCR catalysts: A critical review, Appl. Catal. B, (2021) 120388.
[38] T. Tong, J. Chen, S. Xiong, W. Yang, Q. Yang, L. Yang, Y. Peng, Z. Liu, J. Li, Vanadium-density-dependent thermal decomposition of NH_4HSO_4 on V_2O_5/TiO_2 SCR catalysts, Catal. Sci. Technol., 9 (2019) 3779-3787.
[39] I. Song, H. Lee, S.W. Jeon, I.A. Ibrahim, J. Kim, Y. Byun, D.J. Koh, J.W. Han, D.H. Kim, Simple physical mixing of zeolite prevents sulfur deactivation of vanadia catalysts for NOx removal, Nat. Commun, 12 (2021) 901.
[40] I.E. Wachs, G. Deo, B.M. Weckhuysen, A. Andreini, M.A. Vuurman, M. De Boer, M.D. Amiridis, Selective catalytic reduction of NO with NH_3 over supported vanadia catalysts, J. Catal., 161 (1996) 211-221.
[41] W. Yu, X. Wu, Z. Si, D. Weng, Influences of impregnation procedure on the SCR activity and alkali resistance of $V_2O_5–WO_3/TiO_2$ catalyst, Appl. Surf. Sci., 283 (2013) 209-214.

[42] S.-H. Cai, S.N. Rashkeev, S.T. Pantelides, K. Sohlberg, Phase transformation mechanism between γ-and θ-alumina, Phys. Rev. B, 67 (2003) 224104.
[43] C. Li, M. Shen, T. Yu, J. Wang, J. Wang, Y. Zhai, The mechanism of ammonium bisulfate formation and decomposition over V/WTi catalysts for NH_3-selective catalytic reduction at various temperatures, Phys. Chem. Chem. Phys., 19 (2017) 15194-15206.
[44] L.K. Noda, R.M. de Almeida, N.S. Gonçalves, L.F.D. Probst, O. Sala, TiO_2 with a high sulfate content—thermogravimetric analysis, determination of acid sites by infrared spectroscopy and catalytic activity, Catal. Today, 85 (2003) 69-74.
[45] M. Ghasri-Khouzani, M. Meratian, M. Panjepour, Effect of mechanical activation on structure and thermal decomposition of aluminum sulfate, J. Alloys Compd, 472 (2009) 535-539.
[46] Y. Pelovski, W. Pietkova, I. Gruncharov, B. Pacewska, J. Pysiak, The thermal decomposition of aluminum sulfate in different gas phase environments, Thermochim. Acta, 205 (1992) 219-224.
[47] C.C. Chang, Infrared studies of SO_2 on γ-alumina, J. Catal., 53 (1978) 374-385.
[48] G. Busca, The surface of transitional aluminas: A critical review, Catal. Today, 226 (2014) 2-13.
[49] J. Gangwar, B.K. Gupta, S.K. Tripathi, A.K. Srivastava, Phase dependent thermal and spectroscopic responses of Al_2O_3 nanostructures with different morphogenesis, Nanoscale, 7 (2015) 13313-13344.
[50] C. Pecharroman, I. Sobrados, J. Iglesias, T. Gonzalez-Carreno, J. Sanz, Thermal evolution of transitional aluminas followed by NMR and IR spectroscopies, J. Phys. Chem. B, 103 (1999) 6160-6170.
[51] W. Xu, H. He, Y. Yu, Deactivation of a Ce/TiO_2 catalyst by SO_2 in the selective catalytic reduction of NO by NH_3, J. Phys. Chem. C, 113 (2009) 4426-4432.
[52] L. Xu, C. Wang, H. Chang, Q. Wu, T. Zhang, J. Li, New insight into SO_2 poisoning and regeneration of CeO_2–WO_3/TiO_2 and V_2O_5–WO_3/TiO_2 catalysts for low-temperature NH_3–SCR, Environ. Sci. Technol., 52 (2018) 7064-7071.
[53] S. Mateti, M. Mathesh, Z. Liu, T. Tao, T. Ramireddy, A.M. Glushenkov, W. Yang, Y.I. Chen, Mechanochemistry: A force in disguise and conditional effects towards chemical reactions, Chem. Comm., (2021) 1080–1092.
[54] K. Ralphs, C. Hardacre, S.L. James, Application of heterogeneous catalysts prepared by mechanochemical synthesis, Chem. Soc. Rev, 42 (2013) 7701-7718.
[55] M.K. Beyer, H. Clausen-Schaumann, Mechanochemistry: the mechanical activation of covalent bonds, Chemical Reviews, 105 (2005) 2921-2948.
[56] M.J. Muñoz-Batista, D. Rodriguez-Padron, A.R. Puente-Santiago, R. Luque, Mechanochemistry: Toward sustainable design of advanced nanomaterials for electrochemical energy storage and catalytic applications, ACS Sustain. Chem. Eng., 6 (2018) 9530-9544.
[57] Y. Chen, L. Soler, M. Armengol-Profitós, C. Xie, D. Crespo, J. Llorca, Enhanced photoproduction of hydrogen on Pd/TiO_2 prepared by mechanochemistry, Appl. Catal. B: Environ., (2022) 121275.
[58] T. Friščić, C. Mottillo, H.M. Titi, Mechanochemistry for synthesis, Angew. Chem. Int. Ed., 59 (2020) 1018-1029.
[59] C. Bolm, J.G. Hernández, Mechanochemistry of gaseous reactants, Angew. Chem. Int. Ed., 58 (2019) 3285-3299.
[60] H. Lee, I. Song, S.W. Jeon, D.H. Kim, Inter-particle migration of Cu ions in physically mixed Cu-SSZ-13 and H-SSZ-13 treated by hydrothermal aging, Reaction Chemistry & Engineering, 4 (2019) 1059-1066.
[61] I. Song, S. Youn, H. Lee, D.H. Kim, CeO_2-TiO_2 catalyst prepared by physical mixing for NH_3 selective catalytic reduction: Evidence about the migration of sulfates from TiO_2 to CeO_2 via simple calcination, Korean J Chem Eng, 33 (2016) 2547-2554.
[62] M. Danielis, L.E. Betancourt, I. Orozco, N.J. Divins, J. Llorca, J.A. Rodríguez, S.D. Senanayake, S. Colussi, A. Trovarelli, Methane oxidation activity and nanoscale

characterization of Pd/CeO_2 catalysts prepared by dry milling Pd acetate and ceria, Appl. Catal. B: Environ., 282 (2021) 119567.
[63] A.P. Amrute, Z. Łodziana, H. Schreyer, C. Weidenthaler, F. Schüth, High-surface-area corundum by mechanochemically induced phase transformation of boehmite, Science, 366 (2019) 485-489.
[64] M. Bilke, P. Losch, O. Vozniuk, A. Bodach, F. Schüth, Methane to Chloromethane by Mechanochemical Activation: A Selective Radical Pathway, J. Am. Chem. Soc., 141 (2019) 11212-11218.
[65] G.-F. Han, F. Li, Z.-W. Chen, C. Coppex, S.-J. Kim, H.-J. Noh, Z. Fu, Y. Lu, C.V. Singh, S. Siahrostami, Mechanochemistry for ammonia synthesis under mild conditions, Nat. Nanotechnol, (2020) 1-6.
[66] H. Schreyer, R. Eckert, S. Immohr, J. de Bellis, M. Felderhoff, F. Schüth, Milling down to nanometers: a general process for the direct dry synthesis of supported metal catalysts, Angew. Chem. Int. Ed., 58 (2019) 11262-11265.
[67] S. Ndayiragije, Y. Zhang, Y. Zhou, Z. Song, N. Wang, T. Majima, L. Zhu, Mechanochemically tailoring oxygen vacancies of MnO_2 for efficient degradation of tetrabromobisphenol A with peroxymonosulfate, Appl. Catal. B: Environ., 307 (2022) 121168.
[68] X. Wang, X. Du, S. Liu, G. Yang, Y. Chen, L. Zhang, X. Tu, Understanding the deposition and reaction mechanism of ammonium bisulfate on a vanadia SCR catalyst: A combined DFT and experimental study, Appl. Catal. B: Environ., 260 (2020) 118168.
[69] K. Guo, G. Fan, D. Gu, S. Yu, K. Ma, A. Liu, W. Tan, J. Wang, X. Du, W. Zou, Pore size expansion accelerates ammonium bisulfate decomposition for improved sulfur resistance in low-temperature NH3-SCR, ACS Appl. Mater. Interfaces, 11 (2019) 4900-4907.
[70] J. Li, H. Chang, L. Ma, J. Hao, R.T. Yang, Low-temperature selective catalytic reduction of NOx with NH_3 over metal oxide and zeolite catalysts—A review, Catal. Today, 175 (2011) 147-156.
[71] S.W. Jeon, I. Song, H. Lee, J. Kim, Y. Byun, D.J. Koh, D.H. Kim, Enhanced SO_2 resistance of V_2O_5/WO_3-TiO_2 catalyst physically mixed with alumina for the selective catalytic reduction of NOx with NH_3, Chem. Eng. J., 433 (2022) 133836.
[72] P.A. Zapata, Y. Huang, M.A. Gonzalez-Borja, D.E. Resasco, Silylated hydrophobic zeolites with enhanced tolerance to hot liquid water, J. Catal., 308 (2013) 82-97.
[73] G. Engelhardt, U. Lohse, A. Samoson, M. Mägi, M. Tarmak, E. Lippmaa, High resolution ^{29}Si nmr of dealuminated and ultrastable Y-zéolites, Zeolites, 2 (1982) 59-62.
[74] B. Xu, S. Bordiga, R. Prins, J.A. van Bokhoven, Effect of framework Si/Al ratio and extra-framework aluminum on the catalytic activity of Y zeolite, Appl. Catal. A: Gen., 333 (2007) 245-253.
[75] S. Li, A. Zheng, Y. Su, H. Fang, W. Shen, Z. Yu, L. Chen, F. Deng, Extra-framework aluminium species in hydrated faujasite zeolite as investigated by two-dimensional solid-state NMR spectroscopy and theoretical calculations, Phys. Chem. Chem. Phys., 12 (2010) 3895-3903.
[76] A. Miecznikowski, J. Hanuza, Application of the long chain approach to the structure and vibrational spectra of X and Y zeolites, Zeolites, 5 (1985) 188-193.
[77] N.R. Jaegers, J.K. Lai, Y. He, E. Walter, D.A. Dixon, M. Vasiliu, Y. Chen, C. Wang, M.Y. Hu, K.T. Mueller, Mechanism by which tungsten oxide promotes the activity of supported V_2O_5/TiO_2 catalysts for NOx abatement: structural effects revealed by ^{51}V MAS NMR spectroscopy, Angew. Chem. Int. Ed., 58 (2019) 12609-12616.
[78] L. Kovarik, N. Jaegers, J. Szanyi, M. Derewinski, Y. Wang, K. Khivantsev, PdO self-assembly on zeolite SSZ-13 with rows of O_3Al (IV) OH selectively incorporated in PdO (101) facets for moisture-resistant methane oxidation, (2021).
[79] Z. Lian, J. Wei, W. Shan, Y. Yu, P.M. Radjenovic, H. Zhang, G. He, F. Liu, J.-F. Li, Z.-Q. Tian, Adsorption-Induced Active Vanadium Species Facilitate Excellent Performance in Low-Temperature Catalytic NOx Abatement, J. Am. Chem. Soc., 143 (2021) 10454-10461.

[80] P.G. Kompio, A. Brückner, F. Hipler, G. Auer, E. Löffler, W. Grünert, A new view on the relations between tungsten and vanadium in V_2O_5-WO_3/TiO_2 catalysts for the selective reduction of NO with NH_3, J. Catal., 286 (2012) 237-247.
[81] P.G. Kompio, A. Brückner, F. Hipler, O. Manoylova, G. Auer, G. Mestl, W. Grünert, V_2O_5-WO_3/TiO_2 catalysts under thermal stress: Responses of structure and catalytic behavior in the selective catalytic reduction of NO by NH_3, Appl. Catal. B: Environ., 217 (2017) 365-377.
[82] R.J.G. Nuguid, L. Ortino-Ghini, V.L. Suskevich, J. Yang, L. Lietti, O. Kröcher, D. Ferri, Interconversion between Lewis and Brønsted–Lowry acid sites on vanadia-based catalysts, Phys. Chem. Chem. Phys., 24 (2022) 4555-4561.
[83] G. Xu, H. Li, Y. Yu, H. He, Dynamic Change of Active Sites of Supported Vanadia Catalysts for Selective Catalytic Reduction of Nitrogen Oxides, Environ. Sci. Technol., (2022) 3710–3718.
[84] I. Song, H. Lee, S.W. Jeon, D.H. Kim, Understanding the dynamic behavior of acid sites on TiO_2-supported vanadia catalysts via operando DRIFTS under SCR-relevant conditions, J. Catal., 382 (2020) 269-279.
[85] Y. Ganjkhanlou, T.V. Janssens, P.N. Vennestrøm, L. Mino, M.C. Paganini, M. Signorile, S. Bordiga, G. Berlier, Location and activity of VOx species on TiO_2 particles for NH_3-SCR catalysis, Appl. Catal. B, 278 (2020) 119337.
[86] M.D. Amiridis, J.P. Solar, Selective catalytic reduction of nitric oxide by ammonia over V_2O_5/TiO_2, V_2O_5/TiO_2/SiO_2, and V_2O_5− WO_3/TiO_2 catalysts: effect of vanadia content on the activation energy, Ind. Eng. Chem. Res., 35 (1996) 978-981.
[87] Y. Xi, N.A. Ottinger, Z.G. Liu, New insights into sulfur poisoning on a vanadia SCR catalyst under simulated diesel engine operating conditions, Appl. Catal. B, 160 (2014) 1-9.
[88] Z. Lian, M. Zheng, Q. Wang, Y. Li, F. Deng, W. Shan, H. He, Water in the ball-milling process affects the dispersion of vanadia species on V_2O_5/TiO_2 catalysts for NH_3-SCR, New Journal of Chemistry, 47 (2023) 1027-1030.
[89] J. Song, S. Liu, Y. Ji, W. Xu, J. Yu, B. Liu, W. Chen, J. Zhang, L. Jia, T. Zhu, Dual single-atom Ce-Ti/MnO_2 catalyst enhances low-temperature NH_3-SCR performance with high H_2O and SO_2 resistance, Nano Research, 16 (2023) 299-308.
[90] H. Chang, X. Qin, L. Ma, T. Zhang, J. Li, Cu/SAPO-34 prepared by a facile ball milling method for enhanced catalytic performance in the selective catalytic reduction of NO_x with NH_3, Phys. Chem. Chem. Phys., 21 (2019) 22113-22120.
[91] C. Koch, Synthesis of nanostructured materials by mechanical milling: problems and opportunities, Nanostructured Materials, 9 (1997) 13-22.
[92] Y. Pan, B. Shen, L. Liu, Y. Yao, H. Gao, C. Liang, H. Xu, Develop high efficient of NH_3-SCR catalysts with wide temperature range by ball-milled method, Fuel, 282 (2020) 118834.
[93] A. Stolle, T. Szuppa, S.E. Leonhardt, B. Ondruschka, Ball milling in organic synthesis: solutions and challenges, Chem. Soc. Rev, 40 (2011) 2317-2329.
[94] D.W. Kwon, D.H. Kim, S. Lee, J. Kim, H.P. Ha, A dual catalytic strategy by the nature of the functionalization effect as well as active species on vanadium-based catalyst for enhanced low temperature SCR, Appl. Catal. B: Environ., 289 (2021) 120032.
[95] I. Song, H. Lee, S.W. Jeon, I.A.M. Ibrahim, J. Kim, Y. Byun, D.J. Koh, J.W. Han, D.H. Kim, Simple physical mixing of zeolite prevents sulfur deactivation of vanadia catalysts for NOx removal, Nat. Commun, 12 (2021) 901.
[96] I. Song, S.W. Jeon, H. Lee, D.H. Kim, Tailoring the mechanochemical interaction between vanadium oxides and zeolite for sulfur-resistant DeNOx catalysts, Appl. Catal. B: Environ., 316 (2022) 121672.
[97] X. Zhao, Y. Yan, L. Mao, M. Fu, H. Zhao, L. Sun, Y. Xiao, G. Dong, A relationship between the V^{4+}/V^{5+} ratio and the surface dispersion, surface acidity, and redox performance of V_2O_5–WO_3/TiO_2 SCR catalysts, RSC Adv., 8 (2018) 31081-31093.
[98] G. He, Z. Lian, Y. Yu, Y. Yang, K. Liu, X. Shi, Z. Yan, W. Shan, H. He, Polymeric vanadyl species determine the low-temperature activity of V-based catalysts for the SCR of

NO_x with NH_3, Science advances, 4 (2018) eaau4637.
[99] N.R. Jaegers, J.K. Lai, Y. He, E. Walter, D.A. Dixon, M. Vasiliu, Y. Chen, C. Wang, M.Y. Hu, K.T. Mueller, Mechanism by which tungsten oxide promotes the activity of supported V_2O_5/TiO_2 catalysts for NOx abatement: structural effects revealed by ^{51}V MAS NMR spectroscopy, Angew. Chem., 131 (2019) 12739-12746.

초 록

암모니아를 활용한 선택적 촉매 환원기술은 높은 효율성과 낮은 운영 비용으로 대기 오염물질 질소산화물 제거에 탁월하여 각광받아 오고 있으나 매년 강화되는 질소산화물 배출 규정을 준수하기 위해서는 종래의 기술들보다 더욱 효과적인 선택적 촉매 환원 기술이 도입되어야 하는 실정이다. 또한, 해당 기술은 발전소의 후처리 과정에서 많이 활용이 되는데 후처리 과정에 포함된 황산화물은 촉매 수명과 효율에 영향을 미치므로 이에 대한 영향도 고려되어야 한다.

공정의 운용 온도와 배기 가스 조성 등의 요인에 따라, 다양한 금속 산화물 기반 촉매와 제올라이트 기반 촉매들이 암모니아를 활용한 선택적 촉매 환원 기술에 활용되고 있다. 그 중에서도 바나듐 산화물 기반 촉매는 높은 열 안정성과 경제적인 가격 때문에 많이 활용된다. 하지만, 최근 배출 규제를 충족시키기 위해서는 몇 가지 문제점들에 직면해 있다. 첫째, 기존 바나듐 산화물 기반 촉매의 높은 질소산화물 전환율은 300℃ 이상의 높은 온도에서만 달성할 수 있으나 최근 산업에서 실제로 운전되는 온도는 대부분 300℃ 미만이다. 게다가, 후처리 과정에서 황산화물과 물이 존재하게 되는데 황산화물이 산화되어 암모니아와 물의 반응물로 인해, 비활성화 물질인 암모늄

바이설페이트(ABS)가 생성되게 된다. 생성된 암모늄 바이설페이트가 촉매에 침적되게 되어 촉매의 효율과 수명을 감소시킨다는 문제점이 있다. 따라서, 저온에서 높은 질소산화물 제거 효율과 함께 더 적은 에너지 소비로 우수한 내황성을 확보하는 혁신적인 선택적 촉매 환원 기술이 필요하다.

이 같은 목표를 가지고 저온에서 내황성을 향상시키기 위해 V_2O_5/WO_3-TiO_2 촉매와 다양한 온도에서 소성된 알루미나 촉매를 물리혼합방법으로 제조한 촉매들을 개발하였다. 혼합된 촉매 (V_2O_5/WO_3-TiO_2 + Al) 중에서 900℃에서 소성된 알루미나와 혼합된 바나듐 촉매가 강한 산점의 증가로 인해 가장 높은 내황성을 유지하였다. 물리 혼합 과정에서 생성된 물리적 접촉면을 통해 바나듐에 생성된 ABS가 혼합된 알루미나로 이동하여 바나듐 활성점이 황 피독으로부터 보호되어 저온에서도 우수한 내황성과 우수한 재사용성을 가지는 것으로 관찰되었다.

이 연구는 바나듐 산화물 기반 촉매(V_2O_5/WO_3-TiO_2)와 표면을 카본 처리한 제올라이트와 물리 혼합 방법으로 제조하여 물리적 및 화학적 비활성화를 동시에 해결할 수 있는 방법을 제시하였다. V_2O_5/WO_3-TiO_2 촉매 및 알루미늄 사이트가 많은 제올라이트 Y를 물리 혼합방법으로 제조하였을 때, 활성 저하가 관찰되었다. 활성 저하의 주요 원인은 물리 혼합 과정 중 바나듐

종과 제올라이트 표면에 존재하는 알루미나 종의 화학적 상호작용을 통한 활성화 에너지 증가로 밝혀졌다. 이에 따라 제올라이트 표면에 옥타데실트리클로로실란(OTS)을 코팅처리 하여 V_2O_5/WO_3-TiO_2 촉매와 물리 혼합하여 제조하였다. 개발된 촉매(V_2O_5/WO_3-TiO_2 + OTSY)는 물리적 및 화학적 중독을 동시에 억제하여 우수한 저온 활성과 내황성을 가지는 촉매 개발하였다.

더불어, 본 연구에서는 V_2O_5/WO_3-TiO_2 + 제올라이트 Y 촉매를 볼 밀링 머신을 통해 제조함으로서 볼 밀링 효과를 연구하였다. 볼 밀링을 이용한 촉매 제조를 통해 물리 혼합 방법에 따라 변화된 촉매 특성과 활성에 미치는 영향에 대해서 연구를 하였으며, 최적화 연구를 진행하였다.

주요어: 암모니아를 활용한 선택적 촉매 환원, 바나듐 산화물 기반 촉매, 물리혼합방법, 내황성, 제올라이트, 알루미나

학번: 2017-25668